Dynamic Catalytic Microreactor Design and Operation in Overcoming Inherent Thermodynamic Limitations

by

CAMERON DAVID ARMSTRONG

Submitted to the Graduate School of

WORCESTER POLYTECHNIC INSTITUTE

in partial fulfillment of the requirements for the degree of

DOCTOR OF PHILOSOPHY

April 2023

Department of Chemical Engineering

Approved as to style and content by:

Dr. Andrew R. Teixeira, Advisor Chemical Engineering, WPI	Dr. N. Aaron Deskins, Member Chemical Engineering, WPI
Dr. Nikolaos Kazantzis, Member Chemical Engineering, WPI	Dr. Jamal Yagoobi, Member Mechanical Engineering, WPI

ACKNOWLEDGEMENTS

These past 6 years have been some of the most challenging of my life and there are so many people I would not have made it to this point without.

Andrew – Your crazy ideas have taught me to think outside of the box when approaching a problem. Not only have I become a stronger engineer, but the creative problem solving skills you have instilled in me are something that I will take with me the rest of my life. I can't express enough how you've helped and supported me especially in times when I've needed it the most. Throughout all the ups and downs, I couldn't have asked for a better advisor.

To the old guard – Those who were there when I started my time here at WPI (Alex, Avery, Max, Azadeh, Behnam, Satish, Lida, Jim, Natti, Junbo, and anyone else I may have missed) I cant thank you enough for getting me started. You all helped me join a community that was more like a family than anything else when I was just a new, confused first year. For all of the help you have all given me over the years, I have tried to pay it forward as best as I can. It may have taken years of being voluntold to do things, but you taught me how to say no which is something that has never come easily to me. You taught me how to lead and mentor in a way to support, but to also give room for people to rise up and develop their own ideas. I'm excited to join you all in the real world soon!

To Heather and Jacob – Honestly, there's just too much to say. You've been there from the beginning to the end and I can't even start to imagine what my time would have been like here without you. You're both two of my closest friends and I cant wait to see you on the other side!

To Esai, David, and Fatou – It's been so exciting watching you all grow as researchers and going from fumbling around with Swagelok to… well sometimes still fumbling with Swagelok. You are

all great friends and it's always amazing to me how we get the best candidates in our lab (totally unbiased). I know the lab will be left in good hands.

To the rest of the gang – To those that are here now (Liz, Maddie, Muntisir, Karen, Tim, Lily, Kevin, Sydney, Daniel, Januario, Maliha, and any others I may have missed) I've really enjoyed watching the department grow over the years and being able to see the way everyone has brought their own personal touch to the community. It has become such an exciting, energetic, and inclusive environment I'm so excited to see where it goes!

To Geoff, Doug, Ian, and Tom – No research gets done here without input from every one of you. You are all ridiculously skilled in your work and I hope to have close to your levels of expertise in the future.

To Tiffany, Leslie, and Justina – Over my time here I've learned a lot of things, but none of them am I more confident in than the entire department would collapse without you. You support every aspect of what goes on here and, maybe most importantly, you deal with Workday.

To the friends from home – (Adam, Andrew, Dan, Mike, Charlie, Jason, Billy, and any others missed) Thank you for all the times you took my mind away from the stress of the PhD and supporting me along the way.

To the Fam – Thank you for all the support over the years. I will miss watching you try to explain my research to people and I will *not* miss being asked every month when I am going to graduate. Graduation is May 11th by the way.

To the Undergrads – So much of the manpower in troubleshooting and development was done by all of you. I'm especially grateful to Avery Cirincione-Lynch and Eileen Piombino in their work developing the chip microreactor.

To all the friends I've made along the way – I could write another dissertation on the experiences we've shared and the memories we've made. I'd do it all again just to have met each and every one of you.

ABSTRACT

Over a century of catalyst science has proven that kinetic catalytic rates are restricted by the thermodynamics of the surface-species interactions. This kinetic barrier is described by Sabatier's rule and dictated by the scaling relations. These rules tell us that the more a catalyst is able to stabilize a transition state, the lower the activation barrier and thus the higher the kinetic rates. Stabilizing too much, however, becomes a problem as a products may never desorb off the catalyst surface, inhibiting the catalytic binding sites, and thus reaction rates. Sabatier's rule suggests compromising by finding a material where a reactant is stable, but not so stable the product will never desorb. Recent studies have found creative ways to better optimize or even overcome this thermodynamic limitation, including alloyed catalysis, single atom catalysis, and *dynamic catalysis*.

Dynamic catalysis involves periodically operating a reactor in a controlled, oscillatory fashion and is one such way to overcome the scaling relations as it moves away from thermodynamic equilibrated driving forces. Applied thermal oscillations which match the time scales of inherent catalytic phenomena has been a topic of particular interest over the past few years. Although these studies are primarily theoretical, matching an applied frequency to its natural frequency (i.e. catalytic turnover frequency) can lead to order of magnitude rate enhancements.

Here, we investigate the design, fabrication, and validation in developing a catalytic microreactor capable of millisecond heating and cooling and challenge the isothermal paradigm chemical engineers have for so long operated under. We go on to build a full reactor test stand to determine the effects of thermal oscillations on a catalytic system and give insights as to what is happening at a molecular level.

TABLE OF CONTENTS

TABLE OF FIGURES

TABLE OF TABLES

CHAPTER 1

INTRODUCTION

Classical catalytic surface kinetics are fundamentally limited by the thermodynamic interactions between a reacting specie and a catalyst. A specie which is sufficiently relaxed on a surface will be stabilized via strong binding energy between the reactant and the surface. This is what allows this specie to react. Unfortunately, it often follows that as a reactant is more strongly stabilized, its product is as well. This leads to product-surface inhibition which deactivates the catalyst surface. Conversely, the weaker the reactant-surface interaction is, the weaker the product is bound to the surface. This weak binding results in poor catalyst utilization. This phenomena whereby the kinetic activity scales with a thermodynamic binding descriptor is referred to as the linear scaling relations. Entire fields of study have been born to overcome or subvert the limitations imposed by this thermodynamic-kinetic relationship including alloyed catalysts, single atom catalysis, and reaction dynamics.

Reaction dynamics is an approach to reactor operation where one, traditionally static, process variable is made to be transient. The field of reaction dynamics is riddled with creative modes of oscillation to probe the effects of these applied transient waveforms on reaction chemistries. Chapter 2 investigates many of these different modes and provides a fundamental basis for the effect each has on a catalyst surface. This chapter also justifies narrowing down these many different approaches to just two prime candidates: pressure and temperature.

Traditional industrial reactor designs benefit from economies of scale, making then bulky and are not equipped for fast temperature oscillations. Chapter 3 outlines the design considerations and our iterative design process for developing a microreactor which can do just that. Early attempts

in the literature at operating reactors dynamically were often limited by the inability to heat and cool truly at the catalytic time scale (<10 milliseconds). As technology has developed since the early 2000's, increasingly smaller microreactors have become possible. This is important because the ability of a reactor to change temperatures quickly is directly dependent on its thermal mass. This takes us to Chapter 4, where we focused on fabricating a wall-coated capillary microreactor capable of these ultrafast thermal oscillations.

As we began to better understand how to develop these dynamic microreactors, we also began to better understand the transients of the reacting system at a mechanistic level. Chapter 5 describes the experimental and theoretical studies we performed to better understand and characterize our system. These experiments provided insight into the surface phenomena of our catalyst under dynamic operation and helped us to understand that the history of the catalyst plays a significant role in its activity. This all comes together in Chapter 6 where we introduce the theory, microkinetics, and results for dynamic operation.

CHAPTER 2

A BACKGROUND IN DYNAMICALLY CONTROLLED REACTION ENGINEERING

2.1 INTRODUCTION

The field of heterogeneous catalysis has undergone a series of major transformations as our understanding of the physical world has evolved to describe the molecular interactions as *thermostatic* (equilibrium), to *thermodynamic* (dynamic equilibrium), and now finally truly *dynamic* (non-equilibrated) catalysis. *Dynamic catalysis*—the ability of a material to accelerate a reaction under forced periodic input perturbations—promises to fundamentally shift the field of surface catalysis. The concept merges classical catalytic surface kinetics with periodic oscillatory control-theory to unlock a new operating window whereby catalytic activity beyond classically perceived thermodynamic limitations is achievable.

In recent years, this concept of dynamic catalysis has garnered an increasing level of attention from researchers aiming to overcome thermodynamic barriers limiting catalytic turnover rates. The importance has been underscored by Dauenhauer[1,2], Stolte[3], and Silveston.[4–7] While we understand catalysts to be inherently dynamic materials that change continuously over the duration of a chemical reaction, we have demonstrated an otherwise humbling inability to describe their transient nature and predict their behaviour *a priori*. Haber and Bosch screened thousands of materials in pursuit of an ammonia synthesis catalyst leading to their Nobel prizes in 1918 and 1931, respectively;[8] it was not for nearly another century that Ertl would receive a Nobel for being able to describe the mechanism.[9] Only recently with the onset of supercomputing, high throughput

thermodynamic modelling, and machine learning has the predictive nature of static catalytic performance begun to be possible.[10–15]

Notably, both the century-old screening and modern computational approach rely on a single underlying concept: a reaction must occur in a well-controlled, steady, static environment. By operating at such conditions, however, equilibrated surface conditions lead to restrictions on catalytic turnover, often limited by insurmountable constraints such as those described by the linear scaling relationships or volcano plots, despite having global thermodynamically favourable driving forces (e.g. ammonia synthesis; C-H activation). This review aims to lay the historical backdrop for reaction engineering approaches that attempt to dynamically tune the surface toward the eventual implementation of truly dynamic catalysis. As outlined in Figure 1, it will first consider the evolution in our understanding of naturally occurring dynamic reaction oscillations before moving to our ability to achieve stimulated catalytic response through a multitude of engineered forced oscillations.

2.2 THEORETICAL APPROACHES TO FORCED OSCILLATIONS

The history and evolution of heterogeneous catalysis has been extensively chronicled and reviewed by Robertson[16], Lindström and Pettersson[17], and Wisniak[18], among others. The field was founded upon thermodynamic equilibrium relationships pioneered in the mid-1800's by van't Hoff, Ostwald, and Arrhenius. Our mechanistic understanding became a science with the publication of the first true text on chemical kinetics, *Etudes de dynamique chimique* by van't Hoff in 1884.[19] A rapid period of growth made the first major innovation that is foundational today: chemical reactions are dynamically equilibrated (later extended to surface by Langmuir[20]). This was in contrast to the phenomenological kinetics described by Harcourt and Esson of the same era who

described the observable kinetics through differential equations and the law of mass action.[21] The two concepts were reconciled in the unifying theory of Marcelin that introduced standard Gibbs energy to describe a reaction along a potential energy surface. This perspective is combined with several key advances in the 20th century, namely a) statistical and transition state theories of Eyring, b) equilibrated surface kinetics by Langmuir and Hinshelwood, and later c) advanced thermodynamic calculations through density functional theory (DFT). Collectively, this has led us to our current ability to describe in great detail the mechanism, energetics, and kinetics for elementary surface catalysed reactions from first principles.

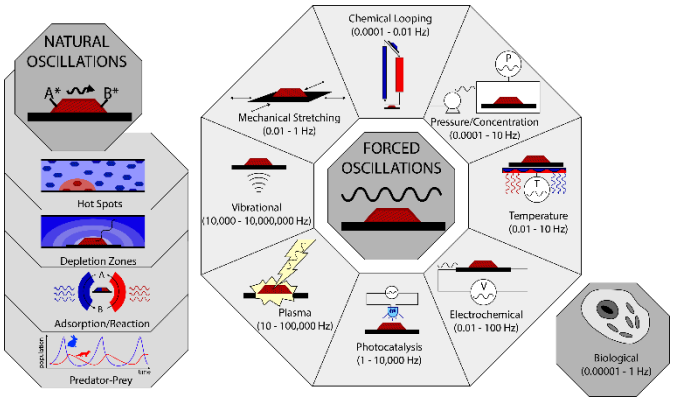

Figure 2-1: Schematic overview of naturally occurring oscillations present in catalytic reacting systems and modes for externally engineered forced catalytic oscillations that periodically perturb the reacting surface

Notably, however, the above-described progression still relies on approximations to dampen dynamical effects resulting from fast equilibrium steps followed by either slow kinetic steps that require overcoming energetic barriers, reaction transients, or spatial gradients. While approximations such as pseudo-steady state (PSS) or most abundant surface intermediate (MASI) are effectively used to reconcile the stiff sets of differential equations that result from rapidly

equilibrated surface phenomena with transient reaction or transport steps, these approaches rely heavily on the existence of static external forces (isothermal, isobaric, potentiostatic, etc.). To that end, extreme efforts are often made to remove inhomogeneity in the system such as hot spots or concentration gradients due to channelling or feed disturbances. Despite these macroscopic efforts, natural microscopic perturbations are inevitable, as described in the Nobel lecture by Gerhard Ertl, where the surface is shown to experience local oscillations in response to reaction events.[22] The question then becomes, what might happen if such micro- or macroscopic perturbations are intentionally imposed upon a surface?

Perhaps the earliest mathematical formulation of externally induced reactor transients for catalytic systems dates back to the 1960's out of Rice University, where Horn and Lin laid out the groundwork conceptualizing the field.[23] They were able to derive iterative and optimization expressions for transient systems, though at the time they did not claim they held any practical applications. At the same time, experiments were explored by other groups that began to study catalytic reactions under dynamic conditions, starting largely through the oscillations of pressure or concentration at externally induced frequencies ranging from tens to ten thousandths of a Hertz, as discussed in the *Pressure/Concentration* section below.

Early studies were typically limited to the bench-scale reactor level which lacked the spatial resolution required to induce rapid surface oscillations, as perturbations would typically be dampened. However, with the advent of microtechnology, improved lasers, and controls, studies performing time dependant experiments through various techniques are becoming more common. Chemical dynamics has been defined differently by scientists over the past hundred and fifty years. According to van't Hoff "[Chemical] dynamics is devoted to the mutual actions of several substances, i.e. to chemical change, affinity, velocity of reaction, and chemical equilibrium".[24]

Ostwald defined it as “the theory of the progress of chemical reactions and the theory of chemical equilibrium”.[25] The most current interpretation considered in the remainder of this review is one in which the surface reaction transiently and periodically changes on the timescale of a elementary surface events (e.g. adsorption, diffusion, reaction), opening the door to macroscopically observed mean field events (turnover frequency) and surface resonance theory.

2.2.1 SABATIERS RULE AND THE VOLCANO PLOT

Catalytic reactions are by their very nature cyclic. In the most simplistic case for a heterogeneous catalysis, this is represented by the periodic cycles of adsorption, surface reaction, and product desorption to regenerate the active site. If any one of these steps is slow---whether due to thermodynamic, kinetic, or transport driving forces---the catalytic turnover will also be slowed. The classical approach for increasing kinetic rates and in turn overcoming activation barriers is achieved by tuning the surface interactions. This can often be done by selecting an active site which stabilizes a transition state, modifying gas-phase pressure, or increasing temperature. While doing so may overcome one barrier, it often inadvertently inhibits a second part of the catalytic cycle. For example, raising temperature may provide enough energy to overcome an activation barrier, but doing so may favour gas phase desorption of reactants, thus depressing the overall kinetics (turnover frequency) by decreasing surface concentrations. This conflicting duality between rate enhancement and inhibition corresponding to the strength of the surface interaction directly gives rise to the multidimensional kinetic optimization function which in its simplest form is linearized as the BEP relations and visualized by way of the volcano plot.[26] This leads catalyst selection to be guided by Sabatier’s rule which suggests that for any given reaction, the optimal catalyst exists at a compromise between two competing surface phenomena.

The concept can be explored through the consideration of a semiempirical derivation of a simple case study, $A \rightarrow B$ where the reaction progresses by serial adsorption to (A^*), first order activated surface reaction ($r = k[A^*]$), and desorption of the product, B. The adsorption equilibrium of A is described as a function of the adsorption energy by the Langmuir isotherm ($K_A = \exp[-\Delta G_{ad}/k_B T]$), and the surface reaction rate constant by an Arrhenius-type relationship ($k = k_0 \exp[-E_a/k_B T]$). As described by the Brønsted-Evans-Polanyi relationship ($E_a = E_a^0 + \gamma_p \Delta H_r$),[27] the activation barrier (E_a) typically scales linearly with the heat of reaction (ΔH_r).[28,29] Combining the two steps, it is clear that increasing surface interactions (i.e. stabilizing surface intermediates/transition states), will certainly favour the adsorption, concentrating the reactants. However, doing so simultaneously increases the energy required for the adsorbed reactant to escape the thermal well, toward the products, hence an increase in activation energy. For this reason, the heat of adsorption of a model compound can typically be taken as a descriptor for catalytic activity, giving rise to linear regions that increase or decrease with the energy—the volcano plot.[27]

Traditionally, Sabatier's rule is used as a guideline in catalyst selection as depicted by a volcano plot, which graphically shows two limiting phenomena as two intersecting lines. The volcano plot practically serves as a predictor of catalytic activity (kinetics) based on a scaling with a thermodynamic descriptor that is readily available (ΔH_{CO}). It is a simple form of mapping activity to a two-dimensional visualization. It often neglects the intrinsic complexity of the multi-step mechanisms and convoluted transport, leading some to criticize it for vastly simplifying reaction mechansisms.[30] To partially address this concern some have adopted n-dimensional volcanos to capture multiple orthogonal descriptors.[31] Notably, however, while the plots are largely

reproducible and show clear trends through computational techniques such as DFT, experimental successes to construct the plot are rare.[32]

In recent years, reviews have focused on understanding the linear scaling relationships, specifically with emphasis on predicting catalytic activity *a priori*[33,34] and overcoming the scaling relationships[35–39]. Chemists and engineers have found creative ways to optimize catalysts at cheaper costs, using alloyed materials that mimic desired single component energetics at the apex of the volcano, often using chemical dopants to functionalize catalyst surfaces and modify its properties.[36] The surface interactions are then further manipulated by creating structures with interesting catalytic interactions by studying metal-organic complexes, unique surface faceting and single atom catalyst structures. Importantly, however, these strategies are still found fundamentally bound by these thermodynamic relations and Sabatier's rule. Recently, we have transitioned into a generation of materials and reactor designs attempting to identify performance beyond this theoretical performance limit.

Pérez-Ramírez and López have compiled a wealth of the most critical ideas and methods for breaking the scaling relations.[36] More narrowly, Kalz and coworkers put together an excellent review describing recent efforts in understanding naturally occurring dynamic behaviour of heterogeneous catalysts.[40] These approaches have been studied to circumvent these kinetic material limitations, including the use of single atom catalysis[35,41], engineering alloyed metal surfaces[42], and process dynamics. Each technique has been studied and built up as they are understood to surpass these catalytic barriers.

2.2.2 NATURAL OSCILLATIONS

As our understanding of the active site evolved into dynamical considerations, the presence of naturally occurring oscillatory behaviour could be observed. Both seminal and recent works demonstrate the natural tendencies of catalytic systems to experience periodic oscillations.

In Gerhard Ertl's Nobel lecture,[43] he cited the tendency in nature for the population of hares and lynx to directly respond to one another per the Lotka-Volterra model.[44,45] This theory models the time dependent predator-prey interactions per the simple equation set:

$$\frac{dX}{dt} = \alpha_1 X - \alpha_2 XY$$

$$\frac{dY}{dt} = \beta_1 XY - \beta_2 Y$$

The theory extends to catalysis. To this end, Ertl identifies the oxidation of carbon monoxide over crystalline platinum catalysts, where "*X*" and "*Y*" correspond to each chemical surface species (O_2 and CO) competing for binding sites. Specifically, Ertl references the way that each species is able to interact with the catalyst surface while minimizing energy. The periodic saturation and cleaning of the surface is what leads to the observable harmonic rate of carbon dioxide production. This natural oscillation and mathematical solution extends to a multitude of naturally occurring phenomena across varied timescales. Some reactions include CO oxidation over noble metals,[46,47] NO reduction over noble metals,[48] and hydrogenation reactions over various metal catalysts,[49,50] with many specific reactions summarized by Imbihl and Ertl[51] as well as Schwartz and Schmidt.[52]

Perhaps among the most well-studied of these self-oscillating experiments is carbon monoxide oxidation over noble catalysts. When oxygen at sufficient pressures is present in the reaction over palladium, platinum, or even sometimes nickel, the pure metal lattice incorporates the oxygen into its lattice structure to become more thermodynamically stable. These two structurally and energetically different materials transition between one another during the course of the reaction, all-together changing the reaction mechanism between a Langmuir-Hinshelwood mechanism on the pure metal and a Mars-Van Krevelen mechanism on the oxide surface.[53]

In the case of the partial oxidation of methane over a NiO/SiO_2 catalyst, redox reactions lead to local temperature oscillations as induced by these endo- and exothermic reactions. The frequency of these oscillations are proportional to the reaction temperature itself, with higher reaction temperatures seemingly leading to higher frequencies and vice versa. These reactions initially occur at the top of the catalyst bed, where the reactants first come in contact with the material. These oscillating hot spots propagate downwards in the bed leading to somewhat discrete layers of catalyst which are "hot" at any given time.[54]

Additionally, some natural oscillations may be due to micro-depletion zones within the vicinity of a catalytically active site. In a recent computational Monte Carlo study, kinetic and diffusive phenomena are coupled to observe the effect of a reaction on the microenvironment about a catalyst site. As the ability of products to diffuse away from the active site diminishes due to increased number density of local particles, there is a trapping effect, meaning that products stay more local and reactants struggle to interact with the catalyst. When the magnitude of the kinetic rate is substantially larger than the diffusive rate, strong oscillations occur. This is because product molecules are able to diffuse away from the active site in batches. Reaction occurs instantaneously upon product removal, leading to a back and forth motion in the product/reactant equilibrium.[55]

Interestingly, single reaction events on catalytic surfaces have been directly observed using operando techniques imaged at <80 ms.[56] Across all the naturally observable oscillations, however, time scales for the oscillation remain orders of magnitude slower (10-10,000 seconds) than that of catalytic turnover phenomena (<1 second). While it is possible there are secondary, much faster vibrations involved (e.g. bond vibrations, steric rearrangements, etc.), resonance between the two is not apparent.

2.2.3 FORCED OSCILLATIONS

Forced oscillations, as described here, constitute an approach to externally apply periodic input perturbations to a reacting system to induce an enhancement of some form. While unique theories for the mechanism of rate enhancement are proposed for each technique discussed below, the mechanism by which rate enhancements can be expected upon periodic external stimuli can be generalized as one of three approaches:

1. Periodic surface loading and cleaning
2. Overcoming activation barriers
3. Operation in multiple thermodynamic regimes

In the first scenario, external pulses cause the surface to experience a different environment (temperature, concentration, voltage, etc.), which may cause it to be regenerated or pre-loaded with a desired reactant. The second case considers high surface coverage of a reaction intermediate which can progress to the products if sufficient energy is provided to overcome an activation barrier. The final case considers a cyclic process where one stage is thermodynamically favoured under a particular set of conditions and the second stage of the cycle is favoured under a distinct

alternate set of conditions; switching between the two (e.g. looping) will allow the surface to turnover.

Process dynamics classically involves using feedback loops to modulate a controllable variable, such as temperature or pressure, among others. By changing a variable, the surface energy or local concentration is changed, which in turn effects the real time kinetics. As such, a standard catalytic volcano plot (which compares kinetics to energetics) can be further interpreted to estimate the corresponding reaction turnover. Ardagh et al. determined that if a surface interaction energy can be periodically oscillated in the absence of any other competing phenomena (e.g. transport), a corresponding rate enhancement due to energetic oscillations is expected, and furthermore the location of the optimal performance should approach the natural resonance (turnover rate) of the catalysed target reaction. This optimized rate could be magnitudes higher than the static counterpart. This concept is referred to as *catalytic resonance theory*.[1] Ardagh and coworkers further identify a new interpretation of the static volcano plot to account for this resonance phenomena; they show it to be a powerful tool for making predictions about dynamic reactions using *forced oscillations*. Notably, even though the net energy input between static and dynamic operation is identical, increased production is predicted due to the theorized rate enhancements.

There are a multitude of approaches that have been used to modulate inputs in chemical reactions at an expansive range of frequencies. In this review, we will assess some of these techniques, their attainable time scales, and resulting rate enhancements.

Catalytic resonance theory combined with foundational knowledge of natural surface oscillations in kinetic cycles present an exciting new lens through which we can interpret modern dynamic catalysis. By understanding, matching, and amplifying natural surface resonances, it appears to be possible to achieve enhanced catalytic reaction rates. While *catalytic resonance theory* presents a

sound theoretical basis for achieving forced dynamic catalysis, its translation beyond the theoretical landscape has not yet been realized. Notably, reaction dynamics have been applied extensively in experimentally reacting systems: temperature, light, over potential, vibrations, etcetera—many of which observe enhancements. Each of these technologies, however, introduce distinct oscillations which may not resonate with intrinsic kinetic phenomena**.** In Figure 7, the vertical axis represents the dimensionless frequency which is defined as the timescale for the externally forced oscillation ($\tau_{ext} = f_{ext}^{-1}$) divided by the intrinsic kinetic timescale ($\tau_{rxn} = TOF^{-1}$). Resonance between the two is achieved when the external oscillation frequency is identical to the observed response frequency (i.e. $TOF/f_{ext} = 1$). Harmonics occur at integer values, but are beyond the scope of this review. While no literature references to this ratio are known for catalytic resonance, in fluid mechanics the rate of an external pressure perturbation on the dampening fluid velocity is described by the Hodgson number ($Ho = fV\Delta P/\bar{q}\bar{p}$), where f is the frequency, V is the system volume, ΔP is the pressure drop, p is the average static pressure, and q is the average volumetric flowrate.[57] Similarly, in acoustics, the ratio of natural resonance of a material to an externally applied excitation frequency is used in frequency response analyses to identify peak resonance and dampening.[58] The figure summarizes that only a few technologies induce oscillations that resonate with natural kinetic frequencies on the order of the observed reactions (grey box). Question of whether those oscillations are dampened out or truly felt by the surface is even further suspect, especially at higher frequencies. Lower frequencies likely achieve time-averaged responses consistent with the weighted average of the static cases as oscillations occur much slower than the kinetic steps. It is important to note that while resonance may not exist under these situations, several cases described in the forced oscillations section below do still merit

further consideration for overcoming other limitations (e.g. periodic surface regeneration). Each case will be evaluated individually in the subsequent sections.

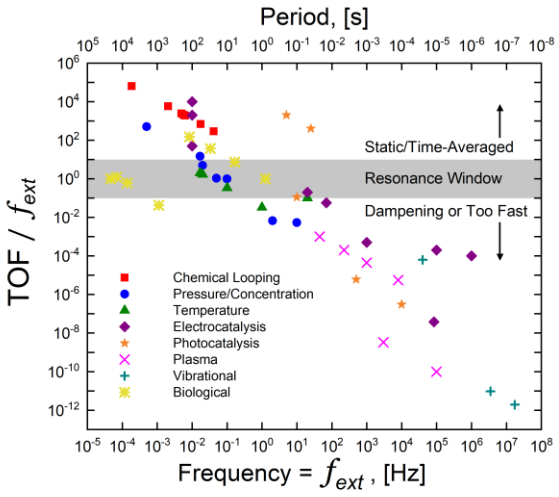

Figure 2-2: Typical oscillation ranges found in literature for different pulsing techniques as compared to the resonant frequency for the reaction. For full list of literature citations see †.

2.2.4 WAVEFORMS

Process dynamics are externally controlled by applying waveforms that generally fall into one of four categories: square/pulse, sinusoidal, sawtooth, or triangle. As described in Figure 8, each waveform consists of an amplitude, frequency, and duty. The amplitude describes the magnitude of the signal, the frequency describes how many full wave cycles are completed per second, and the duty cycle describes how often the signal is "on" relative to the total period, and is most relevant to pulse/square wave functions.

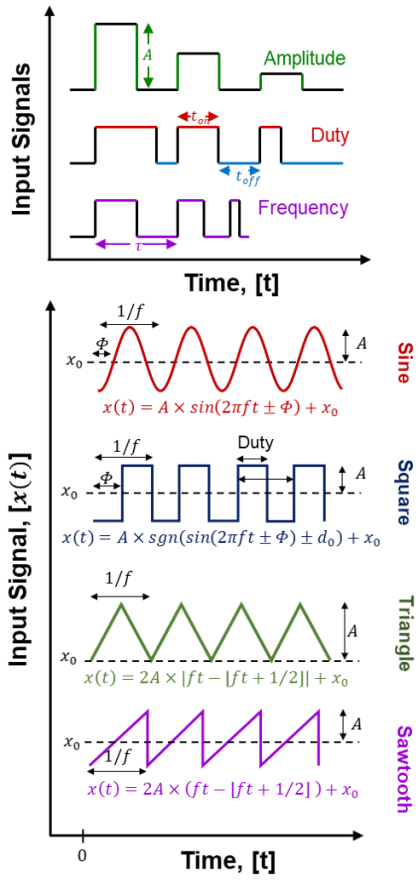

Figure 2-3: (TOP) The tuneable variables for pulse waveforms including amplitude, duty, and frequency (BOTTOM) Graphical interpretations input waveforms and their respective equations as a function of time, t, amplitude, A, frequency, f, phase shift, ϕ, offset, x_0, and duty, d_0.

Generally, amplitude is used to define net magnitude of the perturbation. For example, in periodic temperature oscillations, amplitude may correspond to the temperature swing, ΔT. The specific duty, or relative time spent in each phenomenological regime, is adjusted to achieve the correct time in the excited/base states. For example, the part of the cycle corresponding to the high input may be overcoming a rate limiting kinetic steps ($\tau_{on} = 1 \,/\, k_{rxn}$), while the low input may be necessary for the transport steps of the elementary reactions ($\tau_{off} = 1 \,/\, k_{ads}P$),[59] making the duty cycle with optimal resonance, $Duty = \tau_{on}/(\tau_{on} + \tau_{off}) = k_{ads}P \,/\, (k_{ads}P + k_{rxn})$. Similarly,

the frequency ($f = 1/(\tau_{ON} + \tau_{OFF})$), should be made to match the natural resonance, or turnover, of the reaction itself. Optimizing each of these parameters means having precise knowledge of the reaction kinetics and thermodynamics.

For rapid oscillations rate enhancements, square waves are best suited as they present with the sharpest transition between two distinct regimes; the slower transition experienced in other waveforms dampens this switch. It is important to note, however, that some catalytic applications have benefited from controlled ramping. Sawtooth or triangle waves, for example, are used in intermittent temperature programmed desorption (ITPD)[60] or when clean square steps are not achievable due to dampening. Temperature programmed reactions (TPR) are commonly used to characterize weak and strong binding to material surfaces.[61] This technique is, by its very definition, dynamic. Additionally, sawtooth waveforms are commonly used in battery cycle testing, in charge discharge cycles or cyclic voltammetry to probe electrocatalytic mechanisms.

These waveforms can be mathematically described to represent a controllable system variable x, that is periodically perturbed as a function of time, giving rise to the system input function $x(t)$, as represented in Figure 2-3.

Increasing the amplitude increases the intensity of the oscillation by extending the bounds (e.g. changing your maximum/minimum temperature, pressure, etc.). Increasing the frequency involves increasing the number of oscillations per unit time. Shifting the waveform in time involves either offsetting the reference time conditions for an arbitrary wave by a phase shift, ϕ, which shifts the wave left or right at time zero—this becomes relevant when relating an induced frequency to a measure periodic response. Similarly, the output parameter can be shifted in parameter space by an offset of x_0. Duty is the parameter that describes the relative amount of time the wave is above a certain threshold (i.e. "on" state), and is characteristic of a square (pulsed) waveform. Duty can

be modulated with the relationship $d_0 = -\cos(\pi \times Duty)$ in the respective equation and is some number between 0 and 1. Decreasing the duty means decreasing the relative time spent at the upper limit; as the duty approaches zero, the square wave approaches a periodic pulse input.

In static systems, process inputs are simply represented as scalar values representing a steady and spatially constant parameter (e.g. temperature is 300 K or pressure is 100 bar). Because parameters are constantly changing during dynamic reactions, one value would often leave the system underspecified. Parameterization thus requires specification of parameters such as the amplitude, duty, and frequency or period for dynamic systems. This leaves the challenge of comparing static to dynamic systems side-by-side. To do this end, dynamic variables (input parameters) are commonly reported as *time averaged values*.

$$\bar{x} = f \int_0^{1/f} x(t)dt$$

It is important to note that this time-averaging can also be performed on the response ($\bar{y}$).

$$\bar{y} = f \int_0^{1/f} y(t)\, dt$$

In the case where the time-averaged response is identical to the weighted average of the static responses, no kinetic resonance or rate enhancement is observed. For example, for a square wave, the time averaged response would be the time-weighted response of the two static systems corresponding to the "on" and "off" states:

$$\bar{y}_{sq} = \frac{\tau_{ON} \times y_{ON} + \tau_{OFF} \times y_{OFF}}{\tau_{ON} + \tau_{OFF}}$$

In kinetic resonance theory, a corresponding kinetic response specifically deviated from the time-averaged response to the static stimuli. This is owing to the nonlinear nature of the coupled dynamic equations as discussed earlier and the short periods preventing equilibrium of all elementary steps.

It is sometimes beneficial to consider a pulse effectiveness factor.[3] The metric compares the performance (e.g. rate or TOF) at steady state $y(\bar{x})$ to pulsed performance $y(x)$:

$$\eta = \frac{y(x) - y(\bar{x})}{y(\bar{x})}$$

For example, if the output measurement is the turnover frequency, $\eta_{TOF} = \left(TOF_{pulsed} - TOF_{SS}\right) / TOF_{SS}$. Notably, this effectiveness factor can be calculated on the basis of TOF, conversion, yield, or effluent concentration, underscoring the necessity to explicitly define the basis for calculation.

2.2.5 FREQUENCY RESPONSE

A common technique for assessing rate enhancements due to periodic input perturbation is the frequency response method. This is a mathematically intensive method, which is nicely outlined by Petrovska and colleagues.[62] In brevity, an input variable, $x(t)$, is oscillated at a wide range of frequencies ($\omega = 2\pi f$) and the periodic response, $y(t)$, is observed in the time domain. These perturbations are added to the steady state values of the input (x_s) or output (y_s) as denoted by the subscript "s". A mathematical transformation is then used to interpret the real and imaginary parts

of the frequency domain (e.g. Laplace or Fourier transforms). A frequency that resonates with the characteristic timescale for a physical phenomenon (e.g. TOF or diffusional time constant) will show an elevated response (peak) in this transformed domain.

There are two primary types of frequency response, shown here for a sinusoidal input function: linear,

$$x(t) = x_s + Acos(\omega t) \xrightarrow{t\to\infty} y = y_s + Bcos(\omega t + \phi)$$

and non linear:

$$x(t) = x_s + Acos(\omega t) \xrightarrow{t\to\infty} y = y_s + y_{DC} + B_I \cos(\omega t + \phi_I) + B_{II} \cos(2\omega t + \phi_{II}) + \cdots$$

The output of the linear frequency response is more straightforward and is represented comparably to the input and the output of the nonlinear frequency response is more complex and must be captured by additional terms including the higher order harmonic terms and the "non-periodic" DC term.[62] Linear frequency response is used when the output holds the same shape and frequency of the input and nonlinear frequency response is used for weakly nonlinear systems. It is often useful to transform these functions to the frequency domain such that the response or resonance can be assessed at a particular frequency using Laplace transforms[59],

$$\hat{x}(\omega) = \mathcal{L}\{x(t)\}$$

$$\hat{y}(\omega) = \mathcal{L}\{y(t)\}$$

And the corresponding impedance caused by the kinetic or transport step is,

$$Z = \frac{\hat{x}(f)}{\hat{y}(f)}$$

Similar approaches analyses can be performed in the frequency domain using Fourier transforms. Reversing the transformation back to the time domain leads to a frequency waveform characterized by the Volterra series,[63] for the nonlinearly related case. This is expanded in the form:

$$y(t) = \sum_{n=1}^{\infty} y_{x,n}(t)$$

Physically, these equations mean that if a time dependent parameter is introduced to a system (such as pulsing temperature), then the form and anticipated time-dependent response (such as observed reaction rate), may be mathematically formulated by using some intermediary function, such as the Arrhenius equation coupled with a rate expression that caused some impedance.

Panic et al. performed a study where they compared the experimental and computational results of a frequency response study for ferrocyanide oxidation kinetics while oscillating applied potential and electrode rotation speeds.[64] The study found that using the nonlinear frequency response analysis method was valid for fitting the kinetics of electrochemical reactions. Others have periodically modulated system volume to measure diffusion in microporous materials.[59,65]

2.2.6 THEORETICAL EVOLUTION OF DYNAMIC CATALYSIS

Substantial progress has been made in the computational evaluation of static catalysis, as discussed earlier in this review and by many others.[10,66,67] Similarly, substantial work performed on the dynamics of reactor operation under relatively slow perturbations was performed in the 1960's, as reviewed by Bailey, Amundsen, and Lapidus.[68] Computational approaches are also appropriate to make direct predictions relating applied external perturbations to intrinsic rate enhancements using techniques ranging from first principle quantum simulations to continuum calculations. They may

also allow for more rapid scanning of a multidimensional parameter space (amplitude, frequency, duty, etc.) in the absence of erroneous secondary effects often present in experiments (e.g. mixing, dampening, slow *ex situ* measurements). To date, however, few such studies have been performed to directly assess the effect of such perturbations on the intrinsic catalytic mechanism or rate.

Among the most well established theories for dynamic systems is the Lotka-Volterra model.[44,69] This model, also known as the predator-prey model, was famously related by Ertl[22] to compare the dynamic performance of a catalyst to the periodic population of lynx and hares. This model is detailed above under the "Natural Oscillations" section.

López and Albano performed Monte Carlo simulations to test the effect of periodic pressure oscillation specifically in the case of carbon monoxide oxidation.[70] The simulation was based on a model produced by Ziff, Gulari, and Barshad (ZGB), specifically for monomer-dimer reaction systems. It was assumed that the CO oxidation reaction studied followed a Langmuir-Hinshelwood mechanism. Using this model, the authors were able to test a range of applied amplitudes and frequencies to observe the effect on the production rate of carbon dioxide. The authors determined that by oscillating the pressure of CO to a point near the irreversible poisoning of the catalyst surface, a classical Langmuir-Hinshelwood model under periodic input perturbation predicts optimized surface coverage and a subsequent considerable rate enhancement.

Ardagh et al. developed an analytical CSTR-kinetic model for describing the resonance of a dynamically changing system.[1,2] In their model, they periodically perturbed the binding energy of bound species and calculated the resulting turnover frequencies. They concluded that as the applied frequency approached the inherent frequency (catalytic turnover), massive rate enhancements of 3 to 4 orders of magnitude were observed. This is the first computational work that explicitly identified catalytic resonance theory.

Challenges: The experimentally observed turnover expected under periodic external oscillations is a complex convolution of a multitude of competing and parallel phenomena. These include: transport (heat, mass, fluid), including boundary layers near the catalytic active sites; dynamic adsorption/desorption and surface diffusion; unsteady coverage-dependent surface kinetics; transient thermodynamic barriers/surface energetics integrated with catalytic cycles that experience multiple microenvironments over the period of a turnover. To this end, substantial strides are required in application of dynamic microkinetic surface models, transport reactor-level models, and first principles energetic simulations under non equilibrated surface conditions. Furthermore, multiscale models are required to assess the true performance under dynamic operation.

2.3 EXPERIMENTAL APPROACHES TO FORCED OSCILLATIONS

2.3.1 CHEMICAL LOOPING

Chemical looping is an industrially adopted technology that physically separates two halves of a catalytic cycle into two independently controlled reactors, passing the catalyst back and forth between. It is most commonly used in combustion applications where the oxidizer (air) and reducing stream (fuel) never come in direct contact, but rather a heterogenous catalyst, often metal oxide, is transported (looped) between these two reactors. This term was coined in 1987[71], but the technology has grown substantially since the early 2000's due to efforts to reduce carbon emissions by isolating concentrated CO_2 directly. Reviews of developments in chemical looping technology are written by Moghtaderi[72] and Fang[73].

These reactors currently have many different applications, including chemical looping combustion, gasification reactions, sorbent chemical looping, and chemical looping reforming,[74,72]

all of which focus on carbon capture in different forms with solids residence times around 2 to 3 minutes.[75,76]

More recently, ammonia synthesis has been demonstrated through chemical looping-type systems. This proposed process is a high temperature noncatalytic approach to produce ammonia through the reduction of alumina and subsequent hydrolysis of aluminium nitride. This two-step reactor uses a solar driven thermal heater as well as a hydrolysis reactor to yield ammonia yields of up to 84%.[77] The process, however, suffers from classical thermodynamic barriers by requiring extreme temperatures (nearly 1000 °C[78,79]) to form the nitride.

Challenges: The underlying challenge for chemical looping is the timescale associated with physically transporting a catalyst or switching the reaction environment. Ultrafast chemical looping (<1 s cycles) of just the temperature or concentration would approach the subsequent temperature or concentration oscillation approaches. Even still, the potential benefits would have to outweigh the extreme energy penalties incurred by switching the large thermal masses. Because temperature and pressure swings are so severe across the dual reactor chemical looping systems, using and stabilizing monodispersed catalysts at the nanoscale is also a substantial challenge.[80]

2.3.2 PRESSURE/CONCENTRATION PULSING

Among the first to rigorously study the effect of concentration input transients on catalytic systems were Zhou, Gulari, and Herz who laid the groundwork for this field in the late 70's. Automobile companies such as Toyota and GE were large leaders in the beginning of this research, also in the late-70's to mid-80's.[5] This work had substantial implications to the automotive industry, particularly with transients observed by the three-way catalysts in catalytic converters. At the time,

certain vehicles were achieving naturally oscillating behaviour at a frequency of about 1 Hz.[81] Specifically, the enhancement was attributed to dynamic oscillations in composition, inlet flow rate, and temperature of the reactor feed apparent in automotive operating conditions. There have since been many subsequent studies to test if there is a way to exploit this phenomenon to optimize their activity.

Generally, the controlled input oscillation was achieved by using automated electronic switching valves that switches inlet compositions or pressures at a given rate between two or more feed streams. This is used to control the input which is closely monitored using pressure gauges. This technique, in practice, tends to reach oscillation frequencies in the rage of 0.0001 Hz[82] to 10 Hz[83,84]. The nature of the rate enhancement associated with concentration/pressure pulsing can be found in detail in Silveston's work for the case of carbon monoxide oxidation.[81] To summarize, pressure modulation is proposed to be beneficial for a number of reasons: 1) switching reactant feed streams between pure species allows more fine control of the catalyst surface coverage. In the case of CO oxidation over a precious metal catalysts, CO typically dominates the surface. By allowing only one specie to bind at a time, the composition of each reactant is balanced. 2) Composition modulation has mixing effects of the surface of the catalyst such that the spatial distribution of reactants is ideal for reaction. 3) Pressure modulation can help overcome transport limitations, especially in porous or strongly binding systems which are typically strongly mass transfer limited.[6] Notably, none of these theories directly link the external oscillation to the turnover frequency (resonance) of a particular elementary surface step.

Zhou and colleagues studied carbon monoxide oxidation over a Pd/Al_2O_3 catalyst.[84] They adjusted the concentration of the reactants by switching between a carbon monoxide stream and an oxygen stream, both of which were diluted in nitrogen. They were able to cycle between frequencies of

0.0067 Hz to 0.05 Hz and found that the rate enhancement is up to 44 times higher than respective steady rates. Specifically, for this reaction, the authors found that a duty of 0.3 and cycle time of 20s lead to this large (44 times) rate enhancement. This was attributed to the ability to achieve optimal surface coverages of oxygen on the palladium catalyst.

Oscillating reactant feed concentration consequently leads to catalyst surface changes. This is evident in the work by Hegedus et al. where they did just that.[85] They altered the reaction from reducing to oxidizing for a feed stream of NO, CO, and O_2 (which are typical components for the exhaust from an automobile) at 505°C over an alumina supported platinum catalyst. Further comparing surface specie concentrations at different oscillation rates, the authors found CO is inhibitive at frequencies slower than 1s. At frequencies faster than 1s the time averaged conversion of both CO and NO species increased. Notably, this is the only study reviewed here that directly resolved the transient surface concentration.

In the reduction of nickel oxide, Sohn and Aboukheshem studied the effect of oscillating the pressure of hydrogen gas to regenerate the catalyst at frequencies ranging from 0 to 20 Hz.[86] For this batch type pressure fluctuation reaction, the reduction went to completion in significantly less time when oscillated versus when it is left to steady state. The authors justified this observation by describing the increase in pressure as causing a corresponding increase in the ability of reactant gas to transfer through the porous NiO solid. The authors also note that the effect of pulsing is more obvious towards the end of the reaction than it is towards the beginning. This is explained again as mass transfer is enhanced through periodic forcing which is more relevant to reduce the material in the smaller pores which are the last to be reduced.

Special Case - Sonochemistry: A special consideration of pressure oscillation is sonochemistry.[87] Operating at frequencies between 20kHz to 2MHz, this method exploits cavitation effects that lead

to rapid localized pressure spikes. While such an effect can be convoluted with induced mixing and locally high temperatures which in turn form reactive radical groups, the resulting potential for elevated conversion due to periodic pressure pulses is nonetheless noted and of interest.[6] Due to the highly energetic nature of this technique, sonochemistry is commonly used in degradation reactions[88,89], particularly in wastewater treatment. The cavitation bubble is so energetic that it can split water into radical groups which attack and decompose many different types of pollutants.[90]

Challenges: Specific challenges facing pressure/concentration oscillation are primarily centered about achieving forced local perturbations at the catalytically active site that are not dampened out by competing phenomena (mixing, gas phase diffusion, intraparticle diffusion). For example, while pore diffusion is sufficiently fast relative to the perturbation at low frequency, high amplitude/frequency oscillations may be dampened out by relatively slow pore diffusion. Second, the resulting system should also maintain desirable sharp steps in the gas phase switching (minimize axial dispersion), especially in multiscale regions (boundary layers, pore diffusion, packed beds). Even neglecting mass transfer, induced pressure changes >100 Hz approaches the limit due to the speed of sound (e.g. ~343 m/s through air)—with the exception of local generation as in cavitation. Finally, the ability to describe and account for secondary thermal effects resulting from endothermic/exothermic sorption steps and surface reactions remains understudied. The presence of such effects may convolute the interpretation of rate enhancements, though does not negate the possibility of superior catalytic performance upon forced perturbation.

2.3.3 TEMPERATURE OSCILLATIONS

Dynamic temperature control in reacting systems was studied in the early 2000's by J.J. Brandner and P.L. Silveston. They used their existing backgrounds in microtechnology and pressure oscillations, respectively, to demonstrate the effect of thermal applications in reacting systems.

van't Hoff and Arrhenius demonstrated how the thermodynamic and kinetic rate parameters exhibit an exponential dependence on temperature, later attributed to the activation energy to overcome some transition state energetics. A forced oscillation on temperature, however, causes a perturbation to the elementary process steps which is compounded in multi-step mechanisms. The mathematical propagation of this forced thermal oscillation into the non-linear set of differential equations already exhibiting natural oscillations has not yet been demonstrated from first principle theory or direct experimentation.

The ability to study thermal oscillations on kinetically relevant timescales (>1 Hz) only became a possibility with the advent of microreactor technologies where characteristic heat transfer length scales <10 μm could lead to ultrafast heat transfer. Achieving oscillation frequencies at a magnitude of interest is limited by the heating rate ($\dot{Q}$) of the thermal mass as described by[91] $\dot{Q} = mc_p\Delta T/\Delta t$, where m is the thermal mass being heated with a heat capacity of c_p and temperature swing of ΔT over a time period of Δt.

Evidently, if a large change in temperature is desired in a short amount of time, a small thermal mass is necessary. Even so, thermal oscillations have been shown at a wide range of frequencies over the past 20 years, ranging from 0.01[91] to 10's[3] of oscillations per second.

Oscillation temperature is often controlled by using high power cartridge heaters in microreactors with a constant, thermally bound heat sink or by using direct Joule heating of a metal heating

component. The small length scales allow very rapid heat transfer through system to local catalyst reaction sites.

Jensen and colleagues designed a microsystem with an integrated heater deposited inside oscillated at frequencies between 0.002 Hz to 2.5 Hz.[92] In their system they oscillated the temperature of the catalyst bed at amplitudes between 5°C to 20°C about an offset of 160 °C. They consistently found that for carbon monoxide oxidation over an alumina supported platinum catalyst, a thermal oscillation rate of 1 Hz lead to time averaged rates up to 70% higher than the quasi steady reaction rates. It is important to note that while the enhancement was observed, it was not mathematically related to resonance or intrinsic kinetic barriers. The authors describe that at low frequencies, the reaction rate converges to the individual time averaged response for each temperature regime ($x(t) = T(t),\ y(t) = \bar{y}$), whereas at high frequencies—faster than the time constants characteristic of the reaction—the rate is that of the averaged temperature of the applied signal ($x(T) = \bar{x} = \bar{T},\ y(t) = y(\bar{T})$). It is postulated by the authors that the enhancement comes from unique phenomena at an applied frequencies between these two extremes.

Another study was performed by Brandner et al. who employed a continuous flow through microreactor with cartridge heaters to control the reaction temperature.[91] Their study showed that when oscillating temperature between 50 °C and 150 °C, their oscillating system notably outperformed the reactor operating at steady state conditions at 100 °C, and they claimed that a steady state temperature somewhere between 100 °C and 150 °C would be necessary to match the oscillatory production. Notably, the kinetics are activated with an exponential dependence on temperature, so it is expected that steady conversions would require an elevated temperature to match elevated conversions achieved for brief operation at 150 °C. Again, resonance theory would

apply if the observed rates under dynamic oscillations exceeded even those observed at 150 °C, which was not demonstrated in this study.

Stolte and colleagues designed their own custom microreactor capable of oscillating temperature from 3.3 Hz to 20 Hz for the reaction of carbon monoxide oxidation over platinum.[3] They altered their base temperatures from 150 °C to 210 °C with amplitudes reported in mJ of energy input, which for various experiments ranged from 50 to 300 mJ. They reported a rate enhancement four times greater when normalized to the steady state value at the corresponding conditions as they increased their pulse frequency (or decreased cycle period). Slower cycle times were performed by Luther et al. who observed enhanced conversions and additionally have completed microkinetic computational work to model the surface coverages and reaction rates of such systems.[93]

Challenges: Several challenges exist to demonstrate thermally induced dynamic kinetic resonance in catalytic systems. From a theoretical perspective, the complex coupled kinetic and dynamic inputs must be resolved for the multistep mechanism to establish a basis for rate enhancement. This must be then coupled with continuum modelling to resolve transient hotspots due to reaction/sorption enthalpy coupled with external heating/cooling. From an experimental perspective, materials need to be developed to withstand the rigor from thermally annealing on the order of 0.1 -100 Hz, accounting for mechanical stresses, thermal expansion, and catalyst sintering effects. Careful characterization is also required to characterize the exact temperature of the active site, which has proven challenging to resolve at the stated frequencies and length scales. Similarly, the corresponding analytical tools must be integrated to not only transiently resolve reactor effluents, but also resolve the transient surface composition.

2.3.4 PLASMA

Plasma is a highly energetic state of matter made up of charged particles formed upon ionizing gases. It can take a number of different forms, based on its excitation mode, including microwaves, pulsed discharge, and laser produced. A review on plasma activated heterogeneous catalysis was written by Mehta et al.[94] with a review on the surface-plasma interactions at the nanoscale was written by Neyts et al.[95] The oscillation range in which it has been shown to operate is on the order of 10's[96] to 100,000's[97] of pulses per second.

These types of systems have slight variations in designs, but usually involve a plasma chamber, with their respective induction source connected, and catalyst inside. Induction sources can be microwave excitors with ferroelectric materials[98], a power supply capable of varying the voltage using a charging system[99], or nanosecond pulsed power sources controlled by a waveform generator[97], for example. Reactants pass through this chamber and in line analysis is used for characterization.

A number of possible theories exist for why pulsed plasma leads to rate enhancements. Rousseau et al. report that for their reaction of acetylene oxidation, possible reasons for the observed rate and selectivity enhancement included enhanced flux of the highly reactive, short lived species (e.g. photons, charged particles) or simply thermal effects.[98]

In this study, not only did Rousseau et al. study the effect of frequency on oxidation enhancement, but they observed how it affected the selectivity of the reaction in total. In their experiment, they tested if mixing their alumina catalyst in a ferroelectric $BaTiO_3$ bed or downstream of it had any effect. The ferroelectric material is used to improve reactor energy efficiency as well as enhance the oxidative plasma properties and promotes more desirable reaction pathways. There was a substantial increase in selectivity for this process as the frequency increased to >100 Hz.

Challenges: A recent roadmap has identified that, "the fundamental mechanisms of plasma-catalyst interactions are not yet fully understood. It is a complex environment, as the catalyst may affect the plasma behaviour, and vice versa, the plasma also affects the catalyst and catalysis mechanisms."[100] Furthermore, the enhancement effect is observed at frequencies many orders of magnitude above the typical catalytic TOFs, so it is unclear what if any benefit is observed due to resonance with the physical surface reaction phenomena. Finally, the physical characteristics of the surface have not been transiently resolved over the period of oscillation to resolve surface transients or perturbation dampening, making mechanism resolution challenging.

2.3.5 PHOTOCATALYSIS (LED/LASERS)

Photocatalysts are able to absorb incident light and use the energy to drive a reaction. Several mechanism are proposed and reviewed by Fujishima et al.[101], Mill and Le Hunte[102], and Fox and Dulay[103]. A common proposed mechanism is that this light is able to raise electrons from valence to conduction band, leaving holes on the catalyst surface. These holes are highly oxidative reaction sites.[104] There are a number of different ways to drive these reactions, including lasers, lamps, and LEDs.

In the case of semiconductive, photoactive materials, proposed mechanisms tend to involve the interaction of induced electrons or "holes" (electron "voids" formed by incident photons) with reductive or oxidative species.[105] These reactive species facilitate the separation of electrons and holes when the incident light has enough energy to overcome the band gap, or the energy needed to eject the electron to the conductive band.

Beyond the steady catalytic turnover, the possibility for periodic surface irradiation offers an exciting avenue to dynamically control the catalysis. An extensive dynamic analysis of the

mechanism for pulsed laser catalysis has also been meticulously derived by Vardi and Shapiro.[106] In it, the authors come to a theory that describes laser induced tunnelling through a potential energy barrier via applied high intensity dynamics.

In the case of the reduction of CO_2 over rhenium-based catalysts through photocatalysis, the reaction actually becomes inhibited after a certain amount of exposure to light. The proposed mechanisms for this deactivation include: one-electron-reduced (OER) species react with other radical species which terminates the reaction (radical-radical combination termination) or undesirable side reactions of the OER species at the elevated electron state may terminate the reaction.[107] The authors propose that by only applying very short pulses of light, this can avoid the undesirable reaction of the higher energetic species.

It was found that for lower photon fluxes, the pulsed operation outperformed the continuous LED set up in the reduction of CO_2 to CO. It is also interesting to note that the pulsed set ups did not fully deactivate, leading the authors to believe that the photo-deactivation of the catalyst has been reduced.

Challenges: Especially in the case of laser photocatalysis, the stability of the catalyst and sintering of nanoparticles is a concern due to the high energetic nature.[108] As with other approaches, relation back to the fundamental phenomena---kinetic, mass or electronic transport---has not yet been validated experimentally. Similarly, transient resolution of surface species or any periodic response variable ($\boldsymbol{y}(\boldsymbol{t})$) have not been measured or theorized.

2.3.6 ELECTROCHEMISTRY

Electrocatalysis uses applied voltage to drive a reaction system and is often measured by observing the resultant flow of electrons, or the current passing through the system. Dynamics in electrochemical systems have been well studied since the late 1950's due to an effort to better develop understandings of electrode processes such as the transport and kinetics occurring at the interface of the electrode and surrounding media.[109]

Fedkiw and coworkers studied the anodic oxidation of methanol under pulsed voltage conditions with frequencies ranging from 0.1Hz to 6Hz and two amplitudes, either 0.58V or 0.78V. They claimed that the limiting portion of this reaction on a platinum catalyst was the build-up of reaction products poisoning the surface.[110] Through their experiments they found that oscillating between a high and low potential, they were able to maintain higher oxidation rates that are not observable under steady conditions. This may have been due to higher applied potentials regenerating the catalyst surface such that the reaction can proceed unobstructed (at the lower applied voltage). In this study, they only tested frequencies between 0.1 to 6 Hz. They noted that a study by Adzic et al.[111] tested a wider frequency range, finding an optimal frequency at 2000 Hz, suggesting that while Fedkiw observed improved rates, they may not have been optimal.

Gopeesingh et al. studied the oxidation of formic acid over a platinum catalyst.[112] Using a reactor with in-line gas chromatograph as well as counter, working, and reference electrodes, they were able to obtain turnover frequencies about 45 times that of steady state at 100 Hz applied frequency. This is attributed to how the activation energy of the faradaic steps in this reaction significantly decreases with applied potential.

Special Case - Electrochemical Impedance Spectroscopy: Electrochemical Impedance Spectroscopy (EIS) is a special category of frequency response that is used to characterize the physical and reaction phenomena by inducing small variations in applied potential at a range of frequencies and monitoring the corresponding response as a current (reaction flux). This technique can be particularly useful in determining kinetic rate constants in various electrochemical mechanisms[113,114] and measuring various physical and structural properties[115]. The impedance of a system is defined as the Laplace transform of the applied function (voltage) divided by the response function (current), where the voltage is applied and the current is measured and descriptive of electrochemical reaction rates.[116,117] The outputs for such a technique are often in the form of Nyquist or Bode plots which directly relate the imaginary to real portions of impedance or phase to the applied frequency, respectively, as described earlier in the *Frequency Response* section. The practicality to dynamic measurements is especially of use with resonance theories. EIS makes it possible to scan a large range of frequencies to identify those that resonate with the rate controlling kinetics or transport. The Butler-Volmer relationship then allows for understanding the electrochemical kinetic effects by fitting kinetic and transport parameters to the observed EIS[117,118]The Butler-Volmer relationship allows for understanding the electrochemical kinetic effects by fitting kinetic and transport parameters to the observed EIS. This equation describes electrical current through an electrode for more complex reactions with multiple electron transfer.[117,118]

Challenges: Multiple reactions, side reactions, transport steps and competing impeding phenomena may be occurring simultaneously in an electrochemical system. Measuring current response and attributing it properly to the correct impeding phenomena is difficult, and extreme

caution should be taken, especially at high frequencies. Furthermore, relation to enhancement from first principles, particularly with kinetic resonance or surface coverages would strongly support future electrochemical approaches, as would the operando ability to resolve the transient surface during forced oscillations.

2.3.7 MECHANICAL (STRETCHING/STRAIN/VIBRATION)

There are a number of modes for mechanically altering the surface structure of a catalyst, including: vibration, piezoelectric induced, reaction induced, and acoustic induced. Each of these methods physically flexes, strains, or otherwise changes the structure of the catalyst for a certain amount of time. This, in turn, leads to altering surface energetics that results in interesting effects on the reaction properties.

Systems range in complexity from beaker atop ultrasonic source[119] to acoustically designed catalytic microreactors controlled by piezoelectric strain inducers. Such a broad technology operates across a very broad frequency range, from 0.01 Hz[120] all the way up to 17.4 MHz[121].

Piezoelectric materials are solid materials (e.g. some crystals and ceramics) that gather charge when some external mechanical stress is applied. Some catalysts such as ZnO nanorods[122] and $(Ba,Sr)TiO_3$ nanowires[123] serve as piezoelectrically active materials with catalytic activity. For piezoelectric catalysts, any induced vibrations lead to a build-up of surface charge due to the piezoelectric effect (deformations in crystal structure lead to an electric charge and vice versa). The accumulation of positive and negative charges induce a dipole, facilitating electrochemical reactions, such as HER and OER reactions to occur on the surface.[122] It is interesting to note that unlike many other techniques that rely on externally induced field change (e.g. T or P), this

technique homogeneously induces the piezoelectric effect in response to a fast external stimuli (e.g. current).

Yukawa et al. has experimentally demonstrated that when regions were doped with palladium and gold on either side of a piezoelectrically active z-$LiNbO_3$ material, production rate of ethene from the dehydration of ethanol was increased 16 times in the presence of applied vibration versus the absence of it.[121] This is especially interesting, because the effect was highly selective towards ethylene, more than doubling the selectivity from 36% to 88%, with little effect on the acetaldehyde pathway.

Oh et al. observed the ability to induce pits on the surface of a perovskite during the exsolution of nickel when reduced by hydrogen.[124] Nickel particles began forming in these pits resulting in strongly bound catalytic sites after the 15 minute reduction cycle. Similar pitting is observed with potential-induced pitting.[125] This development is attributed to the relationship between strain energy and surface free energy which drives exsolution towards the unique structure. Approaches like this can induce structural rearrangements or stresses to a catalytic surface, inducing a response in catalytic activity.

Kim and coworkers have recently demonstrated the ability to deposit a catalyst on a stretchable polymeric surface then apply shear to the support to modify the performance of the catalyst[126,127]. In that study, they propose that defects are introduced upon stretching which enhances the catalytic performance. Others have demonstrated reversible or periodic stretching of catalyst pellets.[128]

Challenges: As with other techniques, the mechanical stability of a material exposed to constant periodic strain is always a concern. Furthermore, applied strain to surfaces may affect many different physical properties such as thermal conductivity or diffusivities and phenomena such as

the formation, diffusion, and energy of vacant sites or erroneous hot spots. It is difficult to deconvolute these affects from one another to identify the full, complex mechanism, which also lacks physical derivation from first principles.[129] As the field of flexible electronics progress, there is substantial room for advancement toward heterogeneous catalysis that remains to be explored.

2.3.8 BIOREACTORS

It is important to note the presence and importance of natural and forced oscillations in biological systems. Biological oscillations have been studied for decades and have been reviewed by Silveston et al[4] as well as Hess and Boiteux[130]. Typically in these studies, biological systems are observed under oscillating nutrient or oxygen conditions in order to observe their response. Because the species are living and need to adapt to their new environment, forced oscillation frequencies are typically slower, ranging from 10^{-5} to 10^{-3} Hz.

In the case of the nutrient oscillation of glucose for a sample of *Escherichia coli* in a highly controlled reactor vessel, modulation was achieved by using a solenoid valve to switch between two stock solutions at periodic intervals. The oscillations periods tested were between 0 to 6 hours. Because these biological species are living, fast oscillations are not necessary and would result in a dampened mean response. This study observed not only the rate of growth of the cells, but also the change in macromolecular species (proteins, RNA, and DNA) within the cell itself.

It was proposed that the reason there is an optimum in production of these macromolecules is due to the presence of "active" and "inactive" ribosomes which become activated, for example, when there is a shift towards more beneficial nutrients available.[131] These ribosomes are free to activate and deactivate based on the available nutrients. It was found that the response to the high

concentration (or activation) was notably quicker than the response to the low concentration (or deactivation). This would lead to an overall higher rate at higher frequencies of nutrient supply.

Another study tested the effect of aerobic/anaerobic oscillations on fermentation using *Propionibacterium freudenreichii*.[132] In these experiments it was found that as the oscillations continued, the rate of degradation of the propionate species increased from 0.1 $g/L^{-1}\cdot h^{-1}$ to 0.32 $g/L^{-1}\cdot h^{-1}$. It was claimed that this may be due to the increase in cell concentration in the sample. Oxygen is used in these experiments to adjust the metabolic pathways at given times. While cells are able to grow more quickly under oxygen rich conditions for short periods of time, the presence of oxygen will start to inhibit cell growth at longer times due to the inhibition of cytochrome synthesis. Anaerobic conditions are also beneficial for the decomposition of propionate species which inhibit cell growth.

Special Case - Polymerase Chain Reaction (PCR): PCR was invented by Kary Mullis in 1985 as a technique to rapidly multiply DNA through a series of periodic temperature steps. A review by Kricka and Wilding in 2003 outlines the microchip technology and thermocycling.[133] The process typically includes denaturing, annealing, and extending steps. These steps occur at approximately 95°C, 55°C, and 72°C, respectively and are cycled a total of 30 times. PCR cycling originally took hours to complete, but modern microtechnology has been able to reduce that time to under a minute.[134]

Challenges: Biological systems are living organisms that need to evolve or adapt to external changes, leading to long time scales associated with changing conditions. Furthermore, the complexity of the system requires consideration of thousands of unique pathways, through which a standard frequency response may be difficult to prove. Additionally, because these are living

organisms, they thrive in a narrow window of conditions. Oscillation temperature or chemical environment to extreme conditions will lead to inevitable cell death. In short, strong parallels can be made between catalytic reaction networks and biological or metabolic pathways; if mechanisms for enhancement can be mathematically proven in biological systems, it would offer promise for translation to similarly complex catalytic systems.

2.4 CONCLUSIONS

Despite over half a century of dynamic and periodic catalytic reaction theory, resonance theory had only recently emerged as a potential pathway to operate beyond classical coupled thermodynamic/kinetic limitations. To this end, our progress must be examined both on a theoretical and experimental basis.

From the perspective of theory, the groundwork has only recently been laid for how a periodic perturbation to the catalytic microenvionment might cause an amplified response beyond the time averaged steady state. However, a rigorous analytical model has not yet explored the theoretical solution to such a problem. Similarly, the effect of such a switch on the microstates has not been explored on the quantum scale. Finally, real systems experience impedances from a multitude of kinetic and transport steps at the bulk states, through boundary layers, and at the active site—multiscale models have not been explored for resolving the dampening or amplifying effect of such phenomena.

From an experimental perspective, progress has been made to understand reactor dynamics under slow periodic input perturbations, with time averaged rate enhancements being attributed to: periodic surface cleaning that optimize surface coverage, catalyst regeneration, or enhanced mass and thermal transport removing pore diffusion and hot spot limitations, respectively. Experimental

work with microreactors have shown that pulsed energy inputs allow for periods of conversion, attributed to periodic excitation of the surface. However, the vast majority of these techniques are shown to apply enhancements on timescales that do not resonate with the intrinsic kinetics (Figure 7), leading to the conclusion that the enhancement is on the steady state performance, not the intrinsic catalytic turnover mechanism. Due to the fact that some techniques may inherently be too slow (e.g. biological, chemical looping), or too fast (e.g. plasma, vibration), truly resonant dynamic catalysis may never be observed through these techniques and may instead be due to secondary effects (non-linearity of response, the presence of highly unstable and reactive molecules, etc.). Finally, the first experimental evidence of catalytic resonance has just recently been shown by Abdelrahman and co-workers[112] who used an electrochemical system to demonstrate the enhancement. Despite these strides, substantial efforts are required to develop systems to induce external periodic forced oscillations that are sensed at the surface without having been damped by the external environment. Furthermore, the effect on the catalytic site should be examined operando to prove the existence of surface resonance.

Dynamic catalytic reaction engineering offers an exciting new avenue to explore and further push the limits of heterogeneous catalysis. Natural oscillations are known to exist in reacting systems; exploiting and amplifying those oscillations through external engineered forced periodic stimuli is a new approach that has recently shown great promise to overcome classical barriers. Theoretical approaches have hinted at the ability to externally tune surface energetics to oscillate at frequencies that resonate with intrinsic reaction barriers, thus introducing *catalytic resonance theory*. A multitude of experimental approaches have been reviewed for their ability to induce rate enhancements. While each one faces its own challenges, our overarching assessment is that forced periodic oscillations have the potential to induce substantial rate enhancements in catalytic

systems. However, substantial efforts remain to bridge the gap between the theoretical rate enhancements, kinetic resonance, and reaction engineering with the experimentally observed forced oscillation responses. Furthermore, substantial efforts remain to achieve *a priori* prediction of catalytic rate enhancement and predictive operating windows for forced oscillations.

From a fundamental perspective, particular efforts are required to precisely describe rate enhancements from first principles. Analytical dynamical models that describe the active site and stiff equations governing the predator-prey resonance and corresponding enhancements would motivate the drive to resolve reactor models capable of achieving such environments. Multiscale models are required that are able to resolve the continuum scale from the induced perturbation/transport dampening all the way down to the microkinetics of surface coverage without applying mean field assumptions (PSS or MASI).

Experimentally, kinetic resonance theory remains to be demonstrated and related back to the kinetic turnover phenomena. Techniques must be refined to measure rate enhancements, 1) operando at the active site, 2) in the absence of dampening effects, and 3) in the absence of inadvertent thermal or transport effects.

From an applied perspective, creative ideas are needed to translate these micro-engineered techniques to an industrial scale without losing the critical spatiotemporal resolution necessary for pulsed operation. Catalysts and kinetic expressions are designed with static reaction conditions in mind. To further the advancement of the field, catalysts must be synthesized and kinetic expressions derived that are specific to transients.[40] Furthermore, the economics of operating under dynamically pulsed conditions should be explored, particularly when energy must be rapidly applied then removed from the system.

It is our opinion that if these considerations can be made, the dynamic catalysis concepts reviewed here have the potential to radically transform our knowledge of heterogenous catalysis and more broadly, the chemical manufacturing landscape.

CHAPTER 3

DESIGN AND FABRICATION OF A CATALYTIC MICROREACTOR CAPABLE OF MILLISECOND HEATING AND COOLING

3.1 INTRODUCTION

Millisecond heating and cooling of a chemical reactor is something that has become possible since the early 2000's due to the rise of microreactor technology[135,136]. Traditional chemical reactors (i.e. CSTR, PFR, Batch, etc.) are designed for isothermal operation and their large thermal masses make rapid heating and cooling difficult if not impossible. Microreactor design and fabrication has been the core of this thesis and a lot of time was spent designing, fabricating, validating, and iterating on microreactor designs in the pursuit of this project. This thesis necessitates millisecond time scale heating and cooling of our catalyst meaning we were restricted to a small system with a small thermal mass, where temperature change is governed by the transient heat accumulation energy balance:

$$\dot{Q} = m \times c_P \times \frac{\Delta T}{t}$$

Where $\dot{Q}$ is the rate of heat change in J/s, m is the thermal mass of the reactor in kg (the heated region), c_P is the specific heat capacity of the reactor in kJ/kg-°C, ΔT is temperature swing in °C, and t is time in s over which the heating was applied. Traditional heating options such as furnaces, heating cartridges, or heating tape are not able to supply heat quickly enough to our catalyst to be feasible options for the heating rates that we were looking for to apply millisecond temperature

oscillations. For this reason, we opted to use resistive (or Joule) heating applied across a very short length scale. This method of heating treats our reactor walls as a resistor in line with a high power (2000W) power supply with forced external air convection for cooling. Due to this, a reactor geometry with a high surface to volume ratio is desirable[137]. A reactor with a small volume is one with a small thermal mass meaning that heating and cooling can both become faster than it would be for a more massive reactor. A reactor with high surface area has more active sites for reaction, and also more available surface to be convectively cooled. Heating is a more *active* process in that we are applying high energy inputs to the reactor which accumulates in the form of heat. Cooling, on the other hand, is a more *passive* process where the reactor returns to the bulk temperature proportionally to Newton's law of cooling which is similar to the heat accumulation balance described above[138].

$$Q = hA(T(t) - T_{bulk})$$

Where Q is the rate of heat loss, h is the convection coefficient, A is the area across which cooling can occur, T(t) is the temperature of the cooling body at time, t, and T_{bulk} is the temperature of the convection fluid.

Here we develop a reactor test stand capable of fast, high temperature swing oscillations using resistive (or Joule) heating by applying an external waveform in applied voltage across a microreactor.

3.2 MODELING

Before we started fabricating the microreactor, we had to first determine the necessary design considerations to ensure that rapid heating on the time scale of catalytic relevance is possible. Some of these considerations include: heat transfer timescales, power source specifications, and the different effects of the operating variables (i.e. frequency, duty, amplitude, convection) on the system.

3.2.1 LUMPED CAPACITANCE

To determine the reactor dimensions that would allow for sufficient cooling of the system, we performed a lumped capacitance analysis[139]. Lumped capacitance is a method for approximating complex transient heat transfer models assuming spatial uniformity in temperature. This model assumes a Biot number less than 0.1, meaning that the conductive thermal resistance is significantly smaller than the convective thermal resistance of the body.

$$Bi = \frac{hL_c}{k}$$

Where h is the convective heat transfer coefficient between the gas and the reactor surface in W/m^2-K, L_c is the characteristic length scale of heat transfer in m, in this case the wall thickness, and k is the thermal conductivity of the steel reactor in W/m-K. For a stainless steel 316 capillary reactor, the characteristic length scale is 50um, the thermal conductivity, k, is 16.3 W/m-K, meaning that to achieve a Biot number of less than 0.1, the convective cooling coefficient must be less than 3.3E4 W/m^2-K[140]. If the convection rate is too fast, the condition that there must be no thermal gradient within the body would be lost. For reference, expression for convection coefficients for laminar air flow over a cylinder takes the form:

$$h = 1.42\left(\frac{\Delta T}{L}\right)^{0.25}$$

and for our capillary reactor system is ~2 W/m^2-K making our Biot number ~6E-6 which is significantly lower than 0.1, our Biot condition. It is worth noting that the determination of a convection coefficient is done empirically as it is based on many different considerations including surface geometry, the velocity of the fluid, and even the flow profile of the fluid over the body.

If the Biot number condition is met, lumped capacitance is applicable to the system. The solution to the transient problem in lumped capacitance reduces to it's the dimensionless profile[139]:

$$\theta = \exp\left(-Bi \times Fo\right)$$

Where θ is the dimensionless temperature change of the body, Fo is the Fourier number, representing dimensionless time. The Fourier number is a dimensionless number that describes the rate of heat transfer through a body to the heat stored in that body and is commonly used to better understand systems where heating is transient.

$$Fo = \frac{\alpha t}{L_c^2}$$

$$\alpha = \frac{k}{C_p \rho}$$

Where α is the thermal diffusivity in m/s^2, t is time in s, c_p is the specific heat capacity in J/kg-K, and ρ is the material density in kg/m^3.

Table 3-1: Material properties of stainless steel 316

Material Property	Value
Thermal Diffusivity (α)	3.4E-6 m^2/s
Specific Heat Capacity (c_p)	500 J/kg-K
Density (ρ)	7,980 kg/m^3
Emissivity (ϵ)	0.3

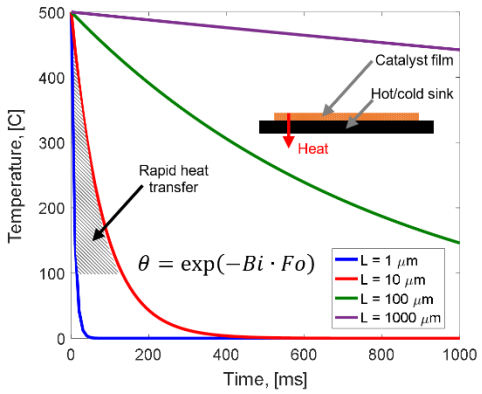

Figure 3-1: Lumped capacitance model for cooling rates at various catalyst layer thicknesses

We can now use the lumped capacitance solution to identify required catalyst thicknesses that are able to achieve sufficiently fast cooling rates (<100ms) given a particular heat transfer coefficient. We determined this thickness to be in the range of 1um to 10um. This gave us a preliminary design directive for achieving ultrafast heating and cooling in our catalytic microreactors.

3.2.2 THEORETICAL HEATING RATES

With an understanding of the approximate thickness necessary to achieve millisecond heating and cooling, we derived a heat transfer expression with electrical power as an input and temperature as an output for a reactor with a tubular geometry[139]:

$$P = I^2RL = \left[\rho C_p \left(\frac{\pi(D_{Outer}^2 - D_{Inner}^2)}{4}\right) L \left(\frac{dT}{dt}\right)\right] + [h\pi DL(T - T_\infty)] + [E\sigma(\pi DL)(T^4 - T_\infty^4)]$$

Where, on the right side of the equation, the first term describes the time dependent heat accumulation within the body of the tubular reactor, the second term describes convective heat loss, and the last term describes radiative heat loss. Using this heat transfer equation, we were able to use known physical values for different metals including nichrome, platinum, iron, and palladium to specify the power capacity necessary for a power source to heat these different materials at a range of thicknesses as fast as 1ms.

Table 3-2: Physical dimensions of capillary tube microreactor

Dimension	Value
Outer Diameter (D_{Outer})	500E-6 m
Inner Diameter (D_{Inner})	400E-6 m
Length (L)	0.09 m

For the material properties seen in Table 3-1 and the dimensions of our capillary microreactor as seen in Table 3-2 we can use this heat transfer equation to approximate the power consumed in the transient heating, convection, and radiative processes. The first term, the accumulation term, describes the power required to heat our reactor at a rate of 250°C/s, or the fastest heating rate we

studied in our experiments (25°C in 100ms). The power input required to heat our reactor at this rate is 6.35W for a 25°C temperature swing. The second term describes the convective heat loss due to room temperature air flowing across the outside of the capillary reactor with the convection coefficient calculated in section 3.2.1 of 2 W/m^2-K. The power offset due to convective heat losses for this reactor is 0.09W at a temperature of 337.5°C (the average temperature of 325°C and 350°C). The third and final term describes the radiative heat loss from the surface of the reactor. The power offset due to radiative heat losses comes to 0.32W at 337.5°C. Radiation losses strongly depend on the emissivity of the hot material which is prone to changing naturally due to metal surface oxidation, composition, or other potentially transient processes. Both convection and radiation losses are functions of the current reactor temperature, which can change from these reported values by as much as 10% across the entire temperature range (325°C to 350°C).

Using the power source, we are able to input a waveform signal in either current or voltage. We chose to use voltage and therefore wanted to know what the expected temperature is after a set period of time based on a specified input voltage. To do this, we used Ohm's law:

$$V = IR \; or \; P = IV$$

Which related the voltage to the current times the resistance of the material or power to the current times voltage. Assuming two of these parameters are known, substituting these equations into each other makes it possible to find either of the other two parameters. Voltage is known as it is the parameter we are setting which means we need the resistance of the material to back calculate the corresponding power or current. To find the resistance of a material with specified dimensions and properties follows the equation:

$$R = \frac{\rho L}{A}$$

Where the resistance is equal to the resistivity, ρ, times the length, L, of the tube, all divided by its cross-sectional area, A. The resistivity of a material is unique meaning that a tube or coating with the same length and cross-sectional area may still have different overall resistances.

Using these equations, we were able to find which materials and geometries would be able to sufficiently provide temperature swings within the limits of the available technology.

3.2.3 TRANSIENT COMPUTATIONAL HEAT TRANSFER

Having narrowed down the feasible materials and geometries for our microreactor, we additionally used Matlab as a tool to observe theoretical heating and cooling rates based on these material properties and to help specify our power supply. This was important to verify that our reactor would be capable of achieving temperature swings on the time scale of kinetic significance.

As we were limited by our heating method, we designed a reactor geometry around the need to be electrically resistive. This is necessary for heat to accumulate within our reactor to reach reaction temperatures. A 400um inner diameter, 500 um outer diameter stainless steel capillary tube reactor satisfies that design consideration while maintaining a small thermal mass and small diffusion length scale for good heat *and* mass transfer. This made it a great candidate for a reactor geometry to allow us to study temperature oscillations in a reactor.

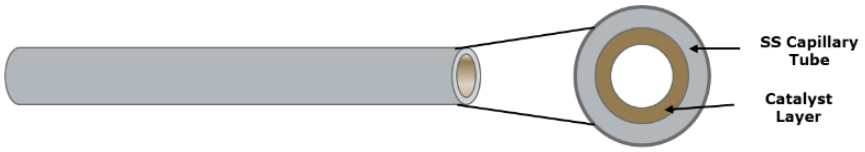

Figure 3-2: Reactor geometry for Matlab modeling

With a geometry in mind, we used our previously derived expression for the heat transfer model as seen in section 3.2.2 for our system. Using Matlab we were able to solve the transient heat

transfer model for a set amplitude, duty, frequency, and convection rates. From this Matlab model we found specifications which allow our reactor to operate in the temperature range as well as the time scale of interest. The Matlab code used can be found in the Appendix. The four primary parameters tested are:

1. Frequency

Frequency was the main parameter of interest. We wanted to make sure that, according to resonance theory, we would be able to match our external temperature oscillations to the intrinsic kinetic turnover of our chemistry[141]. The catalytic turnover of chemical reactions is generally on the time scale between 1ms to 1000ms, depending on the exact chemistry of interest. For this system to be broadly applicable to a wide range of different chemistries, we wanted to make sure that we designed a system capable of a 1-10ms temperature swing.

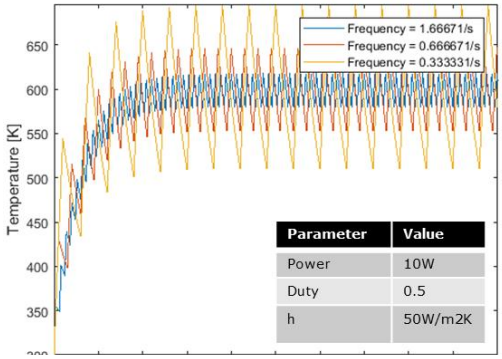

Figure 3-3: Matlab model of frequency dependence on heating and cooling rate in a tubular microreactor

As the applied frequency ramped up with the other parameters help constant at the values shown in the respective plot, we found that the amplitude of the minimum to maximum temperature values diminished. This is because there is not as much time allowed for the temperature to reach the temperature limits as there is when the frequency is lower. This told us that by changing frequency we would be affecting the *temperature amplitude*.

2. Power

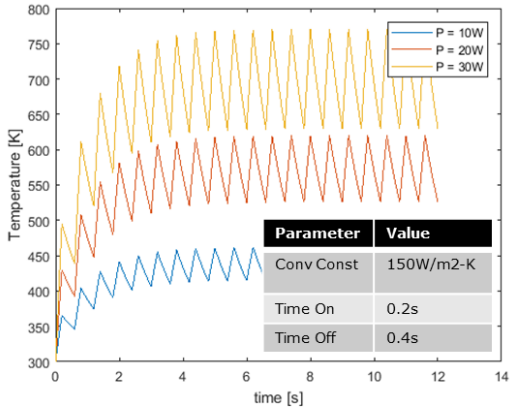

Figure 3-4: Matlab model of the power input dependence of the imposed temperature swing in a tubular microreactor

The power necessary to drive the temperature swing was the next parameter of interest. We wanted to make sure that our power source and reactor specifications would allow for oscillations at a magnitude and a temperature offset in the range of significance to our selected chemistry. The applied power is what drives the temperature accumulation in our reactor so we needed to make sure the power source could provide enough energy to raise the temperature to reaction conditions.

By testing a range of maximum applied powers, we observed its effect on the system. As the applied power to the system increases, the *temperature offset* as well as the *temperature amplitude* were affected. This is because we are inputting more energy into the system which goes towards more rapid heating resulting in a higher average temperature and a more intense temperature swing.

3. Convection Constant

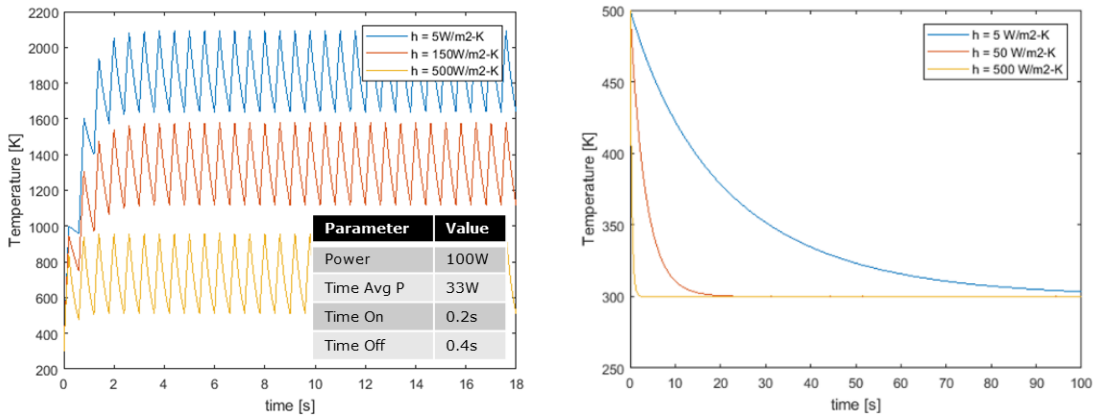

Figure 3-5: Matlab model of the convection rate dependence on the average temperature of the reactor as well as the impact on cooling times

Rapid cooling of the reactor was one of the bigger challenges that we faced in developing this system. The most important characteristics of a good convective fluid for cooling is something that starts off cold (low T_∞), is good at taking up energy (high c_p), and is in close, thermal contact to the hot object. This makes coolant selection difficult as liquid coolants have a high heat capacity but vaporize at reaction temperatures and are often electrically conductive meaning they cannot be used otherwise they would electrically short the reactor or evaporate and create hazardous gases and uncontrollably pressurize the system. This limited us to using forced air to cool our reactor and apply larger voltage swings than we otherwise would have.

We can see that by increasing the convection rate over orders of magnitude there is a significant change in the *temperature offset*, but not in the temperature amplitude as was expected. This is because the cooling is constant and the heating is periodic, meaning that the system exists in an effectively "colder" system making it more difficult to heat the system to consistent temperatures.

4. Duty

The oscillation duty is not something we originally expected to be so relevant to the reaction but becomes important when considering the fundamental phenomena occurring on the catalyst surface. By favoring lower temperatures for longer periods of time, the molecular transport is allowed to dominate. This is because the temperature is too low to drive reactions, so the surface composition becomes more saturated with reactants. When the temperature is allowed to be high for longer periods of time, reaction dominates on the catalyst surface and the surface loading is more vacant. The duty is a significant parameter because it works to balance these two competing phenomena to better cover the surface and react them off.

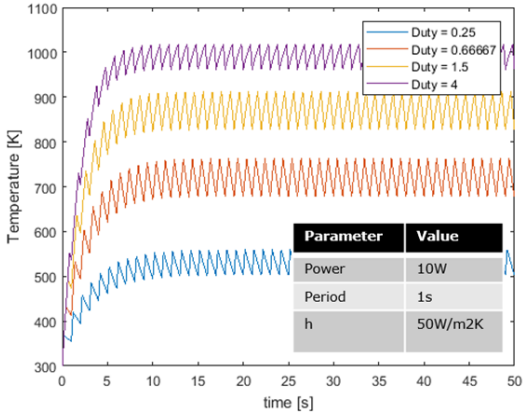

Figure 3-6: Matlab model of the duty dependence on the average temperature of the tubular microreactor

Using Matlab, we tested the effect of duty on the system, or the relative amount of time that the system is "on" at the high temperature condition, versus the time it is "off" at the low temperature condition. The effect of increasing duty is an increase in the *temperature offset*. The average temperature is affected by the relative time that the power is on as might be expected as there is more power in the system.

3.3 REACTOR TEST STAND

We constructed a reactor test stand to run our reactions through. It features three mass flow controllers to mix our reactants for any chemistry of interest. These gases then pass through one of three different paths: the bypass, the isothermal differential reactor, or the dynamic microreactor. The effluent then passes into our in-line analytics for product analysis as seen in Figure 3-7.

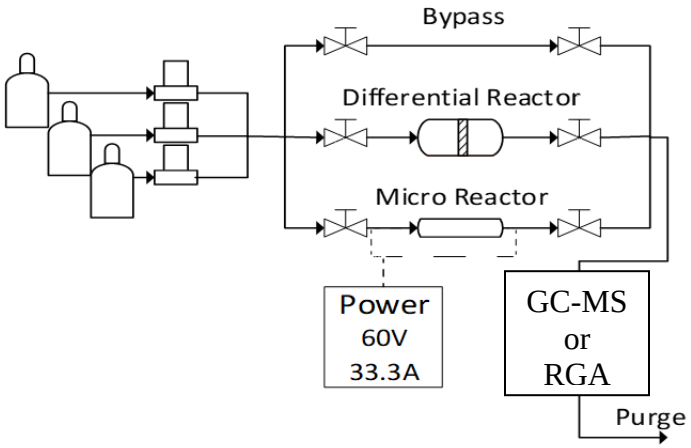

Figure 3-7: Process flow diagram of our catalytic test stand for dynamic microreactions

The system bypass allows for a non-catalyzed pathway to flow our reactants directly into our analytics. This is useful for calibrations and daily checks to make sure the system is operating as intended. The differential reactor is a standard and well accepted method for measuring isothermal kinetics of a reaction. It serves as an important reactor for benchmarking our unconventional, dynamic microreactor. The microreactor itself is connected to our Keysight N7973A power supply which is used to resistively heat our reactor. Our in-line analysis was an Agilent 7890B GC-MS before we purchased a Hiden HPR-20 R&D residual gas analyzer. The system additionally features in-line pressure transducers both before and after the reactors/bypass as well as a mass flow meter downstream of the reactor setup.

3.4 TEMPERATURE CONTROL

The microreactors temperature was controlled using a Keysight 7973A Dynamic DC Power Supply (60V, 33A, 2kW) which is capable of resistively heating and cooling our microreactor on the order of catalytic turnover (~10 milliseconds). Resistively heating the metal microreactor using the power source requires fine control of the applied voltage to the system. Using this power source and a custom-built LabVIEW file we can control the voltage and current of the power source and calculate the real-time resistance of the reactor. The relation between temperature and resistance for a metal is well understood and is given by the equation:

$$R = R_{Ref}\left(1 + \alpha\left(T - T_{Ref}\right)\right)$$

Where α is the temperature coefficient of resistance specific to a metal and the "Ref" parameters are reference resistance in ohms and temperature in degrees Celsius, respectively.

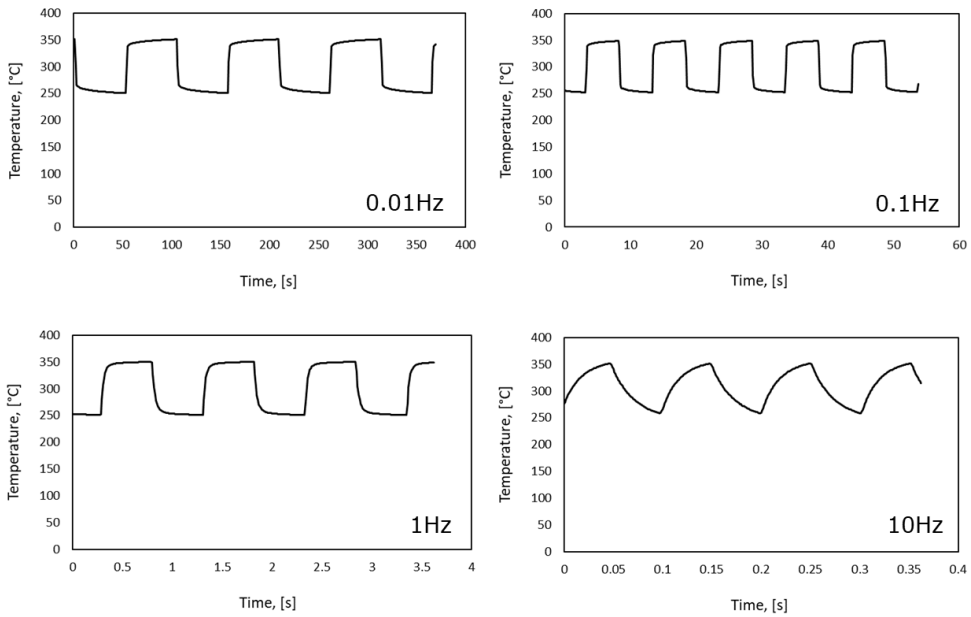

Figure 3-8: Temperature oscillation profiles across four orders of magnitudes of applied frequencies

We can use this relationship to calculate temperature-resistance calibration curves for a known reference temperature and resistance which we can use to monitor real time temperature pulsing with high temporal resolution. Figure 3-8 shows the observed temperature versus time profiles across four orders of magnitude of applied frequencies. We have found that we are able to maintain a square waveform oscillating between 250°C to 350°C at up to 2Hz applied frequency at which point the waveform starts to lose its square shape and transition to more of a sawtooth type waveform. The type of waveform used is important as a square wave input results in maximizing the time at each temperature limit[2]. This is critical in taking advantage of the different transport and kinetic phenomena at the hot and cold temperatures. As we can see in Figure 3-9, the rate of change of the temperature versus time after a new voltage is applied is extremely rapid and, up until 1Hz, the temperature change happens nearly instantaneously even across a range of applied external convection rates.

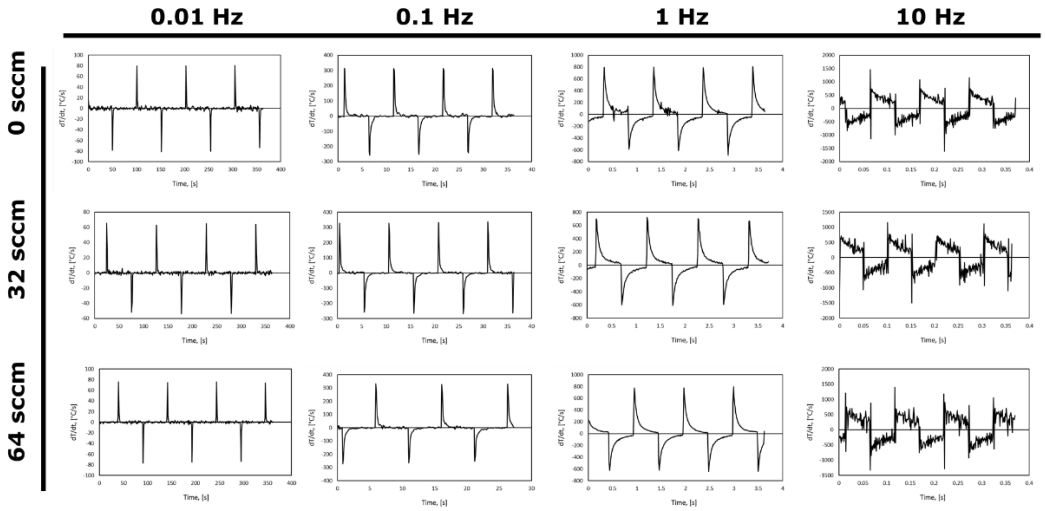

Figure 3-9: Rate of change of temperature oscillations across four orders of magnitude of applied frequencies and 3 different forced convection rates

Other temperature monitoring/control we considered were temperature probes, infrared cameras, and pyroprobes. Unfortunately, temperature probes could not work because they are too slow,

don’t have good enough thermal contact to the reactor to get a reliable reading, and have a thermal mass that could interfere with our heating rate. Infrared cameras and pyroprobes both had resolutions that were too low to focus on and properly detect the temperature of our reactor. The outer diameter of our capillary tube was 500 um which marked the upper limit for the spot size resolution of the non-contact infrared thermal detection. This specification ruled these methods out for our system.

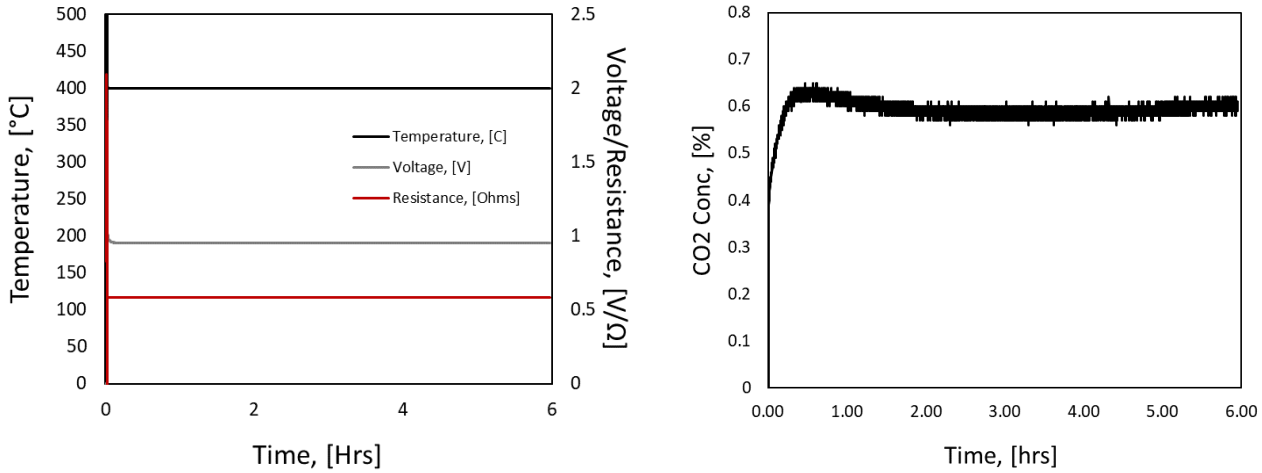

Figure 3-10: Stability test of the temperature, voltage, resistance, and product concentration at 6 hours of run time

To rule out whether the mechanical integrity of our reactor was changing over time, we ran a stability test of our reactor across 6 hours. The temperature monitoring of our system heavily relies on the resistance of our reactor staying constant. As described above, the temperature coefficient of resistance is material specific, meaning that if the composition of our stainless-steel reactor was changing, our temperature-resistance model may not be reliable. Stainless steel is made up of many different metals, such as chromium and nickel, which if leached out of the reactor could alter the material properties. This time on stream experiment showed that our set voltage is constant as expected and that our resistance ($R = V/I$) is also very constant. This indicated to us that the

reactor was mechanically stable enough that we could rely on the temperature-resistance model. The corresponding product concentration profile is also strongly constant after about 2 hours of run time, before which there is some catalyst break in period where the concentration of CO_2 produced slight increases past the steady state conversion before it stabilizes.

These considerations were critical in the initial development of our dynamic microreactors and provided a baseline for us to begin the iterative process of designing, fabricating, and validating our system.

3.5 REACTOR DEVELOPMENT

The first-generation reactor was made of two stainless steel 1/8th inch Swagelok tees connected by a stainless steel 1/8th inch tube. A 6% platinum wire was connected to copper wire leads and was sealed with rubber septa. The chemistry we studied in this version of our microreactor was carbon monoxide oxidation.

$$CO + \frac{1}{2}O_2 \overset{Pt}{\rightarrow} CO_2$$

Carbon monoxide and oxygen diluted in nitrogen were flowed axially over the electrically heated platinum wire to react. The gases were diluted in nitrogen as it was also our carrier phase in our in-line Agilent 7890B GC-MS. This "hid" the reactor sweep phase signal to the GC meaning we narrowed down our chromatographic spectra to just carbon monoxide, oxygen, and carbon dioxide. This version of the reactor was enclosed by a metal tube which made it prone to electrical shorting. This is a significant problem for our reactor design as if we cannot accurately tell through where the applied current is flowing, any temperature measurement we have would be unreliable. This is the same reason we used plastic tubing for the gas inlets and outlets, so we would not short through

some external circuit. The septa which allowed the electrical leads to pass into the reactor were made of plastic and therefore were prone to melting or warping and causing leaks in the system. This was a clear hazard as carbon monoxide oxidation, the chemistry we were studying, is hazardous even at small volumes. This generation of our reactor was designed to be a simple proof of concept reactor, that we could begin developing a system around to achieve dynamic operation. After developing a temperature control system, including receiving our controllable power supply and creating a custom LabVIEW code, we transitioned to a tubular reactor geometry which is more representative of one which we modeled and designed in the previous section.

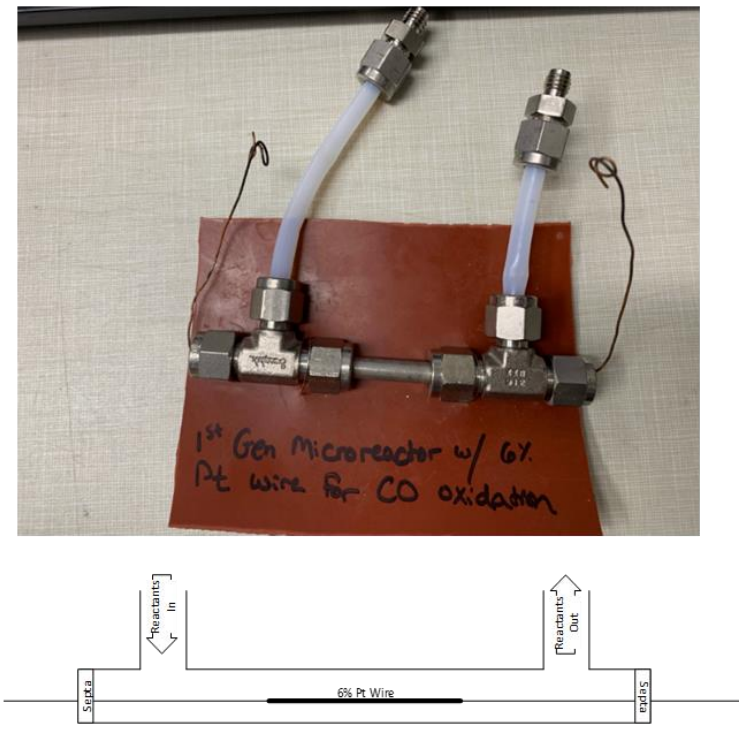

Figure 3-11: First generation dynamic microreactor with a platinum wire catalyst

The second generation of microreactor is when we switched over both to a coated capillary geometry and was also when we moved away from carbon monoxide oxidation and switched to a

methanation reaction. We switched chemistries to move away from using toxic reactants and to use a cheaper, nickel-based catalyst for coating our reactor.

$$CO_2 + 4H_2 \xrightarrow{Ni/\gamma-Al_2O_3} CH_4 + 2H_2O$$

The details of how we coated the capillary reactor can be found in Chapter 4. This reactor was specifically designed to use finely powdered catalyst and was fabricated in such a way to contain a thin wall coated layer of metal nanoparticles. One of the main challenges with this reactor was developing the coating method. Stainless steel is resistant to adhesion meaning that in order to successfully coat the catalyst on the walls of the reactor, we would first need a support layer that acted as an anchor. We used a polymerized, aluminum based, boehmite powder to this end[142]. Mass transport was also enhanced over the previous reactor model as all the reactants were confined to a single, 400um channel with catalyst coating around the inner walls. Additionally, the risk of electrically shorting the reactor or melting plastic components was eliminated entirely in this generation. This is because the electrical leads were connected far enough away from the plastic connections such that the residual heat would not melt them. Since these connections are made of plastic, the reactor was electrically isolated from the rest of the reactor test stand. This reactor does, however, suffer from a lack of real external convection and relies only on the natural cooling and the flow of the carrier gas inside the capillary tube.

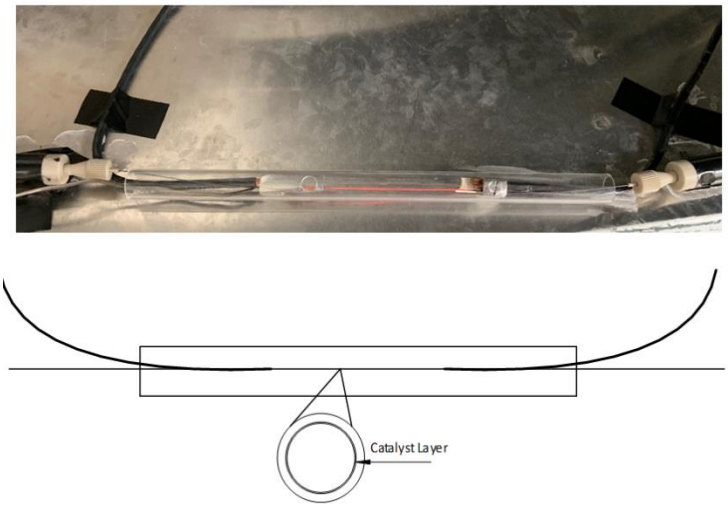

Figure 3-12: Second generation tubular, wall-coated microreactor

The third generation microreactor is modified from the previous generation but is properly sealed to allow for forced convection. Using this design, we were able to maintain the benefits of the previous generation and add air flow to more quickly cool the reactor. This is important to improve the sharpness of our dynamic temperature profile. In this generation we investigated using a coolant with better heat capacity than air. Here we ran into the problem of finding a liquid coolant that was thermally conductive, but electrically insulating. This largely narrowed down the selection to fluorinated coolants which all vaporized at reaction temperatures. This would lead to the issue of pressurizing our cover tube, and volatilizing fluids to toxic gases. Ultimately, because the reactor was coated across a large area inside the tube, we operated at too high a conversion to properly study the kinetics of this dynamic system. The reactants were allowed to react across the entire length of the reactor which ended up resulting in up to 40% conversion which is significantly higher than the 5% to 10% range that is appropriate for studying reaction kinetics.

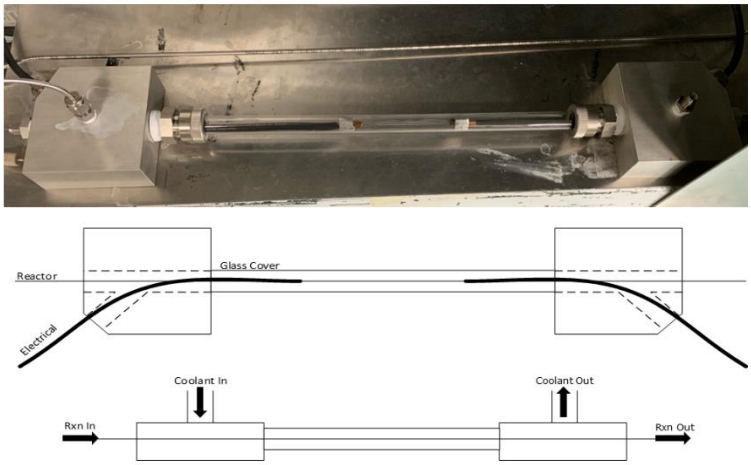

Figure 3-13: Third generation tubular, wall coated microreactor enclosed for the addition of forced convective cooling

In an effort to get around the poor convective cooling ability of the third generation reactor, the fourth generation of reactor design was intended to have as small an aperture as possible to promote very fast convective linear velocities. To do this, we sealed our 76um diameter platinum wire inside of a 400um inner diameter glass capillary tube. This would allow us to heat our reactor without fear of electrical shorting and increase our convection for faster cooling. Instead of the lugs that connected the electrical leads to the reactor in the previous generations of reactors, this model of reactor featured brass connections. The platinum wire was wound around the brass connection inside the reactor and the electrical leads were connected with alligator clips outside of the reactor. Unfortunately, the glass capillary was too delicate and too problematic to properly seal without breaking and this generation of reactor was quickly modified to the next generation of reactor.

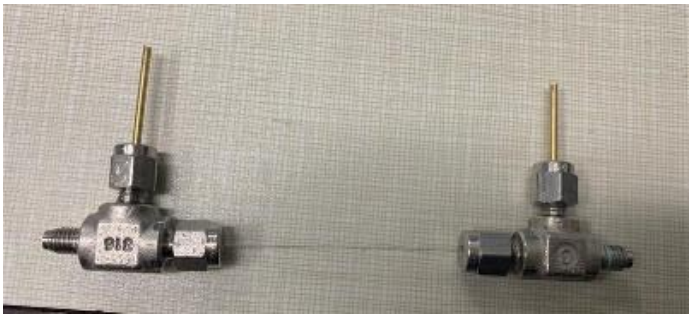

Figure 3-14: Fifth generation microreactor enclosed in a glass capillary tube for faster forced convection rates

With this model of reactor, we had a similar design to the previous, with the exception of the ceramic tube that took the place of the glass capillary. This made properly sealing the reactor feasible without breaking while still maintaining electrical isolation. Unfortunately to do this, we sacrificed the small inner diameter of the capillary resulting in lower cooling rates. Once again this reactor generation featured brass electrical leads that connected the power supply to the platinum wire inside. This was also when we transitioned back to a carbon monoxide oxidation chemistry. At this point we were much more confident in our ability to design and develop a novel microreactor without concern for leaking toxic materials. We also wanted to return to this chemistry due to how well studied and fundamental the reaction is.

Figure 3-15: Sixth generation microreactor with a ceramic tube connector for increased mechanical integrity

The sixth and the final generation of reactor used is when we decided we wanted to operate differentially rather than in plug flow as we had been until this point. This reactor features brass electrical leads that are connected to a platinum wire through an IDEX plastic cross fitting. The electrical leads and sense leads connect externally to the brass leads. In this reactor geometry, the reactants pass over the catalyst radially, rather than axially. This helps to determine the kinetics of the system as reactants have a reduced window to react over the catalyst as opposed to when the geometry was axial. In the previous configuration the reactants would be able to react perhaps until completion making it more difficult to determine the intrinsic kinetics.

$$-r_A' = \frac{F_{A0}X}{\Delta W}$$

This equation describes the surface reaction rate for a differential reactor, where F_{A0} is the molar flowrate of reactant A, X is the conversion to product, and W is the weight of catalyst[143]. This is the reactor model that we used going forward in Chapters 5 and 6.

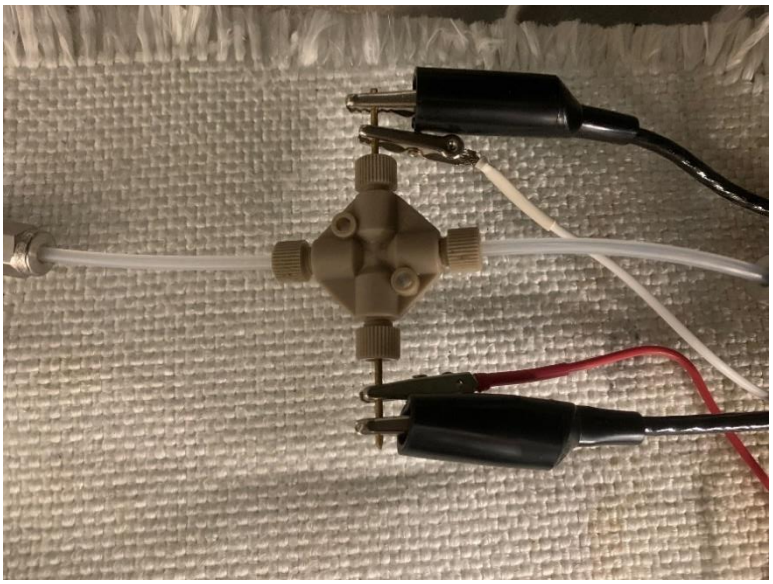

Figure 3-16: Platinum wire cross microreactor for dynamic operation

Finally, we developed a chip reactor with a thin platinum coating over an Aluminum Nitride wafer over which we can react. This reactor geometry is different from the previous iterations as instead of flowing through a capillary tube or over a catalyst wire, the reactants flow over a catalytic platinum strip which is connected to our external power source. This system features an infrared pyroprobe for real-time temperature monitoring, external electrical connections for resistive heating, and gas tight fittings for reactant and product flow. The infrared pyroprobe is an upgrade over the current model as the reactor temperature is here able to be measured *directly* rather than correlated back using an expression for the relationship between temperature and resistance as described previously. This is possible with this generation of microreactor as the catalyst surface is 8mm x 15mm which is sufficiently large enough for the 5mm spot size of the Optris CT 4ML pyrometer. This was not possible in previous designs because the reactor or catalyst were in the 0.5mm range, an order of magnitude smaller than the minimum spot size available for pyroprobes. This generation of reactor is heated in a similar way to the previous microreactors as electrical leads from our tunable power supply connect to copper leads which are connected to the platinum catalyst strip. The last significant improvement of this reactor over previous generations is that

there is forced liquid cooling. Cold water is pumped through a cooling manifold which is in thermal contact with the reactor chip. This way we have a means of convectively cooling the reactor without the trouble of electrical shorting meaning we can achieve faster cooling rates according to Newton's law of cooling[138]:

$$\dot{Q} = hA\Delta T(t)$$

Where $\dot{Q}$ is the heat flux out of the reactor, h is the convective cooling coefficient, A is the surface area in contact with the heat sink, and $\Delta T(t)$ is the temperature difference between the hot reactor and the circulating coolant.

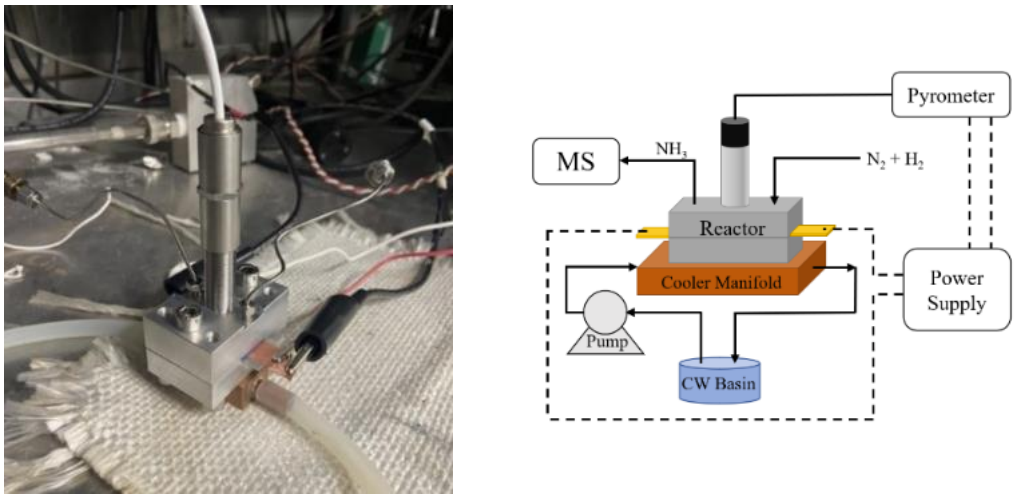

Figure 3-17: (Left) Picture of chip microreactor fully set up with pyrometer, coolant lines, electrical leads, and gas connections and (Right) a process flow diagram of the chip reactor

This microreactor is designed for future dynamic experiments, especially to produce Ammonia. Ammonia is perhaps the most important bulk chemical being produced today because of its significance in fertilizer production to support global food supplies. Although it is such an important chemical, its production is incredibly energy intensive and at the global level ammonia

production consumes as much as 1-2% of the global energy use every single year[144]. For this reason, finding other, novel methods of producing ammonia at a reduced energetic cost is seen as a major challenge within the field.

Although this reactor is left for future experiments and no reactions were run using it, we were able to begin validating the thermal oscillations beyond simply designing it. With this reactor we were able to show that we can maintain square wave oscillations at up to 200°C amplitudes at a frequency of 0.25Hz.

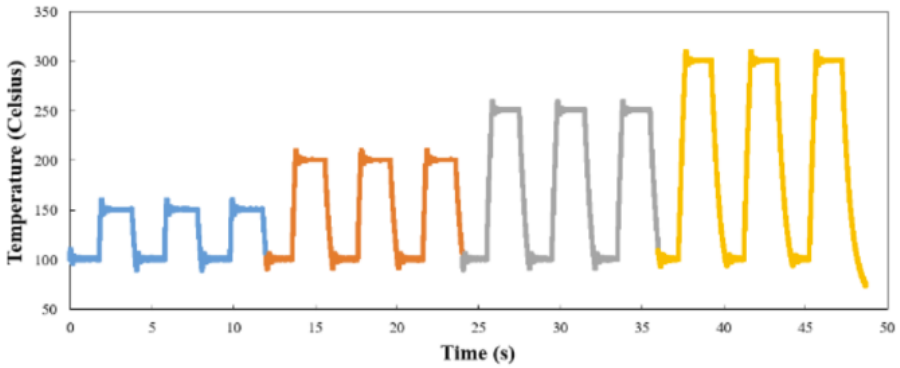

Figure 3-18: Thermal oscillations in the chip microreactor at amplitudes of 50°C, 100°C, 150°C, and 200°C at a frequency of 0.25Hz and a duty cycle of 0.5

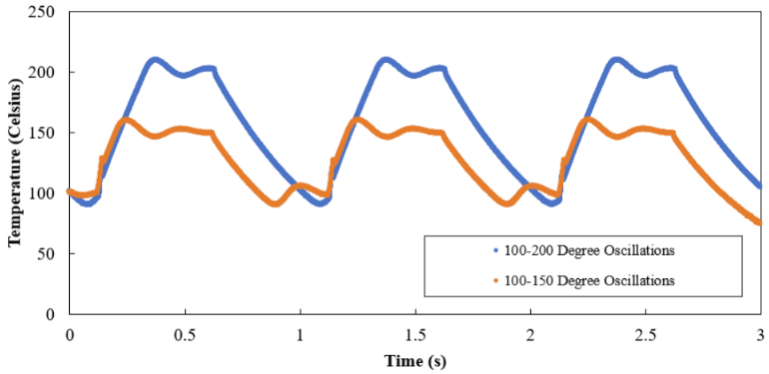

Figure 3-19: 50°C and 100°C temperature oscillations at an applied frequency of 1Hz and a duty cycle of 0.5

As we increase the frequency within this reactor, we see that at a frequency of 1Hz we lose the sharp square waves and transition to more of a sawtooth like waveform. This may be due to the higher thermal mass of the reactor or the controls in the system are not yet developed enough. This final generation chip reactor is shown to be capable of fast oscillations near the time scale of catalytic turnover in a geometry which allows for fine and reliable monitoring of temperature and constant convective cooling for more rapid temperature swings.

3.6 CONCLUSIONS

In this chapter the design considerations, modeling, fabrication, and validation in developing microreactors which are capable of ultrafast heating and cooling for reaction dynamics are explored. Using lumped capacitance approximations and full heat transfer power specifying and Matlab models we were able to develop a theoretical basis to design a dynamic microreactor. From here, we developed a full test stand which includes a differential reactor, custom LabVIEW controls, a highly controllable external power source, and an in-line residual gas analyzer for product analysis. We then worked towards fabricating our dynamic microreactors around the

design parameters we previously determined and developed a system to rapidly heat and cool them through resistive heating. By understanding the relationship between the temperature and resistance of a metal we can back calculate the real time temperature of our reactor by knowing the set *voltage* and *current* across the reactor, both of which are reported by our external power supply. The iterative design of the microreactor geometry led us to a final design which is capable of rapid heating, operates differentially, and is not susceptible to electrical shorting. In Chapter 4 we further describe the developmental process for the wall coated, capillary reactor and in Chapters 5 and 6 we use the platinum wire cross reactor to observe dynamic results.

CHAPTER 4

ANNULAR WALL COATED MICROREACTORS IN DECONVOLUTING TRANSPORT AND KINETIC PHENOMENA

4.1 INTRODUCTION

Chemical reactors are designed with different geometries to promote different phenomena such as throughput, chemical reactivity, and product selectivity. For example, a packed bed reactor facilitates high reactant-catalyst contact to enhance the catalytic effect of the reactor at the expense of a higher pressure drop and the possibility of channeling. Microreactors, on the other hand, are uniquely well suited for resolving reaction kinetics as they are inherently well mixed with a small characteristic length for any kind of heat or mass transfer effects[136]. Here, we explore the construction of an annular, wall coated capillary microreactor. Capillaries are tubes with small (micron to millimeter scale) apertures making them an excellent candidate for use as a microreactor. Because the inner diameter of our reactor is so small (400 um) this allows for the reactant molecules to very easily diffuse to the catalyst site, eliminating mass transport limitations. Similarly, because the capillary is made of stainless steel, the reactor body itself acts as a resistor in our system and heats up the 50um thick, small thermal mass capillary walls very quickly. With a catalyst layer thin enough according to our lumped capacitance model (1 um to 10um) we can additionally eliminate any heat transfer limitations with this geometry. This allows us to study the kinetics of our system deconvoluted from any transport effects. All these conditions are necessary to have a reactor capable of transient heating and cooling in our dynamic system.

4.2 MATERIALS & METHODS

4.2.1 CATALYST SYNTHESIS

Nickel catalyst was synthesized by combining 2.25g of nickel nitrate hexahydrate with 2 mL of water and mixed until it is all dissolved. It was further treated into its nickel nanoparticle form as described in section 4.2.3.

4.2.2 BOEHMITE SYNTHESIS

Boehmite serves as a binding and support layer for catalysts inside of the capillary tubes. 0.5g of P2 disperal boehmite powder is mixed with 10mL of DI water until the boehmite powder has fully dissolved. Hydrochloric acid is then added dropwise until the solution begins to form a gel (~10 drops). The mixture is allowed to continue polymerizing overnight at room temperature.

4.2.3 REACTOR FABRICATION

The boehmite slurry is deposited in a pressurized vessel and flowed through a 400um SS304 capillary tube[145]. Helium was flowed through the tube at a pressure of 60psi for 20 mins to dry out the support layer and further dried in a 120°C oven overnight. We then *slowly* (~1 mL/min) drew the nickel nitrate solution through the capillary using a syringe. Helium is flowed through the tube at 10 sccm for 10 mins to help convectively dry out the catalyst layer. The capillary tubes are placed in an oven at 120°C overnight (for at least 10 hours). The catalyst layer is not deposited the same way as the boehmite layer as not to shear the supporting layer off the capillary walls. The reactors were then calcined as shown in the temperature sequence in Figure 4-1. The reactors were then reduced *in situ* at 400°C at 90 sccm Nitrogen and 11 sccm Hydrogen for 4 hours.

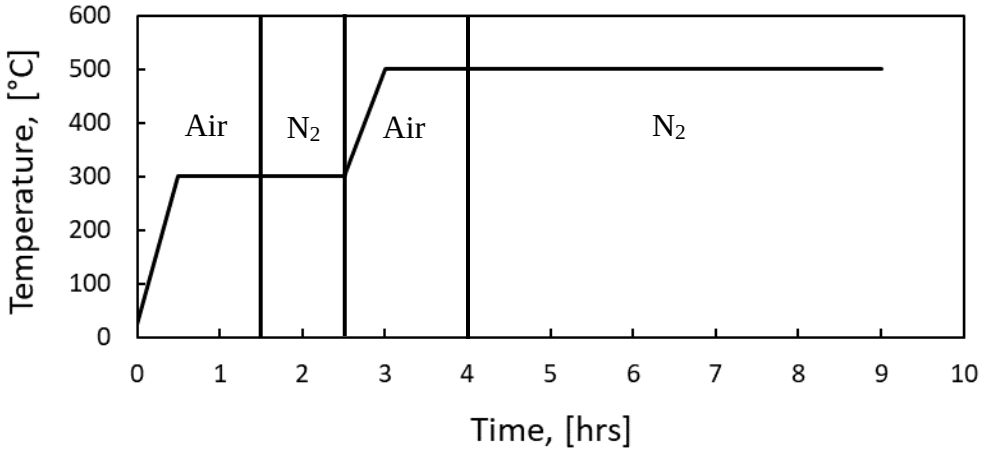

Figure 4-1: Calcination conditions for catalytic capillary reactors

4.3 RESULTS & DISCUSSION

4.3.1 FABRICATION OF THE CAPILLARY MICROREACTOR

Because our stainless-steel capillaries are non-transparent and difficult to cut without disturbing the integrity of the coating inside, we used glass capillaries to help characterize our reactors. Glass capillaries are transparent and are not as mechanically rigid as stainless steel making them easier to see inside. In this work, using a stainless steel, metal capillary reactor was important as it is resistive enough to accumulate heat, but not so much that a current cannot flow through it. Glass capillaries on the other hand are too resistive to allow any current to flow making Joule heating not possible. Glass capillaries are fragile, but transparent and could be a good candidate in isothermal reactions or in systems that do not require an electrical current to pass through them. Another benefit to glass capillaries is that they are widely used in gas chromatographs making them easier to source and there are many different fittings designed to connect them to a larger system. Additionally, GC columns are often coated to increase the degree of separation meaning that coating these columns has been well understood for decades. The glass capillaries used in this

study were used from an old GC column which originally had a coating inside of it which was burned off in a tube furnace.

Because the capillary is so small, there is a high pressure drop across it which makes it difficult to coat if it is too viscous. For this reason, we tested a range of different acid concentrations for boehmite polymerization to find a solution that was not too viscous that it could not be pumped through the capillary, but also not so thin that it wouldn't stick to the walls. In Figure 4-2 we see 9 different boehmite solutions with different numbers of drops of hydrochloric acid (the polymerization agent) 24 hours after mixing. Visually, we can see that the fewer number of drops of HCl lead to a much thinner, more transparent solution, whereas with more drops the degree of polymerization increases to the point where the viscosity is too high. Interestingly, when shaking each of these vials, regardless of degree of polymerization, the solution will return to an almost water-like level of viscosity before re-gelling to its original viscosity. This leads us to believe this mixture to be a shear thinning, non-Newtonian fluid.

Figure 4-2: Visualization of the degree of polymerization of the support boehmite slurry as a function of the amount of hydrochloric acid added

Other than the viscosity of the fluid, the ability of it to maintain a mechanically sound binding to the capillaries was a major area of interest. It is very important that the coating is able to stick to the reactor at elevated temperatures, so our reactors do not deactivate over time. To better visualize our capillary reactor, we coated boehmite gel onto stainless steel and glass slides and were treated the same way we would treat the capillaries. We found that after 3 days post treatment, the thinner

coatings (~0.15mm) showed little to no flaking where the thicker coatings (~0.25mm) showed significant flaking. It is important to note that the 0.147mm coating was the thinnest coating we could make on the slides by hand, using tape and a razor to spread a thin, even coating across the width of the slide. It is also interesting to note the discoloration that occurred on the stainless-steel slide, perhaps due to chemical etching from the hydrochloric acid in the gel. This indicated to us that the stability of a < 10um coating inside our capillary tube would maintain a strong binding to the reactor walls where thicker coatings would be more likely to peel off under a shearing flow.

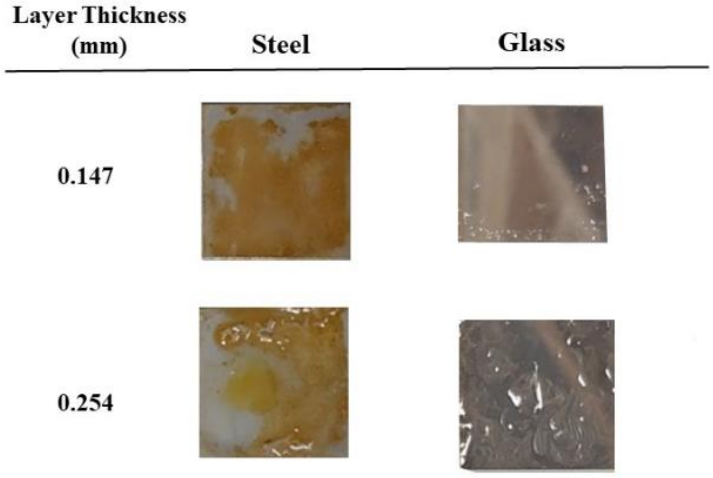

Figure 4-3: Delamination of boehmite support at 0.15mm and 0.25mm thickness on stainless steel and glass substrates after fully drying

To determine the thickness of the coating we developed on the inside of the reactor walls, we broke a glass capillary coating that was coated in the same way as described above for the metal reactors for characterization in the SEM. We found that the wall coating was on the order of 1 um thick, exactly the thickness we aimed for according to our lumped capacitance model. This showed us that our coating technique was sound for wall coating the aperture of a capillary tube.

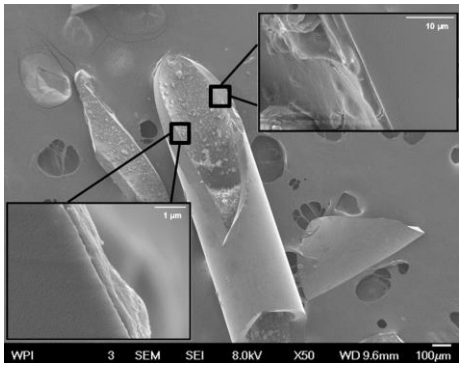

Figure 4-4: SEM image of the deposited boehmite and catalyst layer on a glass capillary with a thickness of less than 10um

4.3.2 VALIDATION OF THE CAPILLARY MICROREACTOR

The activity of each reactor we fabricated was significantly lower than expected and varied significantly from reactor to reactor. To test why this might happen, we took the same nickel catalyst and ran it *ex situ* in a differential reactor to test their activity.

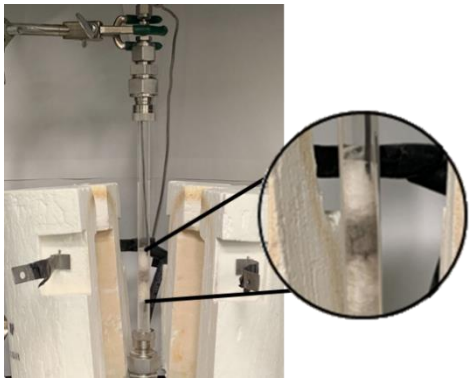

Figure 4-5: Packed differential reactor for comparative, isothermal studies

The difference between these 3 tested catalysts was the presence of boehmite and when the catalyst was synthesized. Catalyst 1 was just the reduced nickel catalyst synthesized as described in the methods section. Catalyst 2 was the nickel catalyst combined with the boehmite gel which was then dehydrated and reduced. Catalyst 3 was dried boehmite gel combined with our nickel nitrate precursor which was then dried, calcined, and reduced. Each of these catalyst synthesis methods

were developed to specifically test if the way we handled or processed our reactors affected the reactivity of the catalysts. In Figure 4-6 we can see that catalyst 1 significantly outperforms the other two catalysts with boehmite followed by catalyst 3 and lastly, with the least activity, catalyst 2. It is important to note that the mass of the nickel metal used in the differential reactors was the same regardless of further preparation, meaning that catalyst 1 had the same amount of metal sites as the other two catalysts.

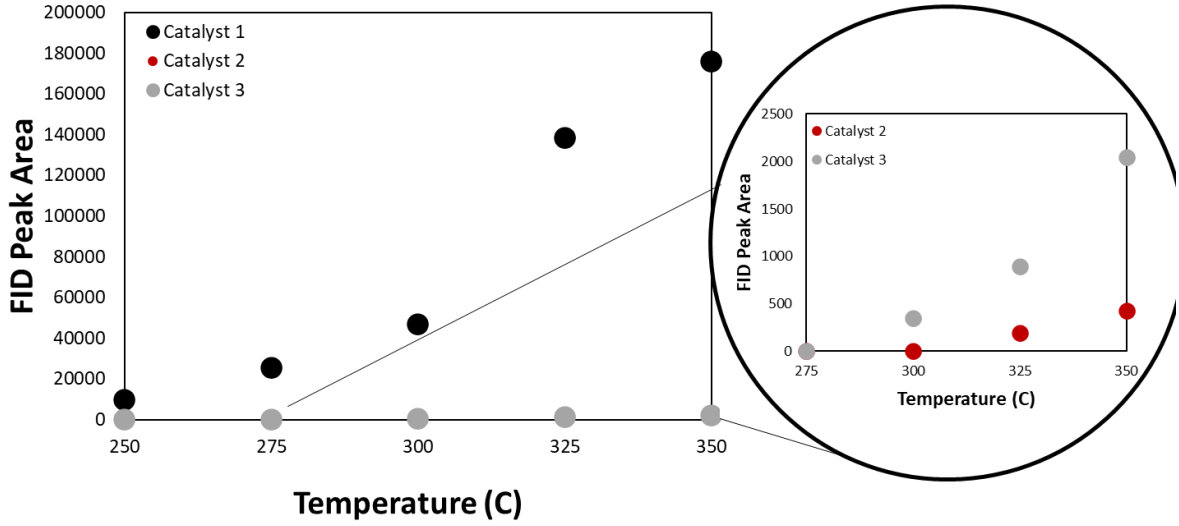

Figure 4-6: Investigative study of Nickel/Al2O3 catalysts synthesized by different methods

From this perspective we considered whether catalyst overcoating may be our problem. Overcoating is when the catalyst sites are blocked by the support making it significantly more difficult for reactants to diffuse to an active site. Because we were mixing our catalyst with a gel directly it seems as though the metal nanoparticles were being inhibited by the gel mixture rather than being taken up into a porous support via capillary effects as expected for an incipient wetness type synthesis. To check this hypothesis we first deposited boehmite onto our capillary walls and dried them in an oven overnight.

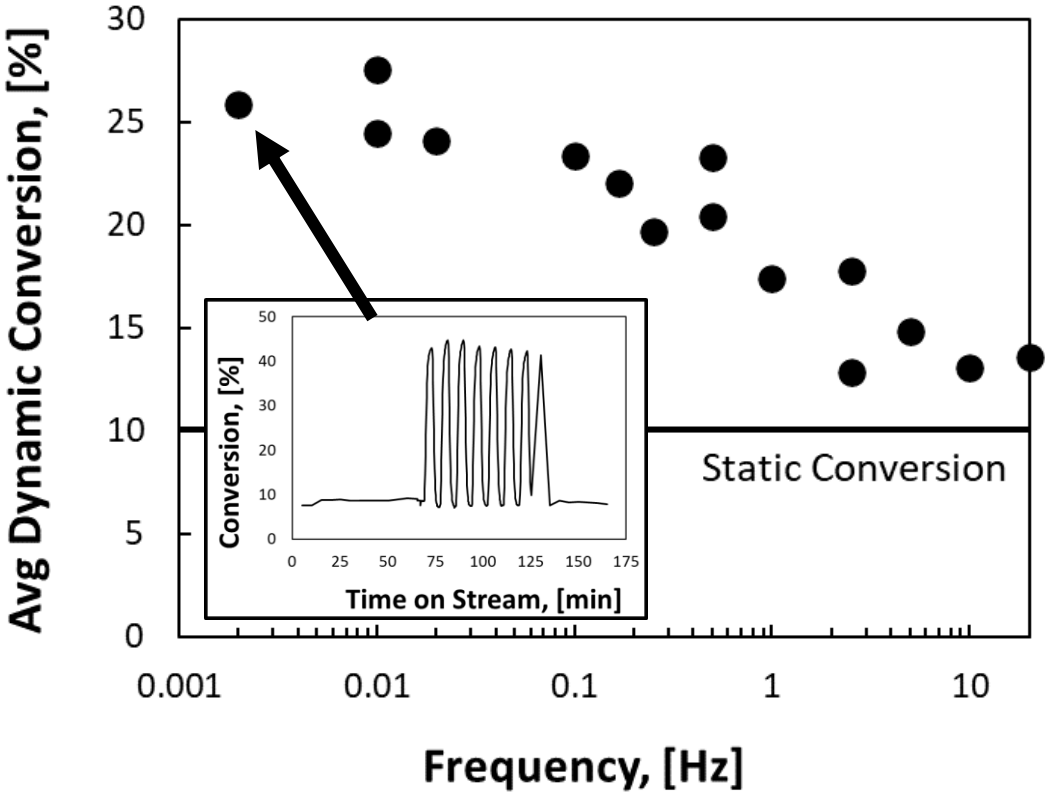

Figure 4-7: Dynamic conversion as a function of frequency for a duty cycle of 0.5 using the wall coated capillary reactor

We used the wall coated capillary microreactor in both dynamic and static (isothermal) operation to compare to each other. As seen in Figure 4-7, we see at low applied frequencies, there is a high (~25% conversion) in a 1:0.1:4 sccm ratio of H_2:CO_2:N_2, a duty cycle of 0.5, an applied voltage amplitude of 4.0V, and a total convection rate of 10 scfm of air. The dynamic conversion drops off at higher applied frequencies, but still outperforms the corresponding static conversion. According to resonance theory, we would expect there to be three major regimes which describe an applied frequency that is too slow, matches the natural frequency of the chemistry, or is too fast. Here we observe two of these three regimes. The inset plot shows the result of the low

frequency experiment which was output by the Agilent 7890B GCMS which was used for our in-line analysis. Each data point on this plot was run in this way. As shown in Figure 4-8, the experimental breakdown was such that for the first hour of the experiment, the reaction was run isothermally, followed by a dynamically operated portion, and finally a "reference" portion. This reference portion was used to compare results day to day to ensure that our results we consistent. In Figure 4-8 we can see that the reference portion of experiment 1 resulted in a significantly higher reactivity than the following two experiments, meaning that the results for experiment 1 were not reliable. For these experiments we used the applied voltage as an indicator of temperature. To match the dynamic and static experiments and to be as consistent as possible, the way we equated the applied voltage was by time averaging the dynamic voltage and matching that to the static voltage. This can be calculated using the known duty of the dynamic waveform and the high and low applied voltages:

$$V_{static} = [V_{Dynamic,On} \times Duty] + [V_{Dynamic,Off} \times (1 - Duty)]$$

The static conversion line was taken from the first portion of the experiment or the "Isothermal" portion. Here we were excited to see that we were able to outperform the static results using dynamic operation and that we were able to see two of the predicted regimes from resonance theory. The high conversion portion of the plot corresponds to where the applied external oscillation matches up nearly or exactly with the natural turnover of the chemistry. This is what we saw here. Additionally, when the applied frequency becomes too fast each individual reaction step experiences the average of the applied temperature swing resulting in diminished returns as we see at the higher applied frequency range. We had two main concerns with these results. One was that there was no presence of the expected first regime, where the conversion initially drops off due to the applied frequency being too slow. This may have been due to a number of reasons,

most obviously due to the fact that we simply did not apply a slow enough frequency to the system. A second, and more concerning explanation is that the high conversion was due to heat accumulation in the reactor at low frequencies and that the drop off in reactivity could have been because heat was not able to accumulate for long enough to lead to a significant conversion at higher frequencies. Either way, the second concern about this data is that the conversions we were getting were *too high*. To reliably measure the kinetics (which was a goal for our dynamic system) we wanted to operate *differentially*[143]. Physically this means that we want our reactants to interact with the catalyst once, then leave it to analysis. In our capillary tube reactor, the molecules were able to interact with the catalyst repeatedly making a reliable measurement of the kinetics difficult and leading to higher reactivity. We were hesitant to try operating at a higher flow rate (lower residence time) which could lead to lower reactivity because we did not want to shear the catalyst coating off the reactor wall. It is worth noting that the GC output only showed a transient waveform during the slow oscillations as the transfer lines from the reactor to analysis lead to mixing which at higher frequencies showed an averaged response.

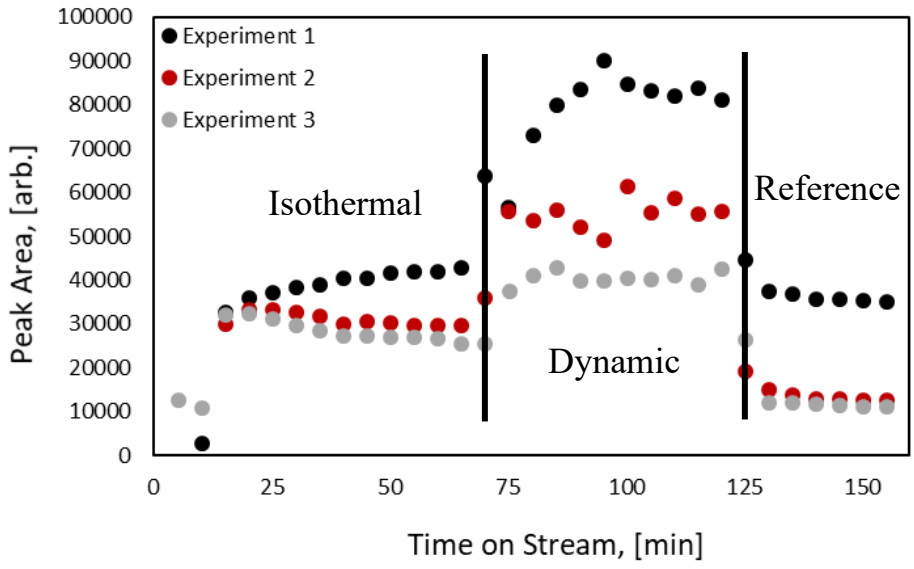

Figure 4-8: Dynamic experiments ran with both a corresponding isothermal and reference portion as a standard to compare experiments

There are a broad range of unique chemical reactors used today dependent on the needs and types of chemistries. To understand how a capillary reactor fits in to the larger picture, we first need to understand some of these different reactors. The general approach to design each type of reactor follows the form[143]:

$$Accumulation = In - Out + Generation - Consumption$$

Or in a mole balance on any species "j":

$$\frac{dN_j}{dt} = F_{j0} - F_j + \int^V r_j dV$$

This design equation is used alongside specific assumptions depending on the reactor type to determine the rate of production or consumption of any species within the chemical reactor.

Perhaps the most well recognized and used type of reactor is the batch reactor. This is simply a sealed vessel with reactants combined within to promote reaction. The vessel is often controlled to a specific temperature and pressure to facilitate the reaction. These reactors are simple to make and use but suffer from poor heat and mass transfer resulting in poor spatial uniformity on shorter

time scales and require longer reaction times for complete conversion. Additionally, these reactors have a fixed volume and therefore a low throughput as reactants cannot be added nor can products be removed during the reaction. The design of these reactors follows the equation[143]:

$$\frac{dN_j}{dt} = \int r_j dV$$

Or if the reactor is assumed to be well-mixed meaning it is spatially uniform in composition and temperature:

$$\frac{dN_j}{dt} = r_j V$$

These equations establish the rate of consumption or generation of moles, N, of species "j" in reactor volume, V at a given rate, r_j. This allows the determination of the effectiveness of the batch reactor given the kinetic rate for the chemistry of interest. Because there is no flow in or out of the batch reactor, the "In" and "Out" terms in the generalized equation are removed, leaving just the accumulation of species "j" dependent on the rate at which the reaction occurs.

The continuous stirred tank reactor (CSTR) is similar to the batch reactor, though it addresses some of the limitations. The CSTR incorporates mixing into the reactor, allowing for a more spatially uniform vessel in both composition and temperature, therefore eliminating some of the transport limitations. This reactor is also constantly adding and removing reactant and product from the vessel, increasing its throughput. This necessitates an additional design consideration. Determining the residence time, or the time that a molecule spends in the reactor, is important for maintaining a high degree of conversion in these reactors, especially if the mixing is highly non-ideal. If the effluent flow rate is too high, the conversion may be too low. If the flow rate is too low, you lose some of the benefit of being able continuously operate this reactor. The CSTR assumes that there is spatial uniformity in concentration and temperature due to the constant

mixing in the reactor. It is important to note that because reactant is constantly being added to the reactor, the mixing rate must be such that the added reactant is nearly instantly incorporated into the bulk of the vessel. Additionally, this reactor is operated at steady state, meaning that there is no accumulation in the reactor or that there is no time dependence on the composition of the reactor. The design equation for a CSTR is therefore[143]:

$$0 = F_{j0} - F_j + Vr_j$$

Or

$$V = \frac{F_{j0} - F_j}{-r_j}$$

This equation sizes a reactor which will reduce the flow rate of species j_0 to the effluent rate of species j for a known reaction rate.

Plug flow reactors (PFRs) are a tubular variation of chemical reactor that is assumed to be well mixed in its radial dimension, but in its axial dimension is spatially non uniform. These reactors are beneficial as they are easy to incorporate in a flow system and they have a high throughput. Unfortunately, if the chemistry is highly exo- or endo- thermic heat generation or consumption may lead to thermal gradients along the axial dimension of the reactor. This is because most of the reactant will be consumed early in the reactor as the composition is higher meaning thermodynamic effects may interfere. The design of these reactors is a little more complicated as they are spatially uniform in one dimension, but not in the other. To do this, the reactor must instead be broken down into differential segments which have an effective spatial uniformity in the axial dimension. The design equation comes to[143]:

$$\frac{dF_j}{dV} = r_j$$

Across the differential segment V to V + ΔV. This equation equates the change in concentration of species j in flow across the differential segment to the reaction rate for that segment.

Differential reactors are commonly used for measuring reaction kinetics. A thin layer of catalyst is deposited in a reactor tube with reactants flowing over it. Because the catalyst layer is thin, it is assumed that the reactor is gradientless and is therefore uniform and well mixed. Due to this design consideration, the relevant equation is similar to that of the CSTR.

$$-r_j' = \frac{F_{j0}X}{W}$$

The conversion is kept low (5% to 10%) to both make the assumption that the reactor is gradientless as well as to obtain reaction rate data to calculate the rate constant, activation energy, and pre-exponential factor.

Packed bed reactors (PBRs) are tubes which are packed with catalyst material that encourages good mixing and high reactant-solid interfacing leading to moderate to high conversions. Although this reactor does well promoting catalytic effects, because it is packed with solid materials, there is often a high pressure drop across the reactor leading to larger costs associated with pumping the reactants through it. Additionally, channeling is a common problem in these reactors, meaning that the reactants tend towards a specific pathway through the solid media which can lead to local hot spots (in exothermic reactions), poor spatial uniformity, and poor utilization of the solid media.

Monolith reactors are mainly seen used in the automotive industry; they are honeycomb-like structures with catalyst deposited across the walls of the many small holes. They have high throughput and moderate pressure drops and can suffer from poor heat transfer and therefore inconsistent product conversions. The design equation for a PBR is very similar to that of the PFR with the exception that the volume term is replaced by the weight of the packed catalyst[143].

$$\frac{dF_j}{dW} = r_j'$$

In this equation, the change in the composition of species j is a function of the weight of the catalyst used, which gives the surface reaction rate, r_j'.

Our capillary microreactor benefits from very small characteristic length scales meaning that transport from the bulk to the reactor walls where the catalyst is deposited is non-intensive. Additionally, the 50um thickness of the capillary wall as well as the ~1um thickness of the catalyst coating means that heat applied through resistive heating can very quickly and easily transfer to the catalyst site. These two considerations mean that we can be confident we are studying the reaction kinetics rather than the energy associated with transport effects. Additionally, because our goal was to create a reactor capable of heating and cooling on the order of catalytic turnover, we needed to make sure our reactor would have a small thermal mass on top of the other considerations. This catalytic, tubular reactor behaves similarly to a PFR and a PBR where the radial composition is uniform, but the axial composition is not. Because our reactor is catalytic, and is operated non-isothermally, the rate of reaction within a differential slice of the reactor is variable with time. Starting from the initial design equation for a catalytic reactor:

$$\frac{d\bar{N}_j}{dt} = F_{j0} - F_j + r_j'\Delta W$$

We can see that the change in moles of species j is *not* constant across all times but *is* constant where $\Delta t = \tau = \frac{1}{f}$. If we make this assumption, we can find that we are at a dynamic steady state where $\frac{d\bar{N}_j}{dt} = 0$. The next consideration is that the surface reaction rate, r' is a function of temperature according to the Arrhenius equation. If we are oscillating the temperature, this also means that the surface rate will be a function of time meaning that the rate must also be evaluated

across this oscillation period, τ. With these assumptions we can reevaluate the general design equation to be:

$$0 = F_{j0} - F_j + \int_0^{\tau} r_j'(\mathrm{T(t)})\Delta W dt$$

Or:

$$\frac{dF_j}{dW} = \int_0^{\tau} r_j'(\mathrm{T(t)})dt$$

Which collapses to a time dependent form of the packed bed design equation. It is important to note that this expression does not consider any dynamic enhancement effects and simply describes a system with time averaged surface reaction rate with an oscillatory temperature input.

4.4 CONCLUSIONS

Here we developed a method for fabricating a wall coated capillary microreactor capable of millisecond heating and cooling rates. We ran into a few issues involving the deposition technique in that a boehmite slurry that was too thick was impossible to pump through the 400um diameter capillary tube, but a slurry that was too thin would not provide enough anchoring support onto the wall. Additionally, the boehmite gel overcoated the catalyst site leading to a stark drop in activity. To overcome these issues, we developed many different boehmite slurries and qualitatively characterized their adhesion onto stainless steel until we had a mixture that worked in the development of these reactors. Additionally, we fabricated catalysts in many different orders to determine why we saw this drop in activity and determined that by mixing the catalyst with the boehmite prior to deposition, the boehmite was blocking reactants from accessing the reactive sites. To overcome this, we changed our fabrication technique in a way that allowed the boehmite layer to be deposited first followed by the catalyst deposition.

In transient operation, this reactor showed up to a 2.5x dynamic enhancements in activity over isothermal operation. We are able to resolve two of the three expected regimes in oscillations, the "resonant" regime, where the imposed frequency matches closely the natural turnover of the chemistry, and the "dampened" regime where the applied oscillations were too fast, so the activity begins to drop down towards isothermal conversions. We did not, however, observe the first "time averaged" regime, where the applied oscillations were too slow. This may be due to several reasons. It is possible that heat accumulated in this reactor at the longer time scales and did not cool fast enough and the high conversion is essentially an artifact of inflated reactor temperatures. This is unlikely as there were no abnormalities while monitoring the temperature as described in chapter 3. This could also simply be because we did not oscillate slow enough to enter this regime. Another problem with this reactor is that the conversion was too high. In studying chemical kinetics you want to operate in the 5-10% conversion range. Here we saw conversions up to 25%. This is likely due to the geometry of this reactor and how reactants were allowed to perform secondary, tertiary, etc reactions along the axial dimension of the reactor.

CHAPTER 5

CATALYTIC HYSTERESIS AND SURFACE EFFECTS

5.1 INTRODUCTION

Hysteresis is the phenomenon where changing a condition in one direction (e.g. increasing temperature) does not result in the same outcome as ramping that condition in the other direction (e.g. decreasing temperature)[146]. For example, one might expect that as you change the temperature of a reactor, the product formation would be the same if the temperature was increased (e.g. 100°C to 200°C) as if the temperature was decreased to the same temperature (e.g. 300°C to 200°C). In each situation, the operating temperature is now 200°C, but because in one case the temperature was increased, and the other it was decreased, you may see different results in product formation based on your chemistry. This is the essence of hysteresis as applied to the temperature of a chemical reactor. The question then becomes, why does this happen? The answer is because of thermodynamics.

The surface composition of a catalyst is heavily dependent on its temperature. For a given temperature, the molecular interactions of reactants with the surface are at equilibrium and so the adsorption/desorption rate of these molecules is constant. This is true when the temperature is insufficient to activate the reaction and this equilibrium becomes a purely adsorption/desorption process. This becomes slightly more complicated when the temperature is elevated to the point that it activates the reaction as the process is no longer just thermodynamic and transport limited, but also kinetically. Even still, the reaction will reach equilibrium, but may become increasingly limited based on the adsorption strength of the product molecule which may begin to deactivate the catalyst surface. This results in a surface composition that is unique for any given temperature.

This is important for dynamic operation because we are continuously changing the temperature between two or more primary regimes which means the system reactivity will be different at each temperature.

The surface of a catalyst can be further broken down into its network of active sites where a molecule can bind[147]. Depending on the surface composition, this may inhibit some of the benefits of a catalyst. There are three primary different orientations of molecules within this active site network, for an example chemistry of $A + B \rightarrow C$. Like molecules (i.e. A + A or B + B) can be adsorbed next to each other, meaning reaction will not occur. A reactant can be next to a vacant site, leading to no reaction. Finally, each reacting molecule can be bound next to each other, which leads to the desired reaction. Reacting molecules must be near each other to react, meaning a surface with a high degree of spatial non-uniformity in reactant molecules is desirable. Molecules on a catalyst surface, to add an extra layer of complexity, are mobile meaning that they can move from site to site in an effort to reach their most stable conformation.

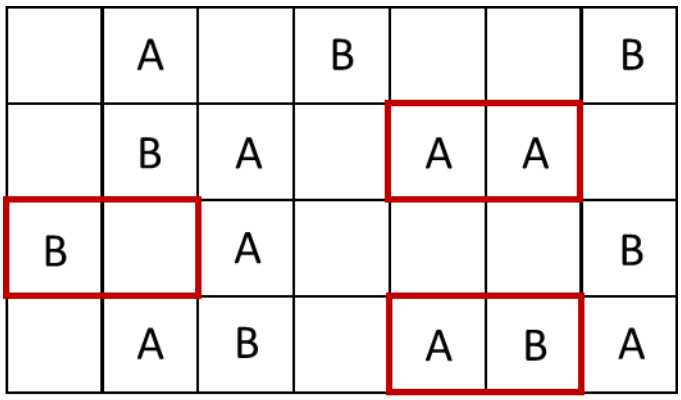

Figure 5-1: Example of different spatial arrangements of reactant molecules, A and B, on the network of catalytic sites

If the binding strength of one molecule dominates over the other, the surface will begin to become saturated with just one species. As the surface approaches total saturation with just one reacting

species, the kinetic mechanism transitions from a Langmuir-Hinshelwood type mechanism to an Eley-Rideal type mechanism.

5.2 RESULTS AND DISCUSSION

5.2.1 EVALUATION OF OBSERVED HYSTERESIS

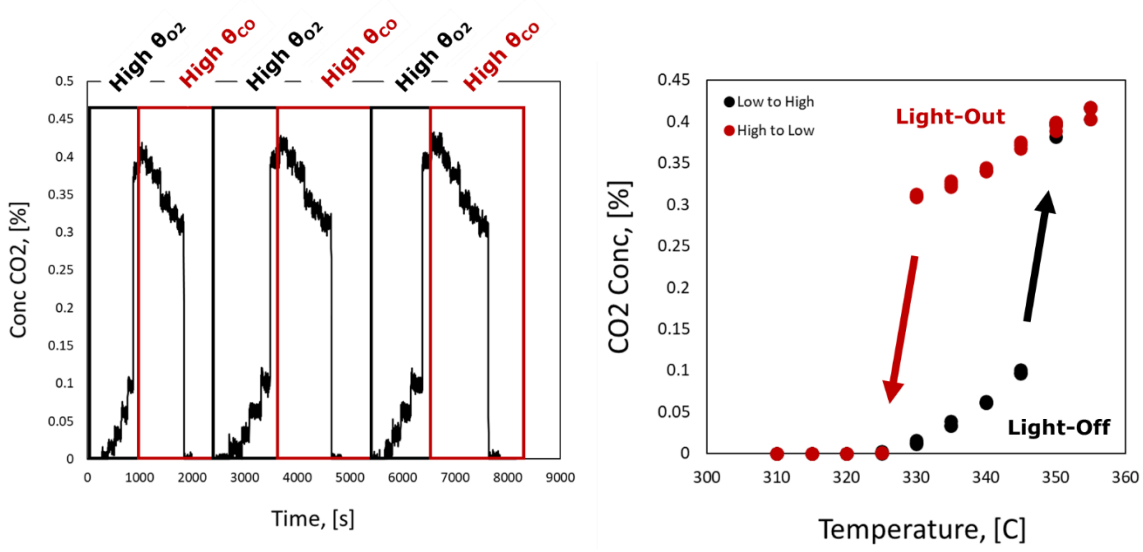

Figure 5-2: Observed hysteresis during isothermal operation of the catalytic microreactor

During daily isothermal operation for standardizing day to day results, we noticed that the direction at which we ramped our temperature led to different results in the forward and reverse directions. We can see in Figure 5-2 that there is a significant difference in the product concentrations depending on the direction of temperature change. When the steady state values at each temperature along the curve are individually averaged and plotted against the temperature, we can see in Figure 5-2 the light-off and light-out temperatures for the system. We can see that when ramping the reaction temperature from low to high (black) there is a traditional Arrhenius exponential increase in conversion until 350°C. When ramping the temperature back down (red) we see that there is a significant hysteresis in the data until 325°C where the conversion returns to

the expected result. This hysteresis indicates that something is happening on an atomic level. Here we propose that as the temperature is *increased*, the surface concentration of each species changes to a composition which is more kinetically favorable. As the temperature is *decreased*, the thermodynamics eventually stabilize back to favoring the less reactive surface composition. This data strongly indicates that the history of the catalyst is very important. This is especially important while working with a transient system where the surface composition is constantly changing and the state of the catalyst surface at any time is dependent on the surface energetics and the temperature. This is the basis for the selection of the temperature oscillation range (325°C to 350°C). This temperature range was specifically selected to include the limits of the observed hysteresis in an effort not to get trapped on one side of the hysteresis curve.

5.2.2 SURFACE PRETREATMENT

From these results, we ran controlled tests to determine the effect of surface coverage on the activity of our catalyst. We controlled the surface composition and temperature by only allowing one molecule to soak the surface for 2 hours at 400°C before introducing the co-reactant. This

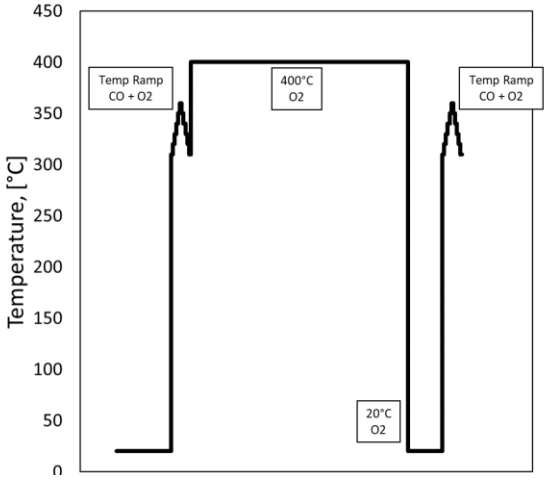

Figure 5-3: Experimental design of catalyst surface loading experiments

allowed us to observe the effects of high surface loadings of each species on the surface and take insight into the surface enhancements or inhibition effects.

As seen in Figure 5-4, there was a significant *inhibitive* effect in the catalyst activity after pretreating the surface with Oxygen. Prior to pretreatment, we see that the light-off temperature is about 310°C and the highest obtained product concentration is 0.45% or a conversion of about 13.6%. After pretreatment, the light off temperature increases to about 330°C and the maximum conversion is 0.12% or a conversion of 3.6%. Clearly there is an effect of high oxygen loading on a catalyst surface.

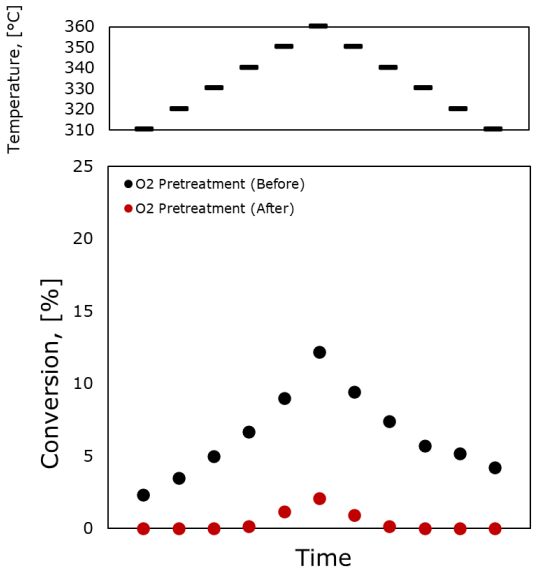

Figure 5-4: Oxygen pretreatment experiments before any pretreatment and after oxygen pretreatment showing catalytic deactivation

From the spike in activity for the CO pretreated system, we take this to mean that the presence of surface CO greatly increases reactivity until the available CO is used up. Once the temperature is stepped up, more surface CO is available to be consumed and leads to the subsequent spikes in activity. Once all the surface CO is used up, the activity returns to its original behavior. This is

very important because we can see that controlling the surface species of the reaction can lead to order of magnitude rate enhancement under the correct conditions.

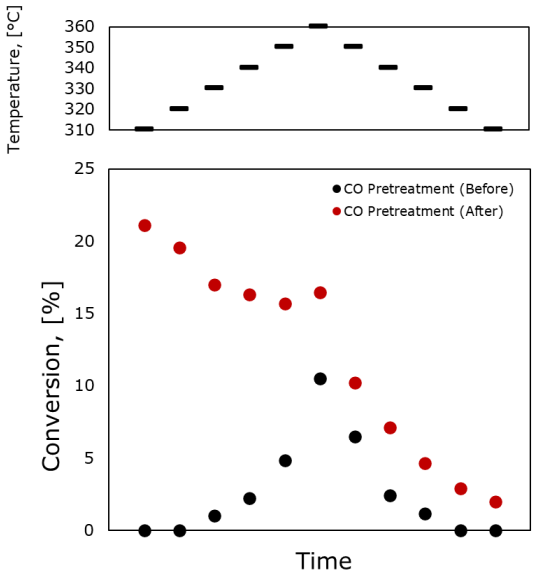

Figure 5-5: Carbon Monoxide pretreatment experiments before any pretreatment and after carbon monoxide pretreatment showing temporary rate enhancement

5.2.3 MODELING

Breaking down the chemistry into its elementary steps provides further insight into what may be happening. In table 5-1 we see the reversable steps for CO oxidation for the adsorption and desorption of each specie (O_2, CO, and CO_2) as well as the reaction steps[148,149]. In this table, the * refers to a surface bound specie if it's an exponent or a free catalyst site if not. Each of these steps can only feasibly happen under the correct circumstance. For example, if the catalyst surface is completely saturated with carbon monoxide, reaction step 1 cannot occur because there are no site vacancies to adsorb to. This is important for several reasons. If the surface is covered by CO, the only possible mechanism of reaction is by Eley-Rideal, or the direct reaction of a gas phase reactant

with a surface bound specie. Alternatively, if the surface is well mixed with both species, both Langmuir-Hinshelwood (the reaction between two or more surface bound species) *and* Eley-Rideal mechanisms are possible. Ultimately what this means is that a reaction will proceed according to the *available pathways.*

Table 5-1: The microkinetic steps and rate expressions for carbon monoxide oxidation

#	Elementary Step	Rate Expression
1	$CO + * \leftrightarrow CO^*$	$r_1 = k_1 P_{CO} C_* - k_{-1} C_{CO^*}$
2	$O_2 + 2* \leftrightarrow 2O^*$	$r_2 = k_2 P_{O_2} C_*^2 - k_{-2} C_{O^*}^2$
3	$CO^* + O^* \rightarrow CO_2 + 2*$	$r_3 = k_3 C_{CO^*} C_{O^*}$
4	$O_2 + * \rightarrow O_2^*$	$r_4 = k_4 P_{O_2} C_*$
5	$O_2^* + * \rightarrow 2O^*$	$r_5 = k_5 C_{O_2^*} C_*$
6	$2CO^* + O_2^* \rightarrow 2CO_2 + 3*$	$r_6 = k_6 C_{CO^*}^2 C_{O_2^*}$
7	$CO + O^* \rightarrow CO_2 + *$	$r_7 = k_7 P_{CO} C_{O^*}$
8	$CO + O_2^* \rightarrow CO_2 + O^*$	$r_8 = k_8 P_{CO} C_{O_2^*}$

In our experiments we are transitioning between two different temperatures, which means that we are oscillating between different surface coverages. This is because as the temperature of a catalyst changes, different numbers of bonds can break and form leading to a range of various surface concentrations. By promoting certain coverages, you are in turn influencing the reaction rates of each individual elementary step. This is particularly important at slower frequencies as thermodynamic equilibrium plays a significant role in the overall reaction. This is because there is sufficient time for molecules to move to the surface and form and break these adsorbing bonds. As the applied frequency increases, we move away from thermodynamic equilibrium as the time scale allowed for surface loading gets smaller and smaller. Each step in the microkinetic model has an associated time scale which is additionally temperature dependent, for example as the temperature is increased, the reaction rate also increases, whereas at lower temperatures surface loading dominates.

The determination of the surface coverage at any given set of conditions is commonly determined by the Langmuir adsorption model, which for the competitive adsorption of CO and O_2 on a platinum catalyst looks like:

$$\theta_{CO} = \frac{K_{co}P_{co}}{1 + \sqrt{K_O P_{O_2}} + K_{CO}P_{CO}}$$

$$\theta_O = \frac{\sqrt{K_O P_O}}{1 + \sqrt{K_O P_{O_2}} + K_{CO}P_{CO}}$$

$$\theta_{CO} + \theta_O + \theta_* = 1$$

Where θ is representative of the fraction of the surface covered by the corresponding molecule, K is ratio of adsorption to desorption rates for the given adsorbate, and P is the system pressure of the reactant.

5.3 CONCLUSIONS

In this chapter we investigated the effects of surface history on the activity of our catalyst. The hysteresis observed in normal operation suggested that something was happening at the surface level. By pretreating the surface with just one reactant, we were able to control the surface composition to determine its effect on the reactivity. Through these experiments we were able to find that the abundance of oxygen *inhibits* the reaction rate whereas saturating the surface with carbon monoxide *enhances* the rate. The spike in activity when pretreated with CO suggests that

the enhancement in activity due to dynamic operation may be due to the surface composition at one or both applied temperature regimes.

CHAPTER 6

DYNAMIC CATALYTIC REACTOR OPERATION AND OVERCOMING THERMODYNAMIC LIMITATIONS

6.1 INTRODUCTION

Full catalytic reactions can be generally broken down to reaction steps and transport steps. In the kinetic steps, the reacting species form new compounds where, in the transport steps, molecules ad- or desorb from a catalyst surface. This is where we can find benefit in operating in two discrete temperature regimes. Per the Arrhenius law, we find that as we increase temperature, we further increase the reactivity of a species:

$$k = Aexp\left(-\frac{E_a}{RT}\right)$$

Bound species tend towards their most relaxed, minimum energy state. This is where we begin to run into competing phenomena. If the system temperature is *high* a reacting species will either react if the temperature is sufficient to activate the reaction (E_a), or it will desorb if the temperature is high enough to overcome the binding energy (ΔH_{ads}). These two phenomena compete at high temperatures. Generally speaking, if $E_a/\Delta H_{ads} > 1$, the activation of the reaction is limited, and molecular desorption will dominate and vice versa. It is important to note that the activation of a reaction is also dependent on the presence of bound reactants in appreciable quantities. If this is not true, then a reaction is *less* likely to occur. If the temperature is *lower*, it is more likely to stay bound to the catalyst. This is because there is not sufficient energy in the system to desorb the reactants *or* to react them. This leads to a higher local concentration of reactive species leading to a higher θ_A. The rate of a reaction is directly dependent on the availability of reactants: $r = k\theta_A$.

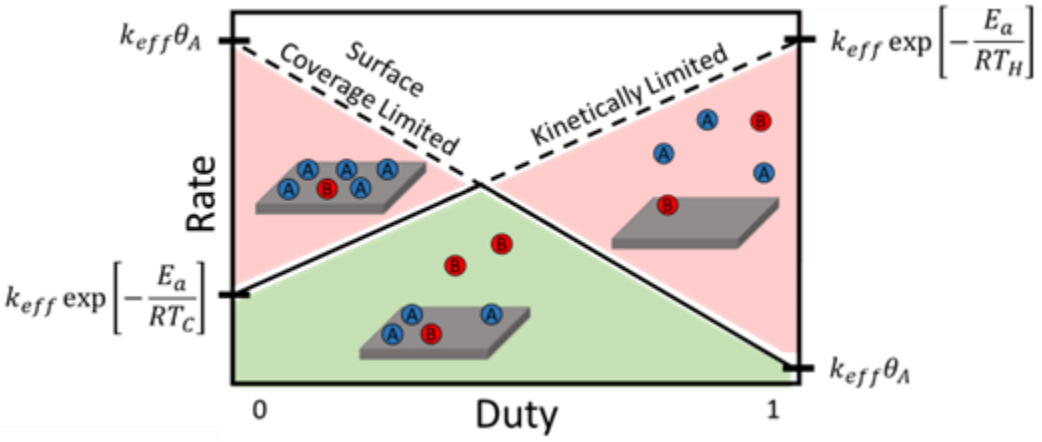

Figure 6-1: Theoretical limitations and maxima for catalytic rate as a function of applied duty

Using dynamic cycling of reaction temperature allows optimization of these two fundamental steps for any given reaction. We are able to increase the surface coverage at low temperatures and increase the rate constant at higher temperatures meaning each catalytic turn over is near optimal. Figure 6-1 illustrates these limitations in the context of an applied duty cycle between 0 to 1 against the catalytic reaction rate. On the vertical axes we can see the form of these limitations. At low duty cycles (low average temperature) the surface concentration is loaded and the reaction rate is fettered by the low rate constant, k, by way of the Arrhenius rate law. In this scenario the rate drops to $k_{eff}\exp\left[-\frac{E_a}{RT_C}\right]$. At higher duty cycles (high average temperature) these limitations change in that the rate constant is high, but the surface interactions are lower. In this case the rate drops to $k_{eff}\theta_A$.

Isothermal reactions are fettered by many competing phenomena every single catalytic turnover. Dynamic operation circumvents these competing steps and transitions from an isothermal, equilibrated reaction to a transient, non-equilibrated process. Low reaction temperatures benefit

from good mass transfer and populating a catalyst surface but are restricted by slow kinetics. High reaction temperatures have good kinetics, but suffer from poor surface-specie interactions. Typically, an isothermal system will balance these effects by taking an operating temperature somewhere at a moderate value to find a balance between kinetics and thermodynamics. Transient operation, however, takes a different approach. By operating at the temperature limits, there exists the possibility to *optimize* both the kinetics and thermodynamics, rather than compromising between the two.

This becomes more complicated for a bimolecular reaction. If one reacting species dominates the surface while the other does not, this will lead to an Eley-Rideal type mechanism. For carbon monoxide oxidation, this may be seen where gas phase CO will react with surface bound O2. If, however, the surface concentrations can be manipulated such that both CO and O2 are found in significant quantities, the overall reaction will include both Eley-Rideal *and* Langmuir-Hinshelwood steps. When O2 dominates the catalyst surface, only the E-R mechanism for bulk CO reacting with bound O2 is available. When both species are present on the surface, both E-R mechanisms (bulk CO/O2 reacting with bound O2/CO) are available *as well as* the L-H mechanism between the bound species.

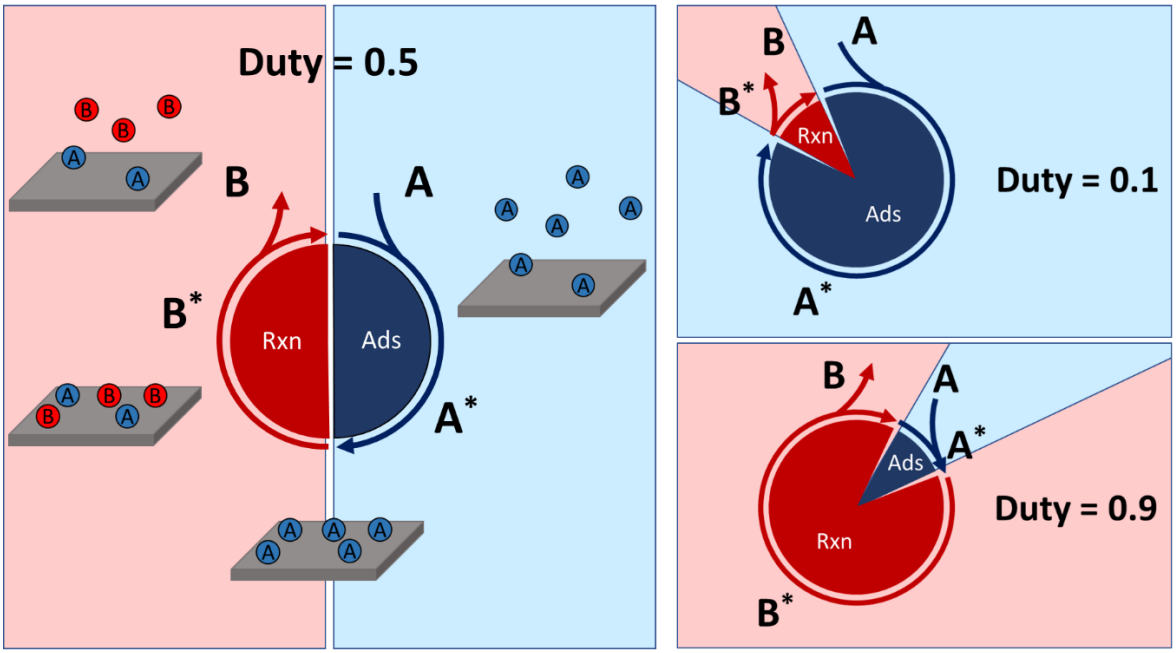

Figure 6-2: The effect of duty cycle on a catalytic turnover

In dynamic operation, we are splitting the different phenomena into different regimes: adsorption and reaction. Whereas in isothermal operation these are all occurring simultaneously and are in equilibrium, dynamic operation is a little different. With knowledge of the turnover frequency for the chemistry, we can narrow down the dynamic optimization to a specific applied frequency/period. With knowledge of the light-off temperature, we can determine our temperature amplitude. This is how we selected our temperature range. Understanding the necessary duty, however, is less straightforward. We need an understanding of the relative time scale associated with the adsorption/desorption transport steps as compared to the time it takes for the kinetic rate determining step. To characterize the entire dynamic operation regime, we studied orders of magnitudes of different applied frequencies and tested the entire range of duty cycles.

6.2 EXPERIMENTAL

6.2.1 CHEMISTRY/CATALYST

The chemistry we studied in these experiments was carbon monoxide oxidation over a platinum wire catalyst. CO oxidation is widely studied in the literature and is a key reaction of interest in the automotive industry.

3.3 v/v% of both carbon monoxide and oxygen were diluted in a helium carrier gas. The total flowrate was 10 sccm.

6.2.2 MICROREACTOR

The microreactor used in these experiments is the cross microreactor as seen in section 3. This microreactor has a platinum wire connected to electrical leads which connect to our dynamic power supply. Gas is flowed across the wire radially such that the reaction can proceed differentially.

6.2.3 JOULE HEATING

The heating and cooling method for this reactor is thoroughly outlined in section 3.4. The temperature oscillations our platinum wire microreactor is capable of are seen in figure X. We are able to oscillate between 250°C and 350°C at frequencies up to about 2Hz while maintaining a square wave before the signal begins to dampen into a more saw-tooth like waveform.

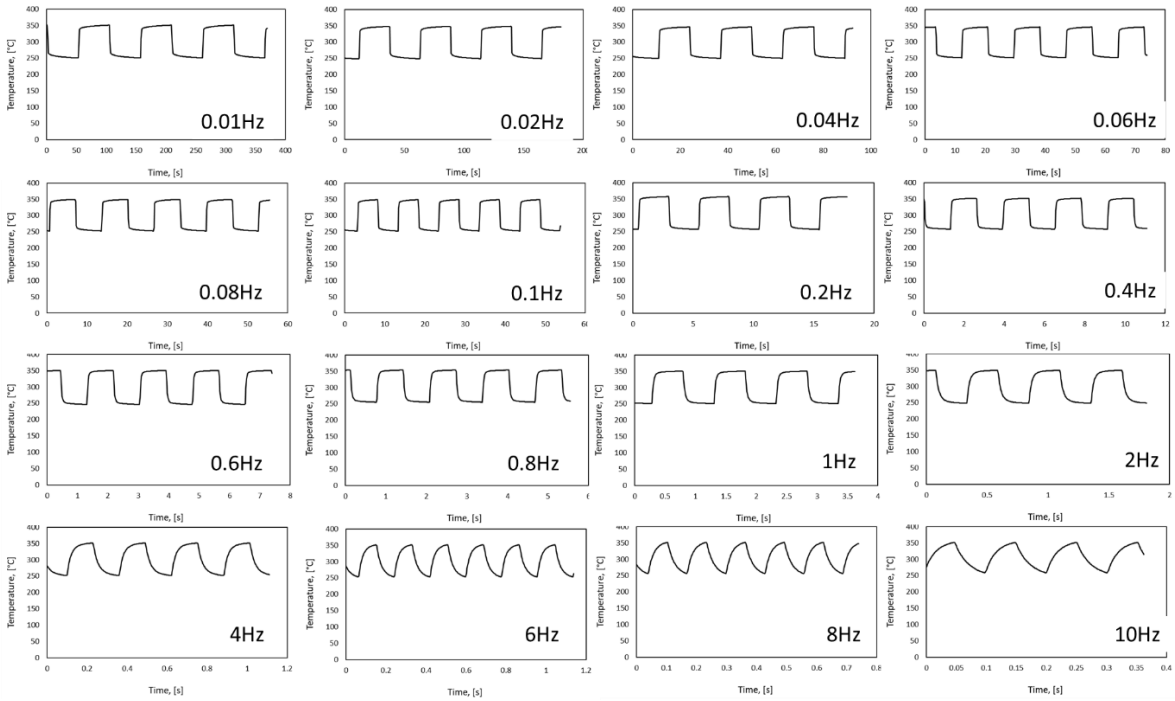

Figure 6-3: 100°C temperature oscillations across a range of applied frequencies between 0.01Hz to 10Hz

6.2.4 ANALYSIS

Product analysis for these experiments was run by our Hiden HPR-20 R&D residual gas analyzer mass spectrometer. The data was processed using their proprietary software QGA Professional.

Temperature data was collected and stored by our custom LabVIEW file by interfacing with the power supply to collect real time voltage and currents to determine the reactor temperature, which is further explained in section 3.4.

6.3 RESULTS & DISCUSSION

There are three main parameters to a waveform that we are able to tune in our dynamic input: amplitude, duty, and frequency. Each of these parameters plays an important role in different ways. The oscillation *amplitude* determines the temperature regimes that we are operating between. The

proper selection of the amplitude allows different surface phenomena to dominate. For example, below the light-off temperature when there is no reaction, surface coverage dominates. Above the light-off temperature, the bonds can break and be formed, and reaction dominates. Selection of the waveform duty means looking towards the microkinetic steps of the chemistry. Table 5-1 breaks down the elementary steps for carbon monoxide oxidation. Each of these steps has a corresponding time associated with it. The proper duty selection for a chemistry considers those elementary steps and tailors the time spent at the high temperature and the low temperature to elementary time scales. Lastly, the selection of frequency is perhaps the most straight forward. The time it takes for one complete catalytic cycle on an individual site is known as a catalytic turnover. The goal is to match the applied frequency to this intrinsic kinetic value. In the following sections we investigate the effect of amplitude, frequency, and duty on the dynamic system.

6.3.1 THE EFFECT OF AMPLITUDE EXPERIMENTS ON DYNAMIC CONVERSION

Here we tested different oscillation amplitudes to determine the role it plays in dynamic operation in the range where we observed conversion. The amplitude parameter is significant in the microkinetics of any given chemistry as it determines which phenomena dominates at any given

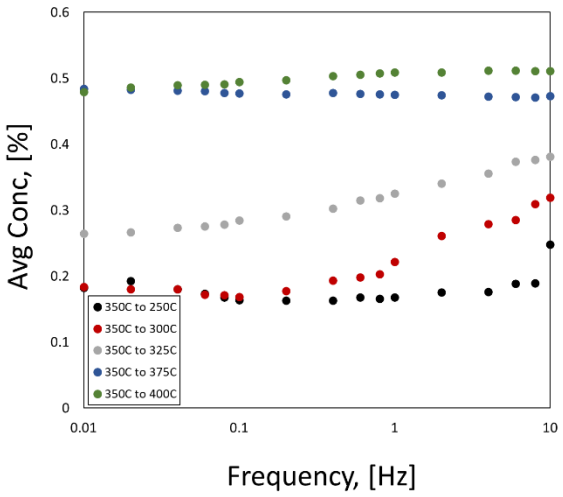

Figure 6-4: The effect of different temperature oscillation amplitudes from 350°C

time – transport effects or kinetic effects. We tested 5 different temperature ranges all around a 350°C starting temperature. The absolute amplitudes tested were between 25°C to 100°C all within the range of previously tested temperature swings giving us confidence our system is capable of achieving these oscillations all at a duty cycle of 0.5. The results of these experiments are seen in Figure 6-4.

The trend that we observe here is that reactivity *decreases* with the average temperature as one might expect according to the Arrhenius equation. The average temperature follows:

$$T_{Avg} = [T_{High} \times Duty] + [T_{Low} \times (1 - Duty)]$$

and can be seen in Table 6-1.

Table 6-1: Temperature conditions for amplitude dynamic experiments

#	Temperature Range	Average Temperature
1	350°C to 250°C	300°C
2	350°C to 300°C	325°C

3	350°C to 325°C	337.5°C
4	350°C to 375°C	362.5°C
5	350°C to 400°C	375°C

Although overall these experiments trend with their average temperature, there are two standout data sets. For the most part, these experiments do not trend with the applied frequency and maintain the same level of activity at low and high rates of oscillations. There are two experiments, however, that seem to show some trends. Experiments 2 and 3 oscillate between 350°C to 300°C and 350°C to 325°C, respectively. Each of these conditions seems to show an upwards trend as frequency is increased. This helped us to select our thermal amplitude in our experiments going forward. As we look back to the observed hysteresis in Chapter 5, these experiments gave us extra confidence in selecting our temperature swing as 350°C to 325°C. This is because our chosen amplitude was selected to encompass the hysteresis effect in our system and is sure to operate above the catalytic light off *and* below the light out as seen in section 5.3.1. The low temperature was 325°C and the high temperature was 350°C. The low temperature covers the lower end of the reaction hysteresis and represents a value where reaction steps cannot yet be activated. The high temperature encompasses the upper range of the hysteresis and lays in the reactive regime.

6.3.2 THE EFFECT OF DUTY EXPERIMENTS ON DYNAMIC CONVERSION

The duty parameter is one that has not been considered previously as most people in their dynamic experiments study a duty cycle of 0.5. Duty is an important parameter as it determines the fraction of time transport and reactions can feasibly occur. Thinking towards the general rate law

$$r = k\theta_A$$

the importance of the duty cycle becomes more evident. When lower temperatures are preferential, reactants are more likely to bind and stay bound to the catalyst surface instead of desorbing. This is because the temperature is low enough such that reaction *cannot* occur. This leads to an increase in θ_A or the fractional coverage of species A on the surface of the catalyst. Now that the surface of our catalyst is saturated as much as possible with reactants, the temperature is increased to the kinetic regime. This follows the Arrhenius rate equation:

$$k = Aexp\left(-\frac{E_a}{RT}\right)$$

Where the rate constant increases with temperature. Now that both terms in the rate equation are enhanced, we observe an increase in the reactivity of the chemistry. This is not true for isothermal

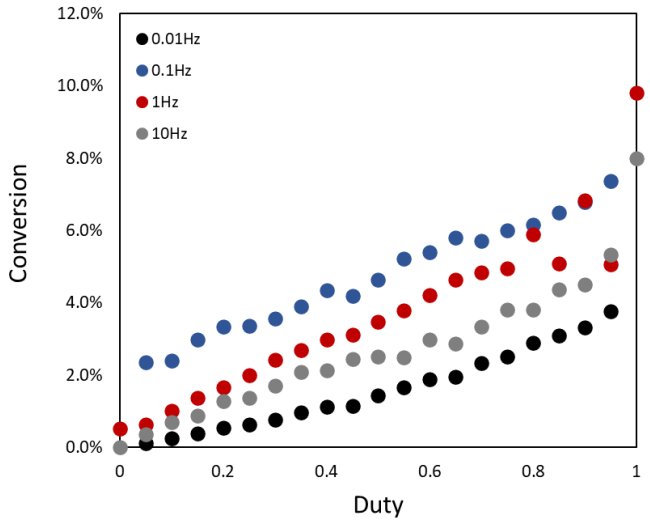

Figure 6-5:Dynamic experiments increasing duty from 0 to 1 for an amplitude between 325C to 350C for a family of applied frequencies

systems because all of the microkinetic steps occur simultaneously. The surface cannot be loaded beyond thermodynamic and kinetic equilibrium and the rate cannot be periodically increased. This is the true benefit of dynamic operation.

In our dynamic duty experiments, we ran reactions between a duty of 0 to 1 in increments of 0.05 for a family of different frequencies between 0.01Hz to 10Hz as seen in Figure 6-5. Here it seems as though there are no dynamic enhancements with duty and that we once again simply follow the trend that as the average temperature of our dynamic signals increases, so too does the conversion as one might expect. Upon closer inspection we see that although there may not be a clear dynamic trend with *duty*, there is in fact a trend with *frequency*. If instead of plotting conversion versus duty we instead look at conversion vs frequency, a trend emerges as seen in Figure 6-6.

When interpreted in this way, we can now see that as frequency increases, the conversion does as

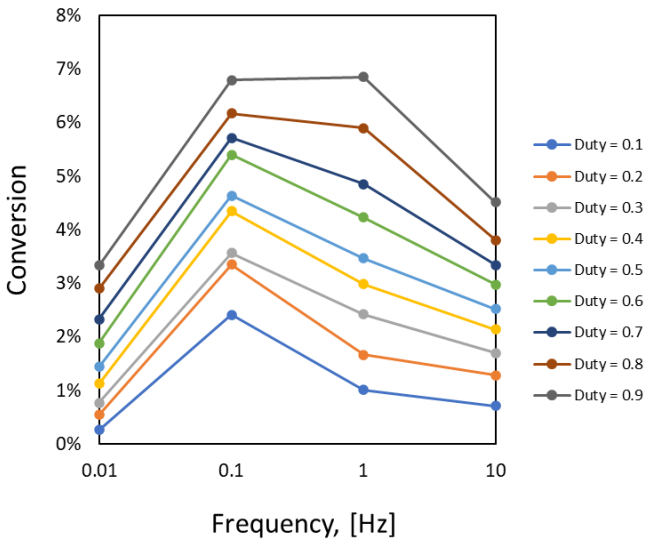

Figure 6-6: Dynamic duty experiments reinterpreted against frequency

well before dropping back down at higher rates. This is an interesting observation that even though we ran our experiments sequentially with duty, a trend emerges with frequency.

6.3.3 THE EFFECT OF FREQUENCY EXPERIMENTS ON DYNAMIC CONVERSION

Frequency is perhaps the first parameter that comes to mind when hearing dynamics. Applied frequency refers to the number of oscillations in a time period and is the inverse of the waveforms' *period*. Here we explore the effect of frequency across four orders of magnitude on the reactivity of our system.

Using our platinum wire, cross microreactor, we designed experiments which would cover a large range from slow to fast oscillations. This is important as there are three major regimes that we would like to elucidate:

1) The applied frequency is *too slow*: the conversion collapses to that of the average of the isothermal limits. There is no dynamic benefit as the individual microkinetic steps of the reaction all experience one temperature, effectively operating under two different static conditions.

$$X = \frac{\left[X\left(T_{High}\right) + X(T_{Low})\right]}{2} = \bar{X}\left(T(t)\right)$$

2) The applied frequency is *just right*: the conversion is enhanced due to dynamic cycling. The microkinetic steps experience conditions that facilitate each individual step. Cooler temperatures enable surface adsorption while hotter temperatures drive the kinetics.
3) The applied frequency is *too fast*: the conversion is dampened to the conversion of the average temperature of the two limits. Each elementary step of the reaction experiences at least one full temperature pulse, meaning that the benefit of temperature oscillations is lost.

$$X = X\left(\frac{T_{High} + T_{Low}}{2}\right) = X\left(\bar{T}(t)\right)$$

With these regimes in mind, we proceeded with our experiments. In running the dynamic experiments, we tested a range of applied frequencies from 0.01Hz to 10Hz. As seen in the temperature oscillation profiles, 10Hz is around the upper limit for our system and 0.01Hz begins to move away from the turnover range of our chemistry (TOF ~0.1 to 20) meaning our oscillation range covers the majority of the expected range for observed turnovers for this chemistry. Additionally, we repeated each set of frequency experiments for a family of different duty cycles between 0 to 1 as seen in Figure 6-7.

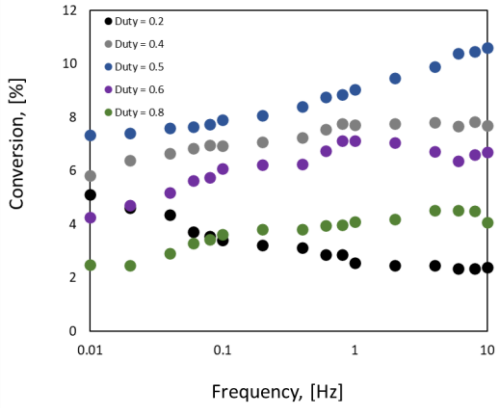

Figure 6-7: Experimental results for the conversion in dynamically operated CO oxidation between 0.01Hz to 10Hz and 0 to 1 duty cycle

Clearly this does not seem to indicate the presence of significant dynamic enhancements as for each set of frequency experiments it appears as though there is a slight increase in conversion with the applied frequency. Once again, if we instead take this data and plot it against duty, we see a trend emerge.

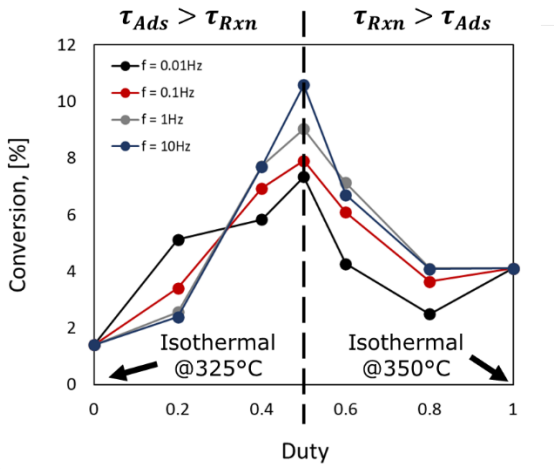

Figure 6-9: Dynamic frequency experiments reinterpreted against duty

Here we once again see a strong trend emerge as we increase duty, the conversion increases to a maxima at 0.5, before falling back off as duty continues to increase. We also see for a subset at different magnitudes of applied frequency that conversion generally increases. It is interesting to note that the conversion reaches its maxima when the time allowed for adsorption processes matches the time allowed for reaction phenomena.

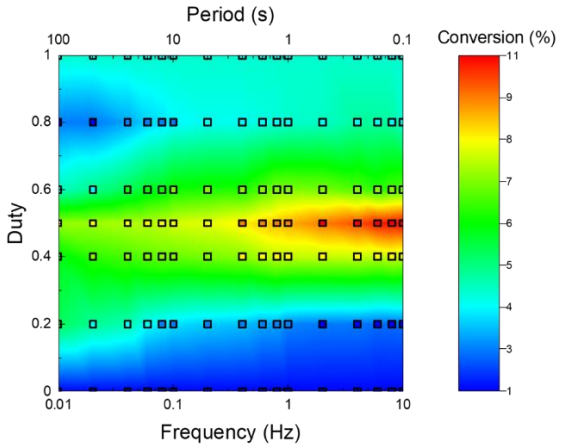

Figure 6-8: 3-D plot of frequency vs duty vs conversion for dynamic experiments between 325C to 350C

If we then turn this data into a 3D representation, as in Figure 6-9, of the conversion as a function of duty and frequency, we can observe some interesting trends. As frequency increases to the range of catalytic turnover for carbon monoxide oxidation (~0.1-20 s^{-1}) a spike in activity occurs. It is

important to note that the maximum conversion occurs at our maximum frequency meaning one of a few things. Either the limitations of our microreactor were not fully able to resolve the entire high frequency regime or heat accumulation in the system leads to inflated conversions. As we have been able to show that we obtain maxima in dynamic conversion in both duty and frequency, it is more likely we are unable to fully resolve this upper regime. As duty is increased we again see a spike in activity before dropping off.

6.4 CONCLUSIONS

Here we ran dynamic experiments on our custom microreactor test stand and tested the effects of amplitude, duty, and frequency on dynamic conversion. We found that amplitude plays an insignificant role if any on the conversion of the system and mostly follows an expected trend for average temperature versus conversion per the Arrhenius rate law. We did observe two specific instances when the amplitude seemed to play a small role, oscillating between 350°C to 300°C and 350°C to 325°C. As 350°C to 325°C fit our hysteresis curve as shown in Chapter 5, it gave us confidence that this amplitude range was appropriate for our system. For our duty experiments we initially found that they also followed the Arrhenius rate expression as increasing the duty (or average temperature) leads to an increase in conversion across frequencies ranging from 0.01Hz to 10Hz. Interestingly, when these data were plotted against frequency instead of duty, an expected trend appeared where we observe all three expected regimes for low, moderate, and high frequencies. Likewise, when running frequency experiments, there was little trend for frequency vs conversion. When these data were plotted against duty, a familiar trend emerged. Our leading idea is that the surface history plays a role and that the sequential operation in one parameter (e.g.

duty 1, duty 2, etc.) has a surface effect that is “reset” when switching to a new family of experiments (e.g. frequency 1, frequency 2, etc.).

CONCLUSIONS

The objective of this thesis was to produce a microreactor capable of millisecond dynamic operation and to use it to probe the effects of transients on the reactivity of the system. This was done to transition the field of catalysis and reaction engineering from a thermodynamic perspective to a truly dynamic one.

Chapter 2 provides background and describes the state of the field and what has been done across many different modes of dynamic operation. It introduces theory that is critical in understanding dynamics. It goes on to describe the understanding of dynamic effects at the time and insights into the gaps of knowledge that may have existed.

Chapter 3 covered the development, fabrication, validation, and the design considerations for successfully producing a microreactor capable of ultra-fast transient operation. It first describes the models that we used to define the geometry and materials necessary to fabricate a reactor capable of dynamics. With these design considerations we began iterating on the design until we had a reactor that was capable of the temperature swings we wanted. Using this microreactor we were able to develop a method for temperature monitoring through resistive heating using an external power source. With a known voltage input and a measured current, we were able to determine the resistance of the reactor in real time and relate it back to temperature in the same way a thermocouple would. We observed temperature swings up to 100°C and up to a frequency of 10Hz, or a temperature rate of change of 1,000°C/s. The temperature profile for these oscillations maintained a strong square-wave type form up to 2Hz before dampening to a sawtooth-like waveform.

Chapter 4 describes the intimate details into how our capillary reactor was fabricated and the thought process that went into it. This was our first truly promising design for a dynamic microreactor and the one we first saw dynamic rate enhancements. It also describes the problems that we had during the development of this reactor and the ways we worked through them to produce a dynamic microreactor that outperformed static operation by as much as 2.5x.

Chapter 5 talks about our working theory on surface coverage and the impact of the history of the catalyst on its activity. We ran pretreatment experiments where we doped the catalyst surface under each reactant (carbon monoxide and oxygen). We found that pretreating the surface with oxygen (high θ_O) seemed to inhibit the reaction when reintroducing carbon monoxide to the system. When we pretreated the surface with carbon monoxide (high θ_{CO}), however, there were large spikes in activity. This tells us that the surface composition prior to reaction plays a significant role in the activity of the current reaction. This drove our understanding of dynamics away from pure resonance theory and more towards surface composition. Due to the fact that we are operating transiently, one single thermodynamically equilibrated surface does not exist meaning that the surface composition from a lower temperature may have profound effects on the reactivity at an elevated temperature.

Chapter 6 described our dynamic experiments through the perspective of each tunable parameter: amplitude, duty, and frequency. Amplitude was shown not to trend with frequency and essentially followed an Arrhenius trend of increasing conversion with average temperature. There was, however, some indication that the temperature range around the hysteresis we observed in Chapter 5 may lead to some *small* enhancements. Duty experiments for a family of frequencies did not initially appear to trend outside of an Arrhenius relationship. We noticed that these experiments, when plotted against frequency, *did* trend in an expected way, where for conversion increased at a

moderate frequency and decreased at low and high frequencies. This was also the case in our frequency experiments for a family of duties. When switching from frequency vs conversion to duty vs conversion, a trend appeared. Our leading theory as to why this is happening is that the history of the catalyst played a significant role in the sequential experimentation (Duty 1, Duty 2, etc.) of one parameter which was "reset" at each new family of tested parameters (Frequency 1, Frequency 2, etc.). Even so, we were able to show that at a duty of 0.5 and a frequency around 1Hz-10Hz a maxima emerged on a 3-D map of frequency vs duty vs conversion where we see up to 5x rate enhancements over isothermal operation.

In this thesis we were successfully able to design and develop a microreactor capable of millisecond heating and cooling rates and we were able to use it to show that dynamic operation does enhance activity over static (isothermal) operation.

FUTURE DIRECTIONS, RECOMMENDATIONS, AND BROADER IMPACTS

Increasing the Waveform Complexity

My primary recommendation is developing this system further to a *truly* dynamic system is based on increasing the complexity of the waveform. In our experiments we worked to encourage certain surface phenomena by transitioning between different thermal regimes which promote either molecular transport or thermal reaction. These two phenomena are generalizations from the microkinetic steps of the reaction. To further dynamic catalysis, an input waveform that does not generalize, but instead satisfies the demands of *each individual reaction step* is important. This means a waveform that matches the proper time scales and energetics of all the elementary steps. This requires some level of molecular modeling (e.g. DFT) to understand the binding and reaction energies necessary to optimize each reaction step. After the conditions and time scales of each elementary reaction are understood, then it would be possible to transition towards a more complex dynamic operation.

Chip Reactor

Additionally, using the chip reactor we developed to run these dynamic experiments would be a good shorter-term recommendation. This chip reactor measures temperature directly using a pyroprobe rather than by calculating it from the applied current and voltage. This reactor also features a liquid forced convection line for cooling. This may ultimately lead to faster heating and cooling rates as the slow portion (cooling) is improved, expanding the frequency range that can be explored. Future generations of the chip reactor should include *operando* analysis such as IR to

measure the surface composition directly at any given time during the reaction as it has been shown to be an important parameter in deciding reactivity.

Chemistry

This system should begin targeting other chemistries. CO oxidation is a convenient chemistry as it is so well studied for the foundational studies, but has limited use in industry. By targeting other chemistries this system can be validated beyond CO oxidation and perhaps methanation, to prove this dynamic process is applicable with nearly *any chemistry.* Chemistries with particular industrial interest such as ammonia synthesis would be a strong candidate.

Beyond the Lab Scale

Perhaps the least attractive feature of microreactors in industry is their low throughput. They are notoriously difficult to scale up to produce relevant quantities of product and scale up usually comes in the form of numbering up (modularity). This is so difficult because microreactors necessitate small length scales for good heat and mass transfer which is especially important in this thesis. For this reason, for practical use of this type of system, looking towards industries which could benefit from smaller quantity, on demand chemicals would be the most impactful. For example, a farmer with such a reactor system could produce fertilizer as needed. Smaller, decentralized chemical production is where a reactor system like this could shine.

Power Comparison and Broader Impacts

Using the heat transfer expression we derived we can make some interesting insights into both the power requirements and potential environmental impacts for a dynamically operated microreactor as compared to an isothermally operated reactor. It is important to note the main difference between the two is that the isothermally operated reactor at steady state does *not*

require the transient heat accumulation term and any power requirements simply offset any convective or radiative heat losses to maintain temperature. The dynamically operated reactor is admittedly thermally very inefficient as one needs to constantly reheat the reactor many times per second.

If we consider our wall coated stainless steel capillary reactor operated dynamically, statically, and a reactor at the industrial scale we can see the power requirements during regular reactor operation looks significantly different. Assuming a square wave temperature profile at 10Hz and the material properties described in Sections 3.2.1 and 3.2.2 and a stainless-steel reactor on the scale of industrial relevance we can begin to compare these different systems as seen in Table 8-1. The industrial scale reactor was probed for a diameter of 1m and a length of 10m and is otherwise tested with the same material.

We can extend the power analysis to environmental impacts we can see how much CO_2 is generated through the electrical demands of the mode of reactor operation. The U.S. Energy Information Administration reported that 0.388kg of CO_2 is generated per kWh used. If we look at each reactor operated for 1 hour we can additionally see the amount of CO_2 generated.

Table 8-1: Power requirements for the accumulation, convection, and radiative heat demands for a microreactor operated dynamically and statically and an industrial scale PFR as well as the CO2 generated from 1 hour of reactor operation

	Dynamic Microreactor	Static Microreactor	Industry Scale Reactor
Accumulation	6.35 W	0 W	0 W
Convection	0.09 W	0.09 W	19.6 kW
Radiation	0.32 W	0.32 W	70.0 kW
Total	6.76 W	0.41 W	89.6 kW
Total CO_2	2.6E-3 kg	1.6E-4 kg	34.7 kg

We can see from these calculated results that the dynamically operated microreactor requires an order of magnitude more power than a statically operated one. This is entirely due to the heat accumulation term which is not ignored in dynamics. This accumulation term directly speaks to the thermal inefficiencies in dynamic operation. When comparing to an industrial scale reactor we see, as expected, a significantly higher power requirement to drive this reactor. Industrial PFRs often use liquids, meaning that convective demand will increase as the convection coefficient gets larger to maintain reactor temperatures.

From a purely power perspective, to make a dynamically operated microreactor on the same energetic scale as an isothermally operated microreactor, the reaction rate would have to be about an order of magnitude higher than static operation which from our results is actually on the order of a 2-5x enhancement. Here it is difficult to further compare the microreactor to an industrial PFR without additional knowledge in the throughput and efficiency, but we can make a general comparison that an industrial PFR product throughput needs to be at least 10,000x higher than dynamic operation of our microreactor to be comparable. The CO_2 generated scale linearly with the power demand meaning that it follows the power analysis just described.

There are a few ways that the dynamic operation inefficiencies could be made less prominent. Coupling thermal oscillations between reactors performing endo-/exo- thermic chemistries could help supplement the needs of each reaction without wasting additional energy. Different reactor geometries where reactants instead pass into different isothermally controlled regions could be another approach to thermal dynamics which would reduce the accumulation inefficiencies.

REFERENCES

1 M. A. Ardagh, T. Birol, Q. Zhang, O. A. Abdelrahman and P. J. Dauenhauer, *Catal. Sci. Technol.*, 2019, **9**, 5058–5076.

2 M. A. Ardagh, O. A. Abdelrahman and P. J. Dauenhauer, *ACS Catal.*, 2019, **9**, 6929–6937.

3 J. Stolte, L. Özkan, P. C. Thüne, J. W. Niemantsverdriet and A. C. P. M. Backx, *Appl. Therm. Eng.*, 2013, **57**, 180–187.

4 P. L. Silveston, H. Budman and E. Jervis, *Chem. Eng. Sci.*, 2008, **63**, 5089–5105.

5 P. L. Silveston, *Chem. Eng. Sci.*, 1996, **51**, 2419–2426.

6 P. L. Silveston and R. R. Hudgins, *Chem. Eng. Sci.*, 2004, **59**, 4055–4064.

7 P. L. Silveston and R. R. Hudgins, *Chem. Eng. Sci.*, 2004, **59**, 4043–4053.

8 F. Haber, *The synthesis of ammonia from its elements*, 1920.

9 G. Ertl, *Catalytic Ammonia Synthesis*, 1991.

10 J. K. Nørskov, T. Bligaard, J. Rossmeisl and C. H. Christensen, *Nat. Chem.*, 2009, 1, 37–46.

11 W. Yang, T. T. Fidelis and W. H. Sun, *ACS Omega*, 2020, 5, 83–88.

12 G. R. Wittreich, K. Alexopoulos and D. G. Vlachos, in *Handbook of Materials Modeling*, 2020, pp. 1377–1404.

13 K. McCullough, T. Williams, K. Mingle, P. Jamshidi and J. Lauterbach, *Phys. Chem. Chem. Phys.*, 2020, 22, 11174–11196.

14 E. J. Kluender, J. L. Hedrick, K. A. Brown, R. Rao, B. Meckes, J. S. Du, L. M. Moreau, B. Maruyama and C. A. Mirkin, *Proc. Natl. Acad. Sci.*, 2019, **116**, 40–45.

15 T. Williams, K. McCullough and J. A. Lauterbach, *Chem. Mater.*, 2020, **32**, 157–165.

16 A. J. B. Robertson, *J. Econ. Hist.*, 1975, **19**, 64–69.

17 B. Lindström and L. J. Pettersson, *CATTECH*, 2003, **7**, 130–138.

18 J. Wisniak, *Educ. Química*, 2010, **21**, 60–69.

19 J. H. van't Hoff, *Etudes de Dynamique Chimique*, 1884.

20 I. Langmuir, *Trans. Faraday Soc.*, 1922, **17**, 607–620.

21 A. V. Harcourt and W. Esson, *Philos. Trans. R. Soc.*, 1866, **156**, 193–221.

22 G. Ertl, *REACTIONS AT SURFACES: FROM ATOMS TO COMPLEXITY*, 2007.

23 F. J. M. Horn and R. C. Lin, *Ind. Eng. Chem. Process Des. Dev.*, 1967, **6**, 21–30.

24 J. H. van't Hoff, *Lectures on Theoretical and Physical Chemistry (translated by R.A. Lehrfeld)*, London, 1900, vol. 3.

25 B. Wilhelm Ostwald, *J. Chem. Soc.*, 1904, **85**, 506–522.

26 J. K. Nørskov, T. Bligaard, B. Hvolbaek, F. Abild-Pedersen, I. Chorkendorff and C. H. Christensen, *Chem. Soc. Rev.*, 2008, **37**, 2163–2171.

27 R. I. Masel, *Chemical Kinetics and Catalysis*, Wiley, 2001.

28 J. N. Bronsted, *Chem. Rev.*

29 M. G. Evans and M. Polanyi, *Trans. Faraday Soc.*, 1938, **34**, 11–24.

30 J. Cheng, P. Hu, P. Ellis, S. French, G. Kelly and C. M. Lok, *J. Phys. Chem. C*, 2008, **112**, 1308–1311.

31 J. Cheng and P. Hu, *J. Am. Chem. Soc. Commun.*, 2008, **130**, 10868–10869.

32 P. Quaino, F. Juarez, E. Santos and W. Schmickler, *Beilstein J. Nanotechnol.*, 2014, **5**, 846–854.

33 A. J. Medford, A. Vojvodic, J. S. Hummelshøj, J. Voss, F. Abild-Pedersen, F. Studt, T. Bligaard, A. Nilsson and J. K. Nørskov, *J. Catal.*, 2015, **328**, 36–42.

34 A. H. Motagamwala, M. R. Ball and J. A. Dumesic, *Annu. Rev. Chem. Biomol. Eng.*, 2018, **9**, 413–450.

35 M. T. Darby, M. Stamatakis, A. Michaelides and E. H. Charles Sykes, *J. Phys. Chem. Lett*, 2018, **9**, 20.

36 J. Pérez-Ramírez and N. López, *Nat. Catal.*, 2019, **2**, 971–976.

37 T. Z. H. Gani and H. J. Kulik, *ACS Catal.*, 2018, **8**, 975–986.

38 P. Mehta, P. Barboun, F. A. Herrera, J. Kim, P. Rumbach, D. B. Go, J. C. Hicks and W. F. Schneider, *Nat. Catal.*, 2018, **1**, 269–275.

39 Y. Li and Q. Sun, *Adv. Energy Mater.*, 2016, **6**, 1600463.

40 K. F. Kalz, R. Kraehnert, M. Dvoyashkin, R. Dittmeyer, R. Gläser, U. Krewer, K. Reuter and J. D. Grunwaldt, *ChemCatChem*, 2017, **9**, 17–29.

41 T. Z. H. Gani and H. J. Kulik, *ACS Catal.*, 2018, **8**, 975–986.

42 T. A. A. Batchelor, J. K. Pedersen, S. H. Winther, I. E. Castelli, K. W. Jacobsen and J. Rossmeisl, *Joule*, 2019, **3**, 834–845.

43 G. Ertl, *Angew. Chemie - Int. Ed.*, 2008, 47, 3524–3535.

44 P. J. Wangersky, *Ann. Rev. Ecol. Syst*, 1978, **9**, 189–218.

45 M. Parker and A. Kamenev, *Phys. Rev. E*, 2009, **80**, 021129-1-021129–10.

46 E. M. Slavinskaya, O. A. Stonkus, R. V. Gulyaev, A. S. Ivanova, V. I. Zaikovskii, P. A. Kuznetsov and A. I. Boronin, *Appl. Catal. A Gen.*, 2011, **401**, 83–97.

47 P. A. Carlsson, V. P. Zhdanov and M. Skoglundh, *Phys. Chem. Chem. Phys.*, 2006, **8**, 2703–2706.

48 T. Katona, L. Guczi and G. A. Somorjai, *J. Catal.*, 1991, **132**, 440–450.

49 H. Niiyama and Y. Suzuki, *Chem. Eng. Commun.*, 1981, **14**, 145–149.

50 T. T. Tsotsis, V. U. S. Rao and L. M. Polinski, *AIChE J.*, 1982, **28**, 847–851.

51 R. Imbihl and G. Ertl, *Oscillatory Kinetics in Heterogeneous Catalysis*, 1995, vol. 95.

52 S. B. Schwartz and L. D. Schmidt, *Surf. Sci. Lett.*, 1987, **183**, L269–L278.

53 B. L. M Hendriksen, M. D. Ackermann, R. van Rijn, D. Stoltz, I. Popa, O. Balmes, A. Resta, D. Wermeille, R. Felici, S. Ferrer and J. W. M Frenken, *Nat. Chem.*, 2010, **2**, 730–734.

54 Y. H. Hu and E. Ruckenstein, *Ind. Eng. Chem. Res*, 1998, **37**, 2333–2335.

55 Y. Li, M. Zhao, C. Li and W. Ge, *Chem. Eng. J.*, 2019, **373**, 744–754.

56 T. Uchihashi, R. Iino, T. Ando and H. Noji, *Science (80-.).*, 2011, **333**, 755–758.

57 R. C. Mottram, *Flow Meas. Instrum.*, 1989, **1**, 15–23.

58 S. Zhu, W. Shen and X. Qian, *Smart Mater. Struct*, 2013, **22**, 115018–115029.

59 A. R. Teixeira, X. Qi, C. C. Chang, W. Fan, W. C. Conner and P. J. Dauenhauer, *J. Phys. Chem. C*, 2014, **118**, 22166–22180.

60 S. Haydar, C. Moreno-Castilla, M. A. Ferro-García, F. Carrasco-Marín, J. Rivera-Utrilla, A. Perrard and J. P. Joly, *Carbon N. Y.*, 2000, **38**, 1297–1308.

61 S. Bhatia, J. Beltramini and D. D. Do, *Catal. Today*, 1990, **7**, 309–438.

62 M. Petkovska, N. Daliborka and A. Seidel-Morgenstern, *Isr. J. Chem.*, 2018, **58**, 663–681.

63 M. Petkovska and D. D. Do, *Nonlinear frequency response of adsorption systems: isothermal batch and continuous flow adsorbers*, 1998, vol. 53.

64 T. R. Vidakovi c-Koch, V. V Panic, M. Andri, M. Petkovska and K. Sundmacher, *J. Phys. Chem. C*, 2011, **115**, 17341–17351.

65 S. C. Reyes, J. H. Sinfelt, G. J. DeMartin, R. H. Ernst and E. Iglesia, *J. Phys. Chem. B*, 1997, **101**, 614–622.

66 J. Greeley, *Annu. Rev. Chem. Biomol. Eng.*, 2016, **7**, 605–635.

67 M. M. Montemore and J. W. Medlin, *Catal. Sci. Technol.*, 2014, 4, 3748–3761.

68 J. E. Bailey, L. Lapidus and N. R. Amundson, in *Chemical Reactor Theory: A Review*, 1977, pp. 758–810.

69 A. J. Lotka, *J. Phys. Chem.*, 1910, **14**, 271–274.

70 A. C. López and E. V. Albano, *J. Chem. Phys.*, 2000, **112**, 3890–3896.

71 M. Ishida, D. Zheng and T. Akehata, *Energy*, 1987, **12**, 147–154.

72 B. Moghtaderi, *Energy and Fuels*, 2011, **26**, 15–40.

73 H. Fang, L. Haibin and Z. Zengli, *Int. J. Chem. Eng.*, 2009, 16.

74 L. F. de Diego, M. Ortiz, J. Adánez, F. García-Labiano, A. Abad and P. Gayán, *Chem. Eng. J.*, 2008, **144**, 289–298.

75 P. Kolbitsch, J. Bolhàr-Nordenkampf, T. Pröll and H. Hofbauer, *Int. J. Greenh. Gas Control*, 2010, **4**, 180–185.

76 R. Naqvi, J. Wolf and O. Bolland, *Energy*, 2007, **32**, 360–370.

77 M. E. Gálvez, M. Halmann and A. Steinfeld, *Ind. Eng. Chem. Res.*, 2007, **46**, 2042–2046.

78 C. Linderholm, A. Abad, T. Mattisson and A. Lyngfelt, *Int. J. Greenh. Gas Control*, 2008, **2**, 520–530.

79 N. Berguerand and A. Lyngfelt, *Int. J. Greenh. Gas Control*, 2008, **2**, 169–179.

80 A. Mishra and F. Li, *Curr. Opin. Chem. Eng.*, 2018, 20, 143–150.

81 P. L. Silveston, *Catal. Today*, 1995, **25**, 175–195.

82 W. R. C. Graham and D. T. Lynch, *AIChE J.*, 1990, **36**, 1796–1806.

83 H. Muraki, H. Sobukawa and Y. Fujitani, *Nippon KAGAKU KAISHI*, 1985, **1985**, 176–181.

84 X. Zhou, Y. Barshad and E. Gulari, *CO OXIDATION ON Pd/Al,O,. TRANSIENT RESPONSE AND RATE ENHANCEMENT THROUGH FORCED CONCENTRATION CYCLING*, 1986, vol. 41.

85 L. L. Hegedus, C. C. Chang, D. J. McEwen and E. M. Sloan, *Ind. Eng. Chem. Fundam.*, 1980, **19**, 367–373.

86 H. Y. Sohn and M. B. Aboukheshem, *Metall. Trans. B*, 1992, 23, 285–294.

87 K. S. Suslick, *Science (80-.).*, 1990, **247**, 1439–1445.

88 J. M. Joseph, H. Destaillats, H.-M. Hung and M. R. Hoffmann, *J. Phys. Chem. A*, 2000, **104**, 301–307.

89 C. Minero, P. Pellizzari, V. Maurino, E. Pelizzetti and D. Vione, *Appl. Catal. B Environ.*, 2008, **77**, 308–3016.

90 M. A. Beckett and I. Hua, *Water Res.*, 2003, **37**, 2372–2376.

91 J. J. Brandner, G. Emig, M. A. Liauw and K. Schubert, *Chem. Eng. J.*, 2004, **101**, 217–224.

92 S. Jensen, J. L. Olsen, S. Thorsteinsson, O. Hansen and U. J. Quaade, *Catal. Commun.*, 2007, **8**, 1985–1990.

93 M. Luther, J. J. Brandner, L. Kiwi-Minsker, A. Renken and K. Schubert, *Chem. Eng. Sci.*,

2008, **63**, 4955–4961.

94 P. Mehta, P. Barboun, D. B. Go, J. C. Hicks and W. F. Schneider, *ACS Energy Lett.*, 2019, 4, 1115–1133.

95 E. C. Neyts, K. Ostrikov, M. K. Sunkara and A. Bogaerts, *Chem. Rev.*, 2015, **115**, 13408–13446.

96 S. Kado, K. Urasaki, Y. Sekine and K. Fujimoto, *Fuel*, 2003, **82**, 1377–1385.

97 E. Delikonstantis, M. Scapinello, O. Van Geenhoven and G. D. Stefanidis, *Chem. Eng. J.*, 2020, **380**, 122477.

98 A. Rousseau, O. Guaitella, J. Röpcke, L. V. Gatilova and Y. A. Tolmachev, *Appl. Phys. Lett.*, 2004, **85**, 2199–2201.

99 S. Yao, A. Nakayama and E. Suzuki, *AIChE J.*, 2001, **47**, 413–418.

100 A. Bogaerts, X. Tu, J. Christopher Whitehead, G. Centi, L. Lefferts, O. Guaitella, F. Azzolina-Jury, H.-H. Kim, A. B. Murphy, W. F. Schneider, T. Nozaki, J. C. Hicks, A. Rousseau, F. Thevenet, A. Khacef and M. Carreon, *J. Phys. D Appl. Phys.* , 2020, **53**, 51.

101 A. Fujishima, T. N. Rao and D. A. Tryk, *J. Photochem. Photobiol. C Photochem. Rev.*, 2000, **1**, 1–21.

102 A. Mills and S. Le Hunte, *J. Photochem. Photobiol. A Chem.*, 1997, **108**, 1–35.

103 M. A. Fox and M. T. Dulay, *Chem. Rev.*, 1993, **93**, 341–357.

104 M. E. Fabiyi and R. L. Skelton, *Process Saf. Environ. Prot.*, 2000, **78**, 399–404.

105 M. A. Fox, *Acc. Chem. Res*, 1983, **16**, 314–321.

106 A. Vardi and M. Shapiro, *Phys. Rev. A*, 1998, **58**, 1352–1360.

107 M. Pschenitza, S. Meister, A. von Weber, A. Kartouzian, U. Heiz and B. Rieger, *ChemCatChem*, 2016, **8**, 2688–2695.

108 Z. H. Yamani, B. Zain and H. Yamani, *Arab J Sci Eng*, 2018, **43**, 423–432.

109 S. SCHULDINER, in *Recent Progress in Surface Science*, eds. J. F. Danielli, K. G. A. Pankhurst and A. C. Riddiford, 1964, vol. 1, pp. 159–218.

110 P. S. Fedkiw, C. L. Traynelis and S.-R. Wang, *J. Electrochem. Soc.*, 1988, **135**, 2459–2465.

111 R. R. Adzic, K. I. Popov and M. A. Pamic, *Electrochim. Acta*, 1978, **23**, 1191–1196.

112 J. Gopeesingh, M. Ardagh, M. Shetty, S. Burke, P. Dauenhauer and O. Abdelrahman, *ACS Catal.*, 2020, **10**, 9932–9942.

113 M. J. Escudero, A. Aguadero, J. A. Alonso and L. Daza, *J. Electroanal. Chem.*, 2007, **611**, 107–116.

114 F. M. Wang and J. Rick, *Solid State Ionics*, 2014, **268**, 31–34.

115 C. Liang, L. Liu, Z. Jia, C. Dai and Y. Xiong, *Electrochim. Acta*, 2015, **186**, 413–419.

116 D. D. MacDonald, *Electrochim. Acta*, 2006, **51**, 1376–1388.

117 B.-Y. Chang and S.-M. Park, *Annu. Rev. Anal. Chem.*, 2010, **3**, 207–229.

118 R. F. Mann, J. C. Amphlett, B. A. Peppley and C. P. Thurgood, *J. Power Sources*, 2006, 775–781.

119 H. You, X. Ma, Z. Wu, L. Fei, X. Chen, J. Yang, Y. Liu, Y. Jia, H. Li, F. Wang and H. Huang, *Nano Energy*, 2018, **52**, 351–359.

120 Q. Deng, M. Smetanin and J. Weissmüller, *J. Catal.*, 2014, **309**, 351–361.

121 Y. Yukawa, N. Saito, H. Nishiyama and Y. Inoue, in *Surface Science*, 2002, vol. 502–503, pp. 527–531.

122 X. Xu, Y. Jia, L. Xiao and Z. Wu, *Chemosphere*, 2018, **193**, 1143–1148.

123 B. Yuan, J. Wu, N. Qin, E. Lin and D. Bao, *ACS Appl. Nano Mater.*, 2018, **1**, 5119–5127.

124 T.-S. Oh, E. K. Rahani, D. Neagu, J. T. S. Irvine, V. B. Shenoy, R. J. Gorte and J. M. Vohs, *J. Phys. Chem. Lett*, 2015, **6**, 57.

125 T. Weber, T. Ortmann, D. Escalera-López, M. J. S. Abb, B. Mogwitz, S. Cherevko, M. Rohnke and H. Over, *ChemCatChem*, 2020, **12**, 855–866.

126 S. M. Kim, C. Y. Ahn, Y. H. Cho, S. Kim, W. Hwang, S. Jang, S. Shin, G. Lee, Y. E. Sung and M. Choi, *Sci. Rep.*, 2016, **6**, 26503.

127 C. Y. Ahn, S. Jang, Y. H. Cho, J. Choi, S. Kim, S. M. Kim, Y. E. Sung and M. Choi, *Sci. Rep.*, 2018, **8**, 1257.

128 H. J. Cho, N. B. Lu, M. P. Howard, R. A. Adams and S. S. Datta, *Soft Matter*, 2019, **15**, 4689.

129 E. E. Benson, M.-A. Ha, B. A. Gregg, J. van de Lagemaat, N. R. Neale and D. Svedruzic, *Sci. Rep.*, 2019, **9**, 15906.

130 B. Hess and A. Boiteux, *Annu. Rev. Biochem.*, 1971, **40**, 237–258.

131 A. L. Koch, *J. Theor. Biol.*, 1970, **28**, 203–231.

132 K. Ye, M. Shijo, S. Jin and K. Shimizu, *J. Ferment. Bioeng.*, 1996, **82**, 484–491.

133 L. J. Kricka and P. Wilding, *Anal Bioanal Chem*, 2003, 820–825.

134 J. S. Farrar and C. T. Wittwer, *Clin. Chem.*, 2015, **61**, 145–153.

135 Y. Asano, S. Togashi, H. Tsudome and S. Murakami, *Pharamceutical Eng.*

136 X. Yao, Y. Zhang, L. Du, J. Liu and J. Yao, *Renew. Sustain. Energy Rev.*, 2015, **47**, 519–539.

137 J. C. Ganley, E. G. Seebauer and R. I. Masel, *J. Power Sources*, 2004, **137**, 53–61.

138 R. H. S. Winterton, *Contemp. Phys.*, 1999, **40**, 205–212.

139 T. L. Bergman, A. S. Lavine, F. P. Incropera and D. P. Dewitt, *Fundamentals of Heat and Mass Transfer - Seventh Edition*, 2011.

140 R. H. Bogaard, *Thermal Conductivity of Selected Stainless Steels*, .

141 M. A. Ardagh, M. Shetty, A. Kuznetsov, Q. Zhang, P. Christopher, D. Vlachos, O. Abdelrahman and P. Dauenhauer, *ChemRxiv*, , DOI:10.26434/chemrxiv.10271090.v1.

142 X. Zhang, M. Honkanen, M. Järn, J. Peltonen, V. Pore, E. Levänen and T. Mäntylä, *Appl. Surf. Sci.*, 2008, **254**, 5129–5133.

143 H. Scott Fogler, *Elements of chemical reaction engineering*, 1987, vol. 42.

144 L. Wang, M. Xia, H. Wang, K. Huang, C. Qian, C. T. Maravelias and G. A. Ozin, *Joule*, 2018, **2**, 1055–1074.

145 J. Bravo, A. Karim, T. Conant, G. P. Lopez and A. Datye, *Chem. Eng. J.*, 2004, **101**, 113–121.

146 R. M. Al Soubaihi, K. M. Saoud and J. Dutta, *Catalysts*, , DOI:10.3390/catal8120660.

147 M. E. Davis and R. J. Davis, *Fundamentals of chemical reaction engineering*, 2003.

148 M. P. Harold and M. E. Garske, *J. Catal.*, 1991, **127**, 524–552.

149 M. P. Harold and M. E. Garske, *J. Catal.*, 1991, **127**, 553–575.

APPENDIX

Transient Heat Transfer Matlab Code

```
function [tf, Tf] = Temperature_SS_Calculator_v4()

global npulse L  Dout  Tinf  epsilon  sigma  Tsurr rho Cp   Din ti Ti W k_ss
close all

%% Variables
if nargin<1
    P       = 8;      %W or J/s
end

% Only one of these can be a vector: h or dt_hot+ht_cold

flag = 2; % 0 = h vector; 1 = duty vector; 2 = power vector; 3 = frequency vector

if flag ==0      % h Vector
    h = [5 150 500];               % W/m2-K
    dt_hot  = 0.0;                 % s
    dt_cold = 5;                   % s
    P       = 100;                 % W or J/s
elseif flag==1   % Duty Vector
    h = 50;                        % W/m2-K
    dt_hot  = [0.2 0.2 0.2];       % s    const period (1s)
    dt_cold = [0.4 0.6 0.8];       % s
    P       = 10;                  % W or J/s
elseif flag==2   % Power Vector
    h = 50;                        % W/m2-K
    dt_hot  = 0.2;                 % s
    dt_cold = 0.4;                 % s
    P       = [6 10 16];           % W or J/s


elseif flag==3   % Frequency Vector
    h = 50;                        % W/m2-K
    dt_hot  = [0.3333 0.1666 0.03333 0.016666 0.01111];       % s    const duty
    dt_cold = [2-dt_hot(1) 1-dt_hot(2) 0.2-dt_hot(3) 0.1-dt_hot(4) 0.066667-
dt_hot(5)];       % s

    P       = 10;                 %W or J/s
end

%% Reactor
Din     = 0.0004;                   %m
Dout    = 0.0005;                   %m
Tinf    = 300;                      %K
epsilon = 0.3;
sigma   = 5.6703E-8;                %(W/m2K4)
Tsurr   = 300;                      %K
rho     = 8000;                     %kg/m3
Cp      = 500;                      %J/kg-K
```

```
L       = 0.1;                          %m
W       = 0.0001;                       %m   capillary wall width
k_ss    = 20;                           %W/m-K    stainless steel 304 ~100C

npulse  = 50;

% Initialize
ti = 0;     %s
Ti = 300;   %K


%% h Calculations
% visc_kin= 3.5E-5;                      %m^2/s
% v       = 0.98;                       %m/s
% kc      = 0.047;                      %W/m-K
% mu      = 2.7E-5;                     %kg/m-s
% Cp      = 1005;                       %J/kg-K
% Re      = v*L/visc_kin;
% Pr      = Cp*mu/kc;
% Nu      = 0.3387*Re^(1/2)*Pr^(1/3)/(1+(0.0468/Pr)^(2/3))^(1/4);
% h       = Nu*kc/L                     %W/m^2

%% Evaluate T Profiles

if flag == 0
    for i = 1:length(h)
        [tprint, Tprint] = Tprofile(h(i), dt_hot, dt_cold, P);
        Tf(:,i)=Tprint;
        tf(:,i)=tprint;

    end
elseif flag==1
    for i = 1:length(dt_hot)
        [tprint, Tprint] = Tprofile(h, dt_hot(i), dt_cold(i), P);
        Tf(:,i)=Tprint;
        tf(:,i)=tprint;

    end
elseif flag==2
    for i = 1:length(P)
        [tprint, Tprint] = Tprofile(h, dt_hot, dt_cold, P(i));
        Tf(:,i)=Tprint;
        tf(:,i)=tprint;

    end
elseif flag==3
    for i = 1:length(dt_hot)
        [tprint, Tprint] = Tprofile(h, dt_hot(i), dt_cold(i), P);
        Tf(:,i)=Tprint;
        tf(:,i)=tprint;
    end
end

%% Biot Number
% for i = 1:length(h)
```

```
%     Bi = h(i)*W/k_ss;



%% Plots
plot(tf,Tf)
    set(gcf, 'color','w')
    xlabel('time [s]')
    ylabel('Temperature [K]')

if flag == 0
    legend(['h = ' num2str(h(1)) 'W/m2-K'],['h = ' num2str(h(2)) 'W/m2-K'],['h = '
num2str(h(3)) 'W/m2-K'])
end

if flag == 1
    legend(['Duty = ' num2str(dt_hot(1)/dt_cold(1))], ['Duty = '
num2str(dt_hot(2)/dt_cold(2))], ['Duty = ' num2str(dt_hot(3)/dt_cold(3))])
end

if flag == 2
    legend(['P = ' num2str(P(1)) 'W'],[ 'P = ' num2str(P(2)) 'W'],[ 'P = '
num2str(P(3)) 'W'],[ 'P = ' num2str(P(4)) 'W'],[ 'P = ' num2str(P(5)) 'W'],[ 'P = '
num2str(P(6)) 'W'])
end

if flag == 3
    legend(['Frequency = ' num2str(1/(dt_hot(1)+dt_cold(1))) ' 1/s'], ['Frequency = '
num2str(1/(dt_hot(2)+dt_cold(2))) ' 1/s'], ['Frequency = '
num2str(1/(dt_hot(3)+dt_cold(3))) ' 1/s'], ['Frequency = '
num2str(1/(dt_hot(4)+dt_cold(4))) ' 1/s'], ['Frequency = '
num2str(1/(dt_hot(5)+dt_cold(5))) ' 1/s'])
end


end

function [t, T] = Tprofile(h, dt_hot, dt_cold, P)
global npulse L  Dout  Tinf  epsilon  sigma  Tsurr rho Cp   Din ti Ti

tspan_hot   = linspace(0,dt_hot,10);
tspan_cold  = linspace(0,dt_cold,10);

tprint= ti; % Initial time (ti = 0 s)
Tprint = Ti; % Initial T

for j = 1:npulse
%     % Solve ODE for Hot half of pulse j
    tspan = tspan_hot;
    T0 = Tprint(end);
    [tout,Tout] = ode45(@(t,T) ( P/L - pi * Dout * h * (T - Tinf) - pi* Dout *
epsilon * sigma * (T^4 - Tsurr^4))/(rho * Cp * pi * (Dout^2 - Din^2) / 4), tspan,T0);
    tprint = [tprint; (tout+tprint(end))];
    Tprint = [Tprint; Tout];
```

```
%     Solve ODE for Cold half of pulse j
     tspan = tspan_cold;
     T0 = Tprint(end);
     [tout,Tout] = ode45(@(t,T) ( - pi * Dout * h * (T - Tinf) - pi* Dout * epsilon *
sigma * (T^4 - Tsurr^4))/(rho * Cp * pi * (Dout^2 - Din^2) / 4), tspan,T0);
     tprint = [tprint; (tout+tprint(end))];
     Tprint = [Tprint; Tout];

end
t = tprint;
T = Tprint;

end
```